Friction in journal bearings

Bennett, James

FRICTION IN JOURNAL BEARINGS

BY JAMES BENNETT B.Sc.

Abstract

Friction in fluid Journal Bearings is usually investigated by measuring the torque which appears on a bearing whilst a shaft is rotated inside it. The bearing is supported hydrostatically which would allow it to rotate freely if otherwise unrestricted. Motion of the bearing is restricted by tension gauges which indicate the frictional force which they are resisting.

The work described in this thesis is concerned with a new method of measuring frictional torque in journal bearings. The method consists of driving a shaft up to a given speed inside a fixed bearing and then permitting it to decelerate freely. The decelerations are timed electronically and almost instantaneous deceleration rates are obtained. From these deceleration rates and known polar moment of inertia, the frictional torque in the bearing can be found for given speeds. The method has been found to be very reliable and also has wider application with other rotating systems.

FRICTION IN JOURNAL BEARINGS

BY JAMES BENNETT B.Sc.

Thesis submitted for the Degree of
Doctor of Philosophy at the University of Durham.
Department of Engineering Science 1981.

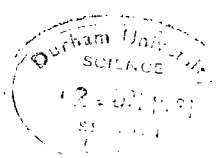

CONTENTS

ILLUSTRATIONS

Acknowledgements

I should like to express my thanks to the members of staff of the Engineering Science Department at Durham University for their help and advice given to me throughout my research, with special thanks to Prof. H. Marsh, Dr. V.G. Endean and Mr. G. Daley.

Declaration

None of the material contained in this thesis has been previously submitted by me for a degree in this or any other University and the work represents my own original contribution.

NOTATION

A, B	constants
c	radial clearance
Cf	non-dimensional bearing frictional torque
Cf_1	uncorrected non-dimensional bearing frictional torque
D	bearing diameter
F	frictional force
h	film thickness
h*	film thickness at the point of maximum pressure
I	inertia
I_p	rotor polar inertia
I_T	rotor transverse inertia
k_1	constant
k_c	bearing angular stiffness
k_L	bearing linear stiffness
k_x, k_y	constants in the turbulent Reynolds equation
L	length of the bearing
l_2	L/2
M	rotor mass
$\dot{m}$	lubricant mass flowrate
$\dot{m}_c$	non-dimensional correction for angular momentum torque
N	rotational frequency
N	integer variable
N_o	initial rotational frequency
N_∞	self drive steady rotational frequency
N_{onset}	onset speed of instability
p	pressure

$\bar{p}$	time mean pressure
p'	pressure fluctation
R	bearing radius
R_1	radius of the inner cylinder
R_2	radius of the outer cylinder
Re	rotational Reynolds number
Re_{axial}	axial Reynolds number
T	frictional torque
T_2	angular momentum torque
Ta	Taylor Number
Tc	eccentric critical Taylor Number
Tco	concentric critical Taylor Number
T_{total}	total frictional torque
T_R	rotor torque
T_B	bearing torque
T_{exp}	experimental frictional torque
T_{th}	theoretical frictional torque
t	time
t_1	time for N pulses
t_2	time for 2N pulses
tc	decelerating time constant
U	surface speed
u, v, w	velocities in coordinate directions
V_x	axial flow velocity
W	bearing load
x	coordinate in the direction of motion
y	coordinate $\perp$ to the direction of motion
z	coordinate across the film
α	deceleration rate

α_T	total deceleration rate of the rotor in the air bearing
α_c	correction for the air bearing drag
D	disc drag deceleration rate
δ	$t_2 - 2t_1$
ε	eccentricity
θ	angle of rotation
θ	angular displacement from the line of centres
μ	dynamic viscosity
ν	kinematic viscosity
ρ	lubricant density
τ	shear stress on any layer of fluid
τ_c	Couette surface shear stress
ψ	attitude angle
ω	angular velocity
ω_o	initial angular velocity
ω_m	angular velocity after time t_1
ω_f	angular velocity after time t_2
ω_s	angular velocity at time t = 0
$\frac{dN}{dt}$	deceleration rate for the bearing torque + mass flow rate torque
$\frac{dN}{dt_1}$	total deceleration rate including windage and mass flow rate effects

INTRODUCTION

A journal bearing can be described as a circular shaft passing through a slightly larger hole in a housing. The two components of a fluid journal bearing are separated under normal operating conditions by a fluid film.

In hydrostatic bearings, the surfaces are forced apart by fluid supplied at high pressure into the bearing clearance.

Hydrodynamic bearings operate by virtue of the entrainment of a fluid between two moving surfaces which form a converging wedge. This produces high pressures in the fluid which force the surfaces apart. In a hydrodynamic journal bearing the shaft is displaced into an eccentric position by radial loads thus forming a convergent-divergent clearance and hence a supporting pressure system.

A resistance to the motion of the parts is caused by the shearing of the fluid film in the clearance. This resistance, or in other words the friction in the bearing, varies with the velocities of the moving surfaces, their separation, the pressure gradient in the film and the nature of the lubricating fluid. Lubricants of a very varied nature are used in journal bearings, such as air, water and oils.

Reynolds* (1) in 1886 carried out an extensive analysis of the hydrodynamic phenomenon and this has provided the basis for all the work that followed. He derived a differential equation for the pressure distribution and presented two analytical solutions. The first was for a squeeze film between two elliptical plates and the second for a plane slider bearing of infinite width. Reynolds also presented approximate solutions for the journal bearing problem. For partial arc and total arc journal bearings he sought the solution by the use of trigonometric

* References are listed at the end of the thesis

series. The series if limited to ten or twelve terms and eccentricities less than 0.6 converged with adequate accuracy. Reynolds found that for a total arc journal bearing with an eccentricity ratio of 0.5 the best agreement between theory and experiment occurred.

Reynolds equation assumes laminar flow, constant viscosity and constant pressure across the film thickness, negligible curvatures, an incompressible Newtonian fluid, negligible body forces, negligible fluid inertia and steady state conditions. As with fluid flow in a pipe, a non-dimensional group called the Reynolds number can be used to predict whether or not a bearing lubricating film is laminar or turbulent in nature. The Reynolds number indicates the relative importance of the inertia forces and the viscous forces in a fluid film. As mentioned previously, Reynolds solved the differential equation for pressure distribution by analytical means and one assumption he made was that laminar flow predominated. When bearings are operating with high Reynolds numbers the fluid film changes from laminar flow into turbulent flow and inertia forces dominate. In fully established turbulent flow the inertia forces predominate over the viscous forces. This is the case, except very near the surfaces of the bearing, where a laminar sublayer exists.

Attempts have been made to solve a modified form of the Reynolds equation for turbulent lubricating films. They are generally based on a pertubation type theory, i.e. considering mean parameters and the fluctuations about the mean, substituting these into the modified Reynolds equation and then solving it to find the pressure distribtion. The modified Reynolds equation and its solution will be discussed later in Chapter 8.

The change from a laminar to a turbulent lubricating film is preceded by a transition region, sometimes known as superlaminar flow. The various

stages in this transition region will be discussed in detail in the following chapter.

The friction which appears in a turbulent film bearing is much greater than that of a laminar bearing operating at the same Reynolds number. The modern trend is to use larger bearings, to run them faster and to lubricate them with low viscosity lubricants. The combination of these factors leads to bearings now commonly being run with a turbulent lubricating film and consequently higher frictional losses. In steam turbines manufacted in Britain bearings up to 0.76 metres in diameter are commonly used, running at 1800 r.p.m. A typical steam turbine may have up to twelve bearings varying in size from 0.25 metres to 0.76 metres in diameter supporting the rotor. The power loss in these bearings can be in the region of 0.1 megawatts for the smaller bearings to 0.52 megawatts for the 0.76 metre bearings. The total power loss from the bearings for a complete machine can be in the order of 5 megawatts.

The above statistics demonstrate the importance of the availability of accurate information on friction to the designer of bearing systems to enable him to minimise the total power consumption of a machine. The object of the research reported in this thesis is to investigate the friction in journal bearings the importance of which is indicated above. Most if not all of the experimental work which has been carried out to date has consisted of measuring the frictional torque which appears on the stationary member of a bearing. The present work consists of measuring the frictional torque which appears on a rotating shaft. The method used to obtain measurements of the frictional torque has not been used before. Whereas previous work involved measuring forces which appeared on a stationary bush, the present work involves the timing of the

decelerations of a rotating shaft and then relating the measurements obtained to the frictional torque resisting the motion of the shaft.

The experimental work reported here was carried out on bearings with clearance ratios which are commonly found in industry whereas most research work reported prior to this thesis has been carried out with large clearance ratios not in common industrial use.

CHAPTER 1

PREVIOUS WORK

Introduction

Lubricating films can be best described with the aid of a non-dimensional group called the Reynolds number. The Reynolds number used in this thesis is defined by the following:-

$$Re = \frac{\omega R c}{\nu}$$

where ω = angular velocity in radians/second

R = shaft radius

c = radial clearance

ν = kinematic viscosity

The general outline of the state of a film at various Reynolds numbers is as follows. At low Reynolds numbers the film is laminar in nature. As the Reynolds number is increased the laminar flow gains secondary flow nature and at even higher Reynolds numbers the flow breaks down into fully established turbulent flow. The region of secondary flow is often referred to as the transition region and this will be described in more detail shortly.

Much research has been carried out on bearings running with a lubricating film in the transition state. The prediction of the onset of transition, its delay and its complete suppression are some of the points which are currently under study. Also under study is the possibility of secondary flow occurring in the lubricating film at very low Reynolds numbers.

G.I. Taylor, (2), (3), (1923,1936), investigated the stability of a fluid film between two cylinders, the inner of which was rotating and the outer at rest. The investigations were both experimental and theoretical in nature and were carried out on cylinders with clearance

ratios quite large in magnitude compared to bearing ratios. The ratios used were 0.06 to 0.34. Although as mentioned, these are relatively large, the work offers information which can be used to interpret bearing films in the transition region. Taylor found that laminar flow prevailed at low Reynolds numbers but broke down into a secondary flow of toroidal vortices as the Reynolds number approached a critical value.

In general, in the flow between two concentric rotating cylinders the transition from laminar to turbulent flow is strongly influenced by centrifugal forces. The effect on the transition depends on whether velocity increases or decreases with increasing radius. When the outer cylinder is at rest and the inner is rotating, i.e. velocity decreasing with increasing radius, the effect of centrifugal forces is a destabilising one. The fluid particles near the inner cylinder experience a higher centrifugal force and show a tendency to be propelled outwards. G.I. Taylor was the first to prove that when a certain Reynolds number has been exceeded, there appear in the flow, vortices whose axes are located along the circumference and which have alternately opposite directions. The toroidal vortices have a height and width approximately equal to the radial clearance of the annulus.

The critical Reynolds number for the onset of Taylor vortices can be predicted from the equation,

$$Re = 41.1 \sqrt{R/c} \qquad (1:1)$$

where Re = Rotational Reynolds number

R = Radius of the shaft

c = Radial clearance of the bearing

Measurements indicated that the cellular vortices remain stable in a fairly wide range of Reynolds numbers above the value predicted in

(1:1). At higher Reynolds numbers the flow breaks down into turbulent flow. A generally agreed value of Reynolds number for the onset of turbulent flow is approximately 2000. When the inner cylinder is at rest and the outer is rotating, i.e. velocity increasing with increasing radius, the effect of centrifugal forces is a stabilising one. Taylor vortices do not occur with this situation, but the turbulent onset is still apparent at Reynolds numbers in the region of 2000. As the radial clearance is increased, with the outer cylinder rotating and the inner static, the stabilising influence of the centrifugal forces causes the critical Reynolds number to become larger than the value of 2000.

The frictional torque which appears in a bearing as it passes through the above-mentioned transitions varies greatly. In the laminar regime the torque is directly proportional to the speed of rotation. In the transition and turbulent regimes the torque is a more complex function of speed such as $(\text{speed})^n$ for turbulent flow. The value of the exponent 'n' will be discussed in the following section.

Reported Experimental and Theoretical Observations

A journal bearing operating over a wide speed range may display the following characteristics. At low Reynolds numbers the fluid film will be laminar in nature. As the Reynolds number is increased with increasing speed, the film will go through a 'transition region' and if the Reynolds number is increased still further the film will become turbulent.

Much work has been carried out on bearings operating in these three regimes. The early work was carried out by Petroff (1883) who produced an expression which is now commonly known as Petroff's law. The law can be used to calculate the frictional torque which appears in a

journal bearing with its members running concentrically and with the bearing clearance filled with lubricant.

The expression is:- $T = \frac{2\pi R^3 L \mu \omega}{c}$

where T = The frictional torque

L = Bearing length

μ = Dynamic viscosity

R = Bearing radius

ω = Angular velocity

This expression for frictional torque is probably that most commonly used in lubrication and provides a good estimate of the frictional torque which a bearing will display whilst operating in a laminar regime.

Wilcock, (1950), (4), carried out the first detailed investigation into the characteristics of loaded journal bearings operating in the turbulent regime. Wilcock used four bearings in his experimental work, three of 0.2 m diameter and one 0.1 m diameter. The bearings were fed with oil through two longitudinal grooves. The clearance ratios used by Wilcock were in the range $(1.7 - 3.8) \times 10^{-3}$. The housing was stationary and loaded by a hydrostatic ram and the shaft was driven by an inline motor. Frictional torque measurements were taken from the housing by using a torque arm arrangement.

Wilcock's frictional torque results are plotted in Fig. (1a). At low Reynolds numbers the plot has a gradient of -1 indicating that the frictional torque is proportional to rotational speed. Wilcock explains that as the Reynolds number is increased a definite transition occurs at about the speed predicted by Taylor for vortex formation and a further increase in speed produced full turbulence. The gradients of Wilcock's curves varied from -1 to nearly zero when turbulence was fully established.

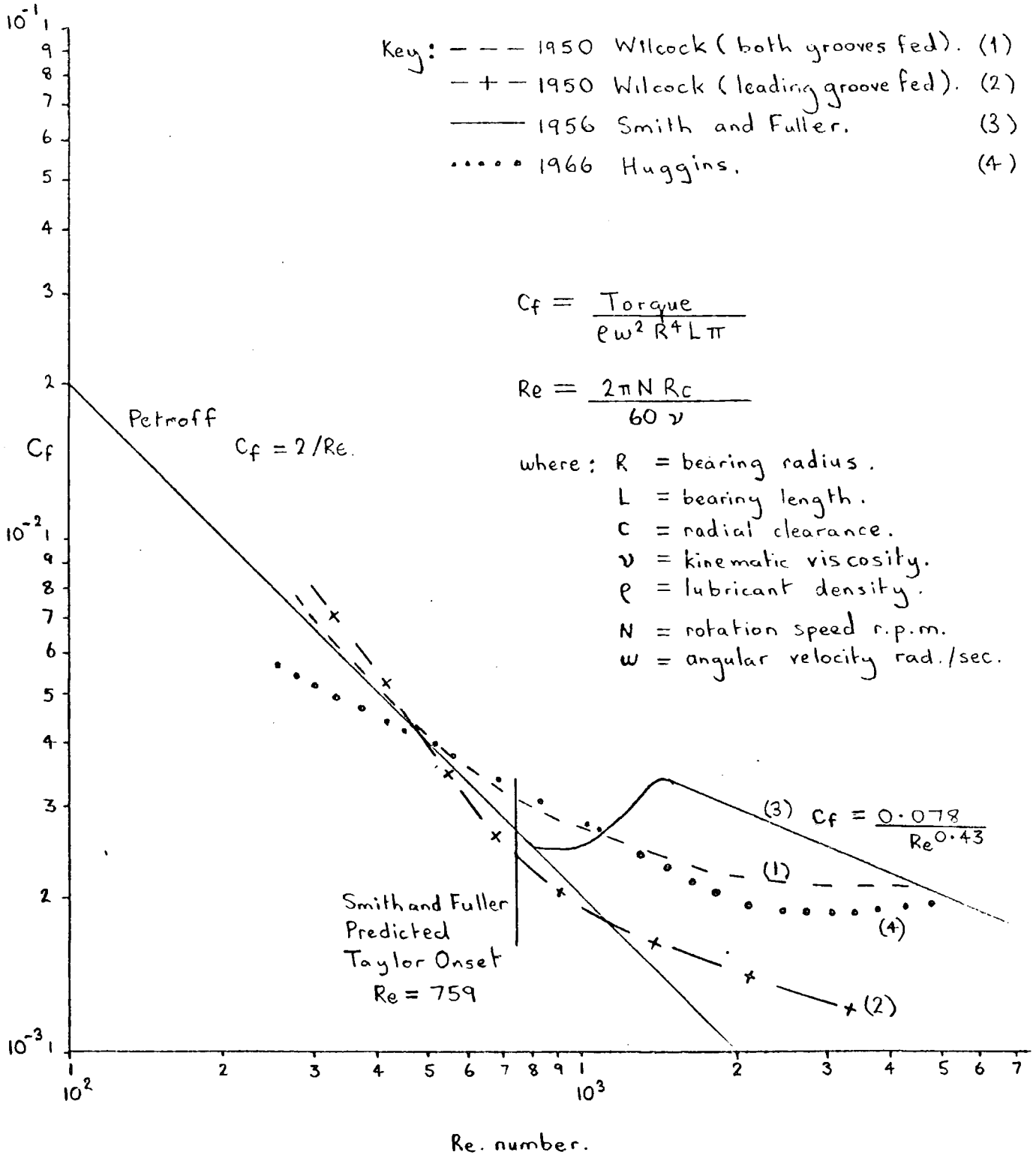

Fig.(1a) Plots of C_f versus Re from early experimental reports.

In the light of more recent work, Wilcock's explanation of his results may be incorrect. Wilcock's bearings were operated with large eccentricity ratios and it has been shown by Mobbs (5) and others, that a bearing run in this way can suppress the vortex formation in the lubricating film to such an extent that the onset of turbulence will be experienced first.

The next reported experimental work was by Smith and Fuller in 1956, (6). The apparatus used by Smith and Fuller consisted of a 0.076 m x 0.076 m bearing with a clearance ratio of $2.93\ 10^{-3}$. The lubricant, which was water and not oil as Wilcock had used, was fed into the bearing through a single 0.006 m hole. Again the bush was stationary and loaded by a hydrostatic ram. The shaft was supported by two rolling element bearings, one at either side and was driven by a pulley system. The frictional torque was measured by a torque arm fitted to the stationary bush. The apparatus used in the current experiments and which will be described in a later chapter was similar in dimensions to the bearing detailed above and also in the use of water as a lubricant although the method used to measure the frictional torque was totally different.

The results obtained by Smith and Fuller are plotted in Fig. (1a). The results follow the Petroff line very closely until almost exactly the predicted Reynolds number of 759 for the onset of Taylor vortices. The plot then indicates a well defined transition region followed by the onset of turbulence. The expression obtained for the frictional torque in the turbulent regime was,

$$Cf = 0.078\ Re^{-0.43}$$

Huggins (7) in 1966 investigated the frictional torque in a large turbogenerator bearing. The apparatus which Huggins used consisted of

a bearing 0.61 m in diameter. His work was connected with a practical situation, that of bearings used in large steam turbogenerators. The rig was designed around a fixed bearing because this arrangement is dynamically more realistic than the fixed shaft usually chosen for experimental equipment. At that time no method existed of taking direct friction measurements on the apparatus chosen. Consequently Huggins resorted to a heat balance calculation.

This method is obviously not as satisfactory as others and therefore leads to a certain amount of doubt about the results. The results obtained from these experiments are plotted in Fig. (1a). With reference to this plot, there is a deviation from the expected results in the low Reynolds number region and also the transition to turbulence at high Reynolds numbers appears to happen without the prior onset of vortices.

Recent investigations into the regimes of a lubricating film have concentrated on the change from a laminar to a turbulent film and the suppression of the early onset of the transition region between these regimes. The onset of the transition region has been found to be affected by the following:-

1. eccentricity, ε
2. axial flow, $\dot{m}$
3. clearance ratio, c/R
4. annulus length, L_a

Much of the experimental work concerned with the above effects has been carried out on rigs in which the rotating parts are separated by clearance ratios which are large in comparison to bearing clearance ratios commonly found in industry. It has been found that care must be exercised when the large clearance results are related to practical bearings. Onset of film changes in the above-mentioned experiments is usually detected

by the use of visual or torque measuring techniques.

It has been found that when a bearing is running eccentrically the film usually tends to be more stable and the laminar regime exists at higher Reynolds numbers than those predicted for the onset of Taylor vortices. Conversely it has also been found in some cases that the onset of secondary flow can be experienced at lower Reynolds numbers than expected.

A useful summary of eccentricity effect findings was presented in a paper by Mobbs (8) and this is illustrated in Fig. (1b). The plot is the ratio of Taylor numbers, (a non-dimensional group derived by G.I. Taylor and defined in Fig. (1b)), for the onset of vortices, in a liquid contained between, eccentric and concentric cylinders, versus cylinder radius ratio. It is apparent, from the plots, that there is a large degree of disparity over the effect of eccentricity. A possible explanation for the spread in the results was suggested in the same paper by Mobbs. He observed secondary flow between rotating cylinders at sub-critical Taylor numbers for both concentric and eccentric cylinders and explained that this could sometimes be responsible for the increased frictional torque observed and interpreted wrongly as the onset of Taylor vortices.

The table in Fig. (1b) shows that a wide range of radius ratios has been used in experimental work. In another paper Mobbs (9) reported an investigation into the effect of cylinder radius ratios on the critical Taylor number. He found that the critical Taylor number was virtually unaffected by radius ratio but that the breakdown of the Taylor vortices into a wavy mode, which is found to precede turbulence, did show a marked dependence when the ratio was less than 0.8 and much less of an effect when greater than 0.8. This then throws some light

$$\text{Taylor Number } (Ta) = \frac{R c^3 w^2}{\nu^2}$$

where R = shaft radius.
c = radial clearance.
w = angular velocity.
ν = kinematic viscosity.

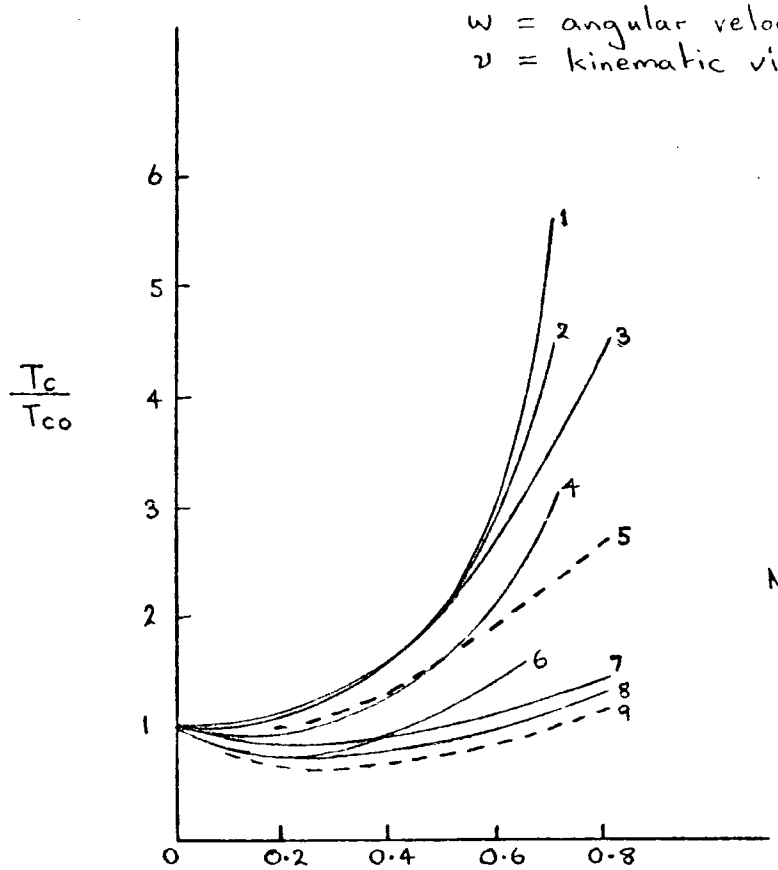

Note: 5 and 9 are theoretical plots.
5 is from the non-local theory.
9 is from the local theory.

	R_1/R_2		R_1/R_2
1. Cole.	0·9	6. Castle et al. Dye injection.	0·91
2. Vohr.	0·91	7. Younes.	0·95
3. Castle et al. Torque measurement.	0·9	8. Frêne and Godet.	0·995
4. Versteegen et al.	0·5	9. Di Prima.	
5. Di Prima and Stuart.			

R_1 = Radius of the inner cylinder. R_2 = Radius of the inner cylinder

Tco = *Critical Taylor Number at zero eccentricity.

Tc = Critical Taylor Number at non-zero eccentricity.

* Note: The 'Critical Taylor Number' is the Taylor Number at which vortices first appear.

Fig.(1b) Variation of Critical Taylor Number with eccentricity ratio [Mobbs(8)].

on the limitations of applying large clearance results to bearing situations.

Cole (10), (11) reported the effects of axial flow and annulus length on Taylor vortex critical speeds. At axial Reynolds numbers related to moderate axial flows it was found that axial flow had negligible effect on the onset of Taylor vortices. It was pointed out that at axial Reynolds numbers approaching 400 the effect of axial flow was becoming more significant, so it would seem that caution must be exercised with large clearance rigs when investigating the onset of Taylor vortices.

Annulus length was found by Cole to have virtually no effect on the onset of Taylor vortices. It did however affect to some degree the onset of a wavy mode to the vortices but only at L_a/c ratios less than 40.

Jackson (12) used a large clearance rig to investigate the onset of wavy modes superimposed on Taylor vortices. He found that three distinct wave modes occurred as the Reynolds number was increased and called these the Primary wave mode, the Transitional state and the Secondary wave mode. Visual and torque changes are found to occur at the transition from one mode to another. It was found also that if the Reynolds number is first increased distinct torque changes could be detected as the modes were encountered but if the Reynolds number is then decreased the torque changes are not apparent at the same Reynolds numbers. The torque changes are only detectable at zero eccentricity and for a small increase in eccentricity the distinct torque discontinuities as the wavy modes are traversed become undetectable.

Two approaches have been used to predict the onset of Taylor ring

vortices for eccentric operation. The first is a local instability theory based on considering the stability of the velocity profile at any section of the flow taken in isolation. The most unstable section is found to be at the widest gap position. The second approach is a non-local stability theory which considers the lubricating film on a macroscopic scale. In Fig. (1b) the local stability theory produces a curve close to the lower set of curves and the non-local theory produces a curve which lies close to the higher set of curves. It has been suggested that these two different approaches could provide an explanation for the spread in results obtained in experiments in that some workers have detected local instabilities and others more macroscopic instabilities.

If we consider the transition from Taylor vortices to fully established turbulence, visual reports indicate that as the Reynolds number is increased the vortices gain a wavy mode superimposed on them. At higher Reynolds numbers the film breaks down further until random eddies are formed. Very little appears to be known about the transition to full turbulence as few reports have been published on this subject. Onset of full turbulence has been predicted to occur at a Reynolds number = 2 Re_{onset} of Taylor vortices.

It would appear great care has to be exercised when the onsets of the wavy mode and turbulence are investigated using large clearance rigs. Clearance ratio and annulus length can have deceptive effects on the results obtained by this method if the onsets are to be related to small clearance bearing situations.

In most of the experimental investigations described, the onset of the various states in the lubricating film is detected either by visual or torque measuring techniques. The torque measuring technique is

generally regarded as the most reliable as the onset of the film change of state is usually marked with a distinct change in displayed frictional torque. With the onset of Taylor vortices difficulties can occur when experiments are being carried out with large eccentricity ratios as the torque change is less distinct. Visual techniques tend to be less accurate as a method of determining onsets. The difficulties are associated with illumination or seeing where in the bearing clearance the transition is starting.

It is apparent that the behaviour of the lubricating film is of a very complex nature and in fact still requires much further investigation.

CHAPTER 2

FRICTION IN AIR BEARINGS

The frictional torque in an unloaded aerodynamic journal bearing can be expressed by the equation,

$$T = \frac{2\pi R^3 L \mu \omega}{c} \quad \text{(for the concentric case)}$$

This is the Petroff frictional torque mentioned previously. If the bearing is running eccentrically the Petroff torque is modified in the following manner,

$$T = \frac{2\pi R^3 L \mu \omega}{c} \left(\frac{1}{1 - \varepsilon^2} \right)^{\frac{1}{2}}$$

For most cases the Petroff equation provides a good estimate of the frictional torque for $\varepsilon < 0.4$. In the experiments reported here a very lightly loaded externally pressurised air bearing was used operating with $\varepsilon \approx 0.1$ so that the correction was negligible.

For an externally pressurised journal bearing, the frictional torque gains a term related to the spinning of the lubricant as it passes through the bearing clearance. This effect was reported reference (13)* by the author and Professor H. Marsh.

It was found that the frictional torque was made up of two components. The first being the usual Petroff friction and the second a torque from providing the lubricant with angular momentum.

i.e. T_{total} = (shear torque) + (angular momentum torque)

$$= \frac{2\pi R^3 L \mu \omega}{c} + \text{(angular momentum torque)} \qquad (2:1)$$

The Angular Momentum Term

When the lubricant enters the bearing it has no net angular momentum, but on passing through the bearing clearance it acquires angular momentum.

* A reprint of this paper can be found in Appendix (1)

This change in angular momentum requires a torque which is supplied by the rotating shaft as explained in Ref. (13). This is, therefore, a restraining torque on the rotor.

For laminar flow the mass averaged tangential velocity of the lubricant exiting from the bearing clearance is $\omega R/_2$. A point to note is that for any asymmetric velocity profile the mass averaged tangential velocity is also $\omega R/2$. As the lubricant enters the bearing clearance with no net angular momentum, the change in angular momentum per unit mass is $\omega R^2/_2$. The lubricant acquires the tangential velocity quickly after leaving the feed holes, this is borne out by markings on the shaft caused by the air flow which show the flow pattern. As the tangential velocity is obtained soon after entry to the bearing clearance the change in angular momentum of the lubricant is caused by viscous forces in the neighbourhood of the supply holes. The provision of angular momentum for the lubricant is thus a frictional effect near the supply holes.

The torque required to change the angular momentum of the lubricant is given by,

$$T_2 = \dot{m}\,\omega R^2/_2$$

where $\dot{m}$ is the mass flow rate. This torque is the sum of the additional torques supplied by the rotor and bearing

$$T_2 = T_R + T_B$$

where, T_R = Torque on the rotor

T_B = Torque on the bearing

A hypothesis, which is borne out by experiments with air bearings having tilted jets, reference Marsh (14), is that the two torques are approximately in the same ratio as the relative tangential velocities between the incoming air and the two moving surfaces. With radial feed

holes the incoming air has no net tangential velocity. Hence,

$$\frac{T_B}{T_R} = \frac{0}{\omega R}$$

Therefore the change in angular momentum of the lubricant requires an additional torque supplied by the rotor which can be expressed by the equation,

$$T_2 = T_R = \dot{m}\omega R^2/_2$$

This torque is a frictional force because although it is connected with the change in angular momentum of the lubricant, it is caused by viscous forces in the neighbourhood of the supply holes.

The total frictional torque experienced by the rotor is obtained by substituting into equation (2:1)

$$T_{\text{total}} = \frac{2\pi R^3 L \mu \omega}{c} + \frac{\dot{m}\omega R^2}{2} \quad (2:2)$$

Experimental Support for Equation 2:2:

To check the validity of equation 2:2, that is the expression for the total frictional torque in an air journal bearing, experiments were carried out, these have been reported in reference (13).

The apparatus consisted of a bearing with the following dimensions:

R = 25.4 mm

L = 66.0 mm

c = 45.2 μm

Ip = 4.237 x 10^{-4} Kgm^2

The bearing was supplied with air at 20°C through two rows of 12 plain jets situated at 0.25 L from each end of the bearing.

The experiments consisted of accelerating the rotor up to the speed required in the stationary bearing and then permitting it to decelerate freely under the restriction of only the frictional torques in the bearing. Data of speed, ω, versus time, t, was obtained by using stop watches and a stroboscope. The mass flow rate through the bearing was varied by using different supply pressures. The variation of the mass flow rate with supply pressure was measured by the weighing method

described in reference (14). A cylinder of compressed air together with the whole apparatus was mounted on a balance and by using a nulling technique, the time to consume a known mass of air was determined.

The deceleration of the rotor is characterised by the time constant tc. The time constant for a given supply pressure was determined by setting a stroboscope to a fixed frequency, driving the rotor to a higher frequency and then measuring the time taken to decelerate from the fixed frequency to various fractions of this frequency, the stroboscope frequency remaining unchanged throughout the deceleration of the rotor.

The equation of motion for the decelerating shaft is,

$$Ip \frac{d\omega}{dt} = - T_{total}$$

where, Ip = The polar inertia of the rotor

or substituting for T_{total}

$$Ip \frac{d\omega}{dt} + \left(\frac{2\pi R^3 L\mu}{c} + \frac{\dot{m} R^2}{2}\right)\omega = 0$$

The solution of this equation is of the form

$$\omega = \omega_o e^{-t/tc}$$

where ω_o is the initial angular velocity and tc is the deceleration time constant. The reciprocal of the time constant for the deceleration is given by,

$$1/tc = 1/Ip \left(\frac{2\pi R^3 L\mu}{c} + \dot{m} R^2/2\right) \qquad (2:3).$$

The results of the deceleration experiments are sketched in Fig. (2a) which is a plot of $1/tc$ versus $\dot{m}$. It can be seen from Fig. (2a) that there is close agreement between predicted and experimental results.

If Petroff's prediction is correct then the plot in Fig. (2a) would be a straight line parallel to the mass flow rate axis. However the

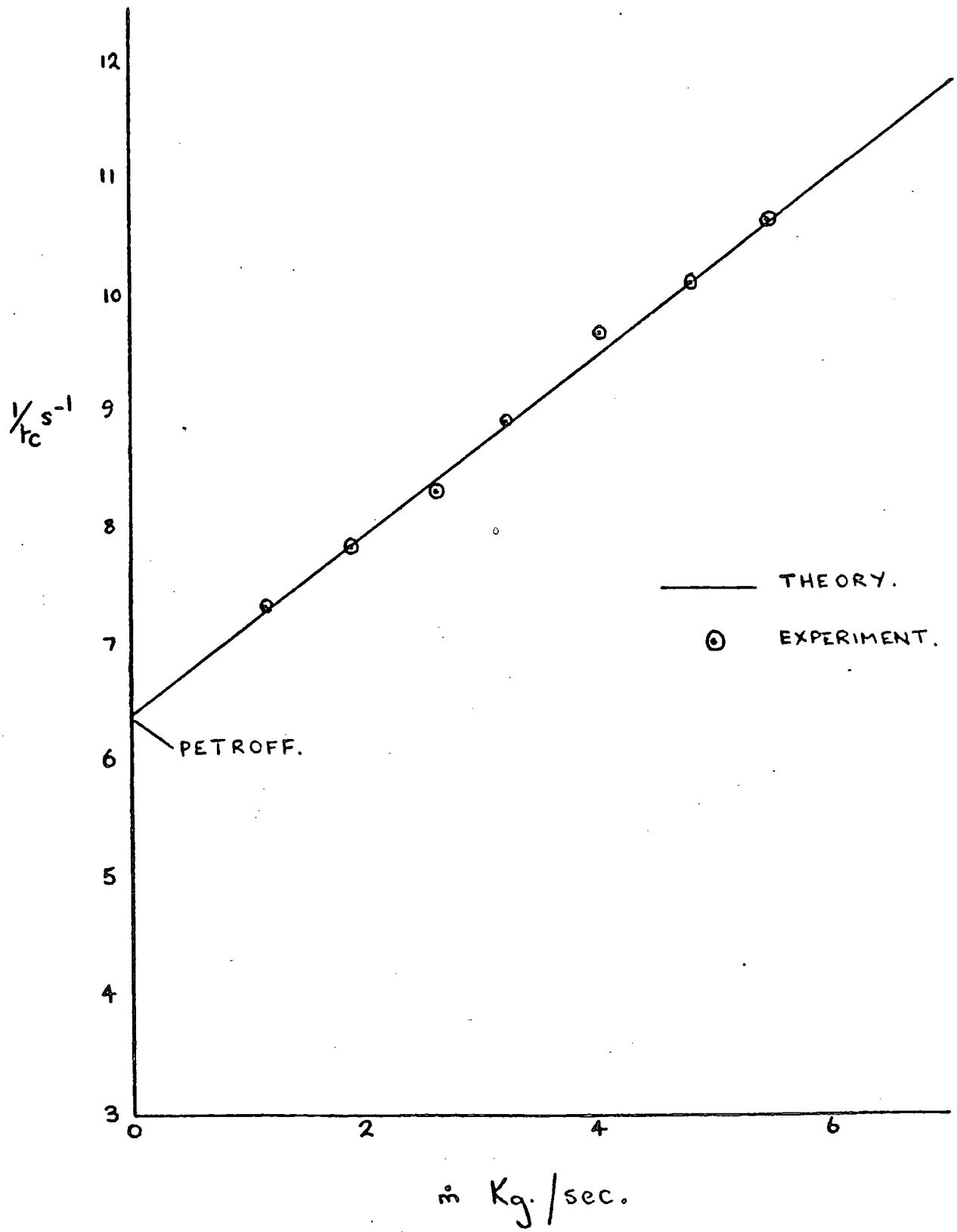

Fig. (2a). Variation of $1/t_c$ with mass flow rate.

experimental plot shows a dependence on the mass flow rate of the lubricant and hence the angular momentum.

These experiments have shown that the angular momentum torque can be greater than the torque predicted by the Petroff formula.

Design Considerations for Minimum Friction

As stated previously the total frictional torque in an externally pressurised bearing is given by

$$T_{total} = \frac{2\pi R^3 L\mu\omega}{c} + \frac{\dot{m}\omega R^2}{2} \qquad (2:2)$$

For a bearing with a given supply pressure, gauge pressure ratio, radius and length, the mass flow rate of the lubricant is proportional to the cube of the clearance. Equation 2:2 can then be written in the form

$$T_{total} = A/c + Bc^3$$

where A and B are constants. The minimum total frictional torque is obtained when the clearance is given by,

$$\frac{dT}{dc} = 0 = -A/c^2 + 3Bc^2$$

or

$$c^4 = A/3B$$

For this value the total torque is given by

$$T_{total} = A/c \left(1 + \frac{Bc^4}{A}\right)$$

$$= 4/3 \; A/c$$

which may be compared to the Petroff equation

$$T_1 = A/c$$

From this analysis it can be seen that if a bearing is to be designed for minimum friction then a clearance should be chosen such that 25% of the total torque is required for changing the angular momentum of the lubricant.

The Turbo-Bearing

If the supply jets in an externally pressurised bearing are not radial, but are tilted the incoming air will enter the bearing with high angular momentum. Instead of requiring angular momentum from the shaft causing a frictional torque, the incoming air will actually drive the shaft. This effect was investigated fully by the author and Professor H. Marsh * (15).

Considering the Turbo-Bearing, gas enters the bearing clearance with high angular momentum and leaves the two ends of the bearing with low angular momentum. This change in angular momentum requires a torque applied to the lubricant, this being provided by the rotor and bearing. There is, therefore, a driving torque on the rotor and the rotor accelerates until the driving torque is equal to the frictional torque predicted from the Petroff analysis. The angular momentum torque in this instance is not a frictional torque, but a driving torque.

* A reprint of this paper can be found in Appendix (2)

CHAPTER 3

LIQUID BEARINGS

The performance of a hydrodynamic journal bearing can be predicted by solving Reynolds equation for the pressure distribution. The method of solution is to first simplify the equation and then apply a set of boundary conditions. In this way the form of the pressure distribution in the bearing can be obtained and hence the load carrying capacity.

Sommerfeld considered a bearing of infinite length with no axial flow. Reynolds equation in this case corresponds to,

$$\frac{dp}{d\theta} = \frac{6\mu UR}{c^2}\left(\frac{1}{(1+\varepsilon\cos\theta)^2} + \frac{h^*}{c(1+\varepsilon\cos\theta)^3}\right)$$

where, U = tangential surface speed of the bearing

θ = angular displacement from the line of centres

p = pressure

h^* = film thickness at point of maximum pressure

The boundary conditions used were that the pressure is equal to zero at both $\theta = \pi$ and 2π. Sommerfeld used the above assumption and boundary conditions with the aid of a substitution known as the Sommerfeld substitution to solve the Reynolds equation and thus obtain an expression for the pressure distribution.

The radial velocity gradient in a journal bearing can be expressed by,

$$\frac{du}{dz} = \frac{U}{h} - \frac{1}{2\mu}(h - 2z)\frac{dp}{dx} \qquad (3:1)$$

where, $\frac{du}{dz}$ = radial velocity gradient of the lubricant

h = film thickness

z = coordinate across the film

x = tangential coordinate

The first term arises from the shearing of the lubricant and the second from a pressure induced flow caused by the variation in pressure around the bearing.

To evaluate the frictional forces in a journal bearing, the definition of Newtonian viscosity is used,

$$\text{i.e. } \tau = \mu \frac{du}{dz} \qquad (3:2)$$

where, τ = shear stress

At the shaft surface z = 0, therefore, using equation (3:1),

$$\frac{du}{dz} = \frac{U}{h} - \frac{h}{2\mu} \frac{dp}{dx} \qquad (3:3)$$

At the bearing surface z = h, again using (3:1),

$$\frac{du}{dz} = \frac{U}{h} + \frac{h}{2\mu} \frac{dp}{dx} \qquad (3:4)$$

Combining equations (3:3) and (3:4) and substituting into equation (3:2) gives,

$$\tau_{h,0} = \mu \frac{du}{dz} = \pm \frac{h}{2} \frac{dp}{dx} + \frac{\mu U}{h} \qquad (3:5)$$

The total frictional forces on the bearing and shaft are given by,

$$F = \int_0^L \int_0^{2\pi R} \tau \; dx \; dy \qquad (3:6)$$

Substituting the expression for the shear stress from equation (3:5) into (3:6) and integrating using the Sommerfeld integration substitution mentioned previously gives,

$$F_{h,0} = \pm \frac{c \varepsilon W \sin \psi}{2R} + \frac{2\pi \mu U R L}{c (1 - \varepsilon^2)^{1/2}} \cdot \qquad (3:7)$$

where, W = bearing load

ψ = attitude angle

which is the total frictional force on the bearing and shaft. The positive sign is for the shaft and the negative for the bearing.

It can be seen from equation (3:7) that the frictional forces on the shaft and bearing differ by the amount $c \varepsilon W \sin \psi / R$. Equilibrium of the oil film is maintained by a couple which arises because of the displacement of the centres of the shaft and bearing with respect to each other. The integrated oil forces on the shaft and bearing act through their respective centres, which are, in the direction normal to the load, a distance $c \varepsilon \sin \psi$ apart. The couple set up because of the displacement is of magnitude $W c \varepsilon \sin \psi$, which corresponds to a frictional force of $(W c \varepsilon \sin \psi)/R$ at the surface of the journal. Considering the moments for the film,

$$R F_0 = R F_h + W c \varepsilon \sin \psi \qquad (3:8)$$

From equation (3:8) it can be seen by substituting values for F_0 and F_h from equation (3:7) that equilibrium of the film is maintained.

For a short bearing that is where $L/D \leqslant 1$ the infinite bearing solution is not very satisfactory. When solving the Reynolds equation for an infinite bearing, axial flow is neglected and only circumferential flow is considered. This is unacceptable with a short bearing in which lubricant is continually being supplied and from which lubricant flows at each end. A method of solving the Reynolds equation for a short bearing was formulated by Ocvirk and DuBois. The Reynolds equation is first simplified by assuming that the pressure gradients around the circumference are very small compared with those along the length. The simplified equation is,

$$\frac{\partial}{\partial y}\left(h^3 \frac{\partial p}{\partial y}\right) = \frac{6 \mu U}{R} \frac{\partial h}{\partial \theta}$$

By integrating twice and applying the boundary condition that $p = 0$ at $y = \pm \frac{L}{2}$, where y is measured from the centreline of the bearing, an expression can be obtained for the pressure distribution and hence the load carrying capacity.

From the Ocvirk considerations, the frictional forces on the shaft and bearing are,

$$F_{h,O} = \frac{2 \pi R^2 L \mu \omega}{c (1 - \varepsilon^2)^{\frac{1}{2}}}$$

so that these forces are equal in magnitude, unlike those obtained from the infinite bearing theory. This is because the pressure induced shear flow is considered to be negligible.

It is found that the Ocvirk solution is generally more acceptable to 'real' bearings than the infinite bearing solution. The Ocvirk solution gives good predictions of load carrying capacity when compared with experimental results for moderate eccentricity ratios, i.e.

$(\varepsilon \leqslant 0.6)$

For an infinite bearing the total frictional force on the shaft is from equation (3:7)

$$F_O = \frac{c \varepsilon W \sin \psi}{2R} + \frac{2 \pi \mu U R L}{c (1 - \varepsilon^2)^{\frac{1}{2}}}$$

The magnitude of the first term, the pressure flow term, for a lightly loaded bearing is very small compared to the second term, the shearing term. For the bearings used in the experimental work reported in this thesis the maximum value of the first term is approximately 3% of the total frictional force. As discussed, for a bearing of finite length, because of large axial pressure gradients the pressure induced circumferential flow is negligible. Therefore the value for a finite bearing is likely to be less than the 3% for an infinite bearing.

Friction in Liquid Bearings:

From the Ocvirk considerations, the frictional torque in a journal bearing operating in the laminar regime is, for both bearing and shaft,

$$T = \frac{2 \pi R^3 L \mu \omega}{c (1 - \varepsilon^2)^{\frac{1}{2}}}$$

From this equation it can be seen that no account has been taken of the extra frictional torque experienced by the journal bearing in connection with the spinning of the lubricant.

In the previous chapter mention was made of the extra frictional torque experienced by an air bearing caused by giving the lubricant flow angular momentum. The magnitude of this torque is $\frac{\dot{m} R^2 \omega}{2}$.

The nature of this extra torque has not been reported before for liquid bearings.

For a liquid bearing the situation is a little more complex than for an air bearing, because of the nature of the lubricant. With an air bearing the air on reaching the ends of the bearing, escapes freely into the atmosphere whereas with a liquid bearing the liquid has to be dribbled over the bearing end face or thrown off the shaft. Under normal operating speeds the liquid is thrown off the shaft with the surface velocity of the shaft. With an air bearing the lubricant at exit has an average circumferential velocity of $\omega R/2$, but with a liquid bearing, all of the liquid on leaving the bearing and being thrown by the shaft gains the shaft velocity, ωR. The extra frictional torque is then $\dot{m} \omega R^2$, that is twice the magnitude of the torque found with an air bearing.

The situation with a liquid bearing can be further complicated by variation of shaft diameter near the exit from the bearing. If the diameter is greater at this point than in the bearing the liquid can be thrown from the larger diameter, thus making the extra torque greater in magnitude. The extra frictional torque then being, $\dot{m} \omega R^2$ (thrown).

From the Ocvirk theory it can be shown that the mass flow rate from

the ends of the bearing is given by,

$$\dot{m} = \rho R L c \varepsilon \omega$$

The total frictional torque experienced by the shaft assuming that the lubricant is thrown from the shaft radius and that the bearing is running full is,

$$T_{total} = \frac{2 \pi R^3 L \mu \omega}{c (1 - \varepsilon^2)^{1/2}} + \rho L c \varepsilon R^3 \omega^2$$

The frictional torque experienced by the bearing depends on whether or not the lubricant when thrown off the shaft is caught by 'catchers' attached to the bearing. If they are not attached to the bearing the frictional torque on the bearing is only the first term of the above equation. If attached then the second term is added.

For clarity, the modification of the shear torque because of eccentric running will be neglected in the following consideration. In fact for small eccentricities the Petroff frictional torque, $\frac{2 \pi R^3 L \mu \omega}{c}$ is a good approximation. For the purpose of comparison the total frictional torque can conveniently be expressed in a non-dimensional form.

For small eccentricities,

$$T_{total} = \frac{2 \pi R^3 L \mu \omega}{c} + \rho L c \varepsilon R^3 \omega^2$$

transforming,

$$\frac{T_{total}}{\pi R^3 L \omega \rho} = \frac{2 \mu}{c \rho} + \frac{c \varepsilon \omega}{\pi}$$

dividing through by ωR,

$$\frac{T_{total}}{\pi R^4 L \omega^2 \rho} = \frac{2 \mu}{c \rho \omega R} + \frac{c \varepsilon}{R \pi}$$

substituting the rotational Reynolds number Re which equals $\frac{R \omega \rho c}{\mu}$

$$\frac{T_{total}}{\pi R^4 L \omega^2 \rho} = \frac{2}{Re} + \frac{c \varepsilon}{R \pi} = Cf$$

The left hand side of the expression is a non-dimensional frictional torque which is equated to Cf. If the correction for the throwing of the lubricant is neglected the value of Cf reduces to 2/Re.

The magnitude of the second term, that from the throwing of the lubricant, can be assessed from Fig. 3(a). This graph was plotted by considering a bearing with a clearance ratio of 0.003 running with various eccentricities. Using equation (3:9) plots of the non-dimensional frictional torque versus the Reynolds number can be obtained for a given eccentricity and these are sketched in Fig. 3(a). Fig. 3(a) indicates that the angular momentum effect is pronounced at high Reynolds numbers and becomes less significant at low Reynolds numbers. Typically at a Reynolds number of 2000 with an eccentricity of 0.3, 23% of the total frictional torque can be attributed to the throwing of the lubricant.

The magnitude and nature of the angular momentum torque can lead to errors in the torque measuring technique for detecting the onset of Taylor vortices in a bearing. The onset of vortices is indicated by the departure of the measured frictional torque from that predicted by Petroff, indicated by the plot of Cf = 2/Re in Fig. 3(a). The departure of the frictional torque from that predicted for laminar flow, which is in fact attributable to an extra torque from the throwing of the lubricant, can be wrongly interpreted as the onset of vortices. Corrections for this angular momentum torque should therefore be made before the true onset can be determined.

As discussed in Chapter 1 a bearing running with a large Reynolds number (> 2000) will usually have a turbulent lubricating film. The frictional torque for a turbulent film is greater than that for a laminar film, so the angular momentum torque will be less significant in this case. A point to note is that irrespective of the turbulent

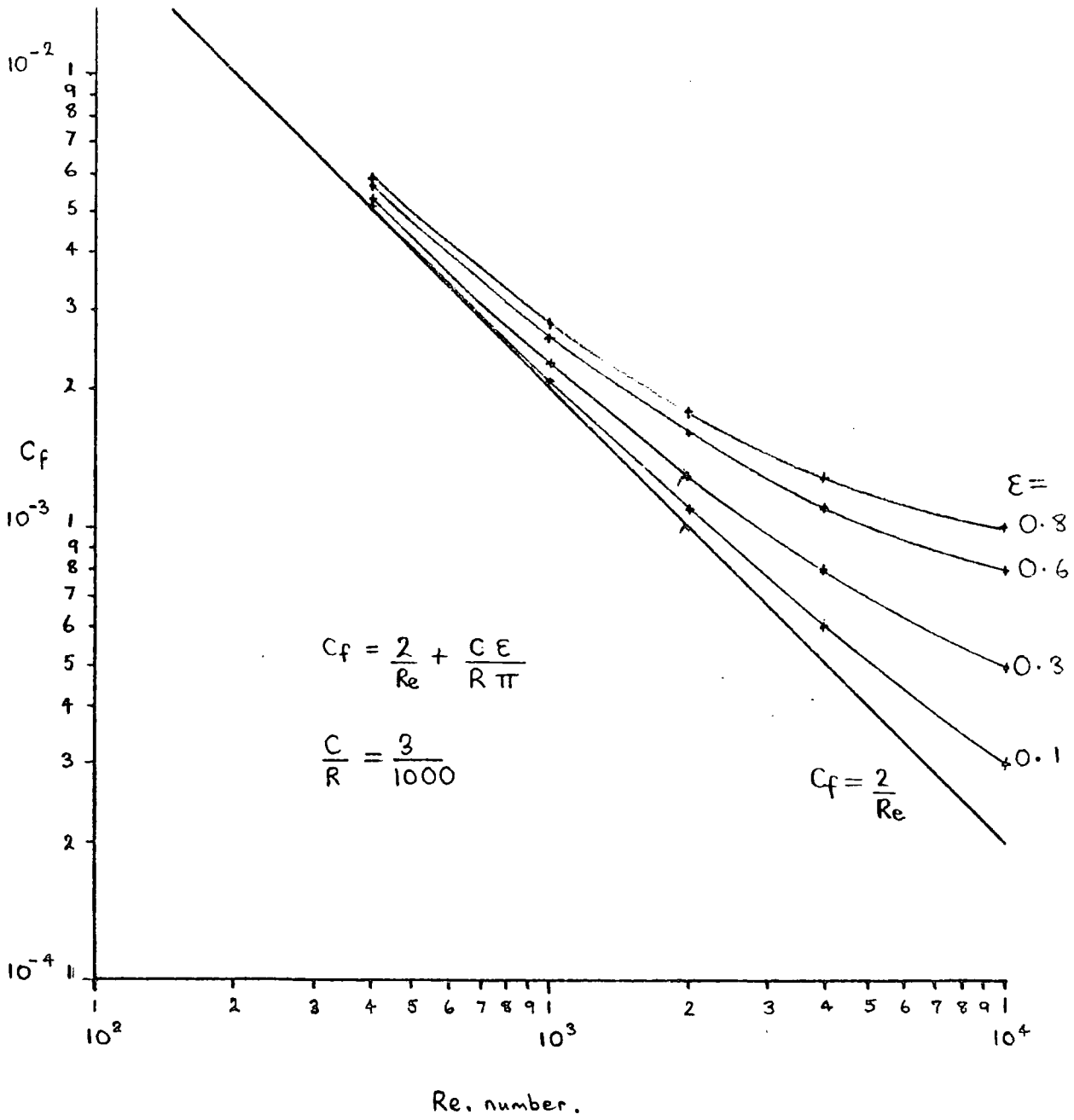

Fig.(3a) Plot of C_f versus Re.

velocities present in a bearing, the lubricant is still thrown from the shaft with the shaft velocity.

The suppression of turbulence and the running of a laminar film bearing at high Reynolds numbers with the corresponding reduction in frictional torque has been attained by using additives in the lubricant.

This effect was investigated at Durham by Hampson (16) who used high molecular weight polymer additives in a water lubricated bearing. Hampson did in fact correct his measured frictional torque for the momentum torque, the importance of which had already been identified in the work on air bearings.

Solutions of Reynolds equation predict a region of negative pressure in a journal bearing and as a liquid cannot maintain negative pressures, the lubricating film cavitates. It has been assumed so far that a bearing runs with a full film and that cavitation is not present. If a lubricating film cavitates, the area over which the lubricant is sheared is reduced with a corresponding reduction in frictional torque. Without the use of special bearings the extent of cavitation in a bearing cannot be easily investigated.

Cavitation can be suppressed by using a pressurised supply of lubricant thus producing a bearing running with a complete film. Pressurised supplies are commonly used in bearings so that spent lubricant can be replaced and also to keep the lubricant from overheating.

In the experiments described in this thesis a pressurised supply was used to simplify the experiments by suppressing cavitation. Another advantage of a pressurised supply in these experiments is

that the flow rate can be varied at will by varying the supply pressure thus permitting useful information to be obtained in connection with the angular momentum torque.

CHAPTER 4

DESIGN OF THE 2" DIAMETER BEARING RIG

The experiments were spread over two bearing rigs, the first rig being a prototype to test ideas and to provide low Reynolds number frictional torque results and a second rig to provide results of the frictional torque of a bearing operating in both laminar and turbulent regimes.

Details of the Prototype Design

Three main problems existed with the design of the prototype rig,

i) To have sufficient polar inertia in the decelerating shaft so that it would slow down at a reasonable rate to permit measurements to be obtained.

ii) To have an easily detachable drive system so that the shaft could be accelerated up to the required speeds and then allowed to decelerate freely.

iii) To have a system with a single bearing which could operate at reasonably high speeds without becoming unstable in a conical mode.

All three of these problems were overcome by using discs attached to the decelerating shaft.

The layout of the prototype rig can be seen in Fig. (4a) and photograph Fig. (4b).

With respect to problem (i), the difficulty of obtaining a sufficiently large deceleration time constant to permit experimental results to be taken was overcome by the following means. Firstly, by the use of discs as mentioned above, which provide the polar inertia so that the shaft decelerates slowly. Secondly, by the choice of a low viscosity lubricant. Water was chosen as the lubricant because of its

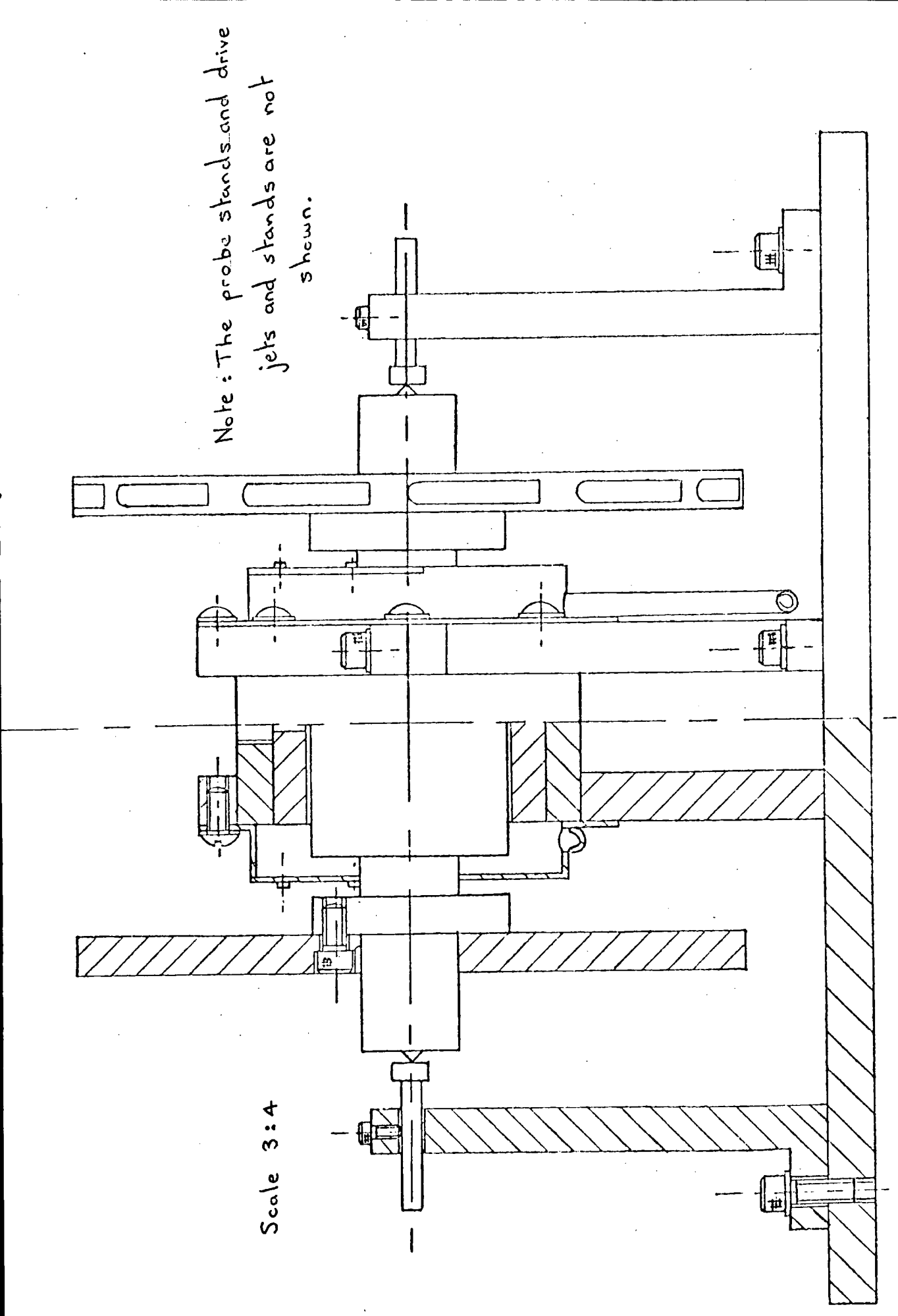

Fig. (4a) Sketch of the 2" Diameter Bearing Rig.

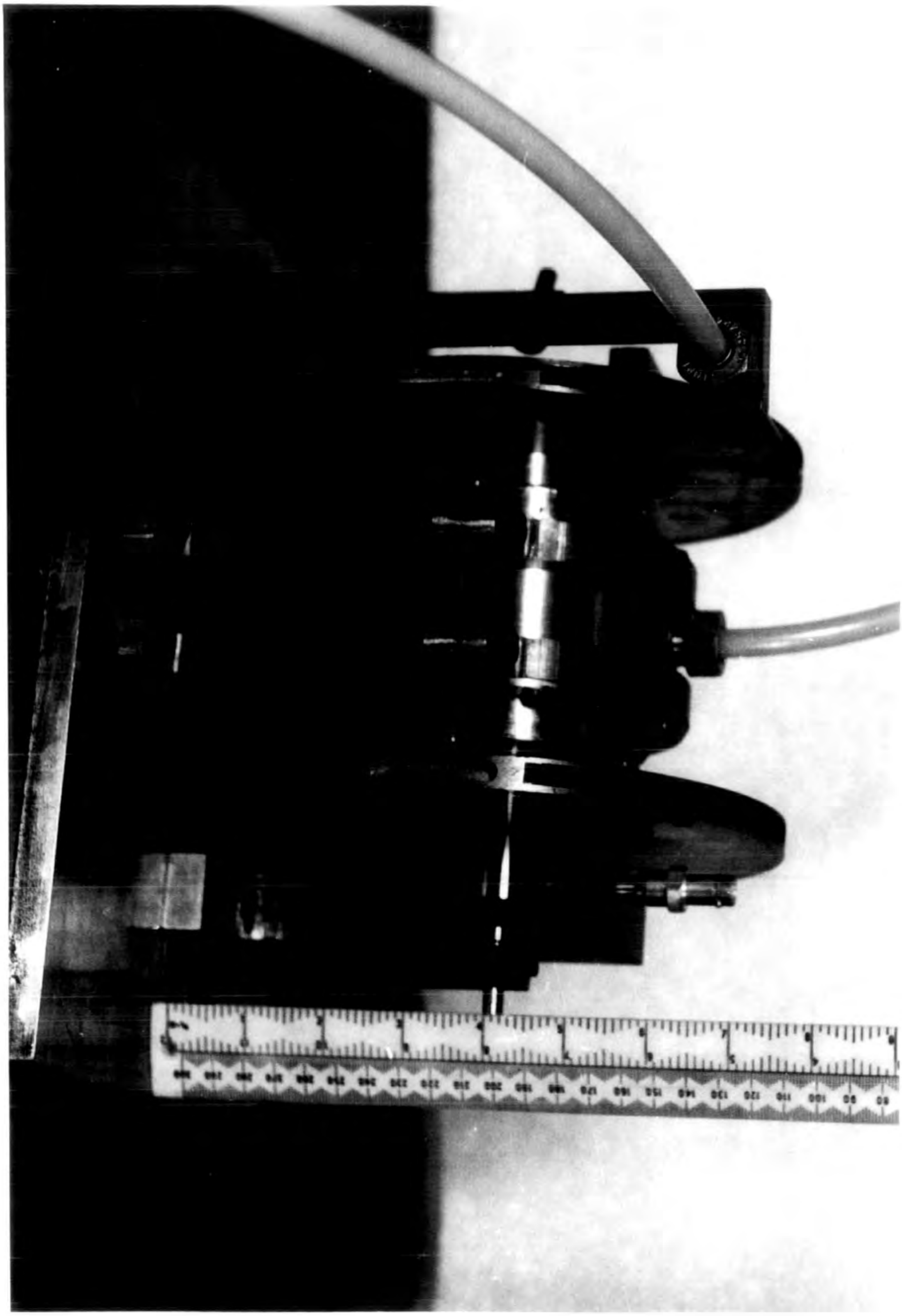

availability, its ease of handling and its relatively low viscosity. The choice of water as a lubricant has other advantages over the use of oils etc. Water has a higher specific heat capacity than oils and also a lower variation of viscosity with temperature. These two facts combined with the low viscosity of water mean that the temperature rise in the bearing is kept to a minimum. Therefore the accuracy with which the viscosity of the lubricant is known is of a high order. The choice of water as a lubricant made it necessary for the bearing and shaft members to be made from materials which did not rust. The shaft was made from stainless steel and the bearing from phosphor-bronze.

The second difficulty, that of an easily detachable drive, was overcome by the use of discs large enough to enable an air turbine system to be used for the drive mechanism. All that was needed to be done to disconnect the drive from the shaft, was to switch off the air supply to the turbine. Because the air turbine operated on a disc of large radius it was possible to obtain a large drive torque to accelerate the shaft without excessive consumption of compressed air.

The third difficulty, that of operation of the bearing at high speed, was overcome in the following manner. Single bearing systems are particularly susceptible to self-excited conical instabilities. These tend to occur at low speeds, hence severely restricting the top speed at which a shaft can be driven. Whirl onset speed depends on bearing design, rotor loading and inertia. Bearings are also susceptible to a second instability of the translational kind, the onset speed of which is usually higher than the conical whirl speed. Both instability modes tend to occur at a frequency close to half the rotational speed. The onset of conical whirl can be estimated by the equation,

$$N_{\substack{\text{onset} \\ \text{conical}}} = \frac{60}{\pi} \frac{(2\, k_c\, l_2^{\,2})}{((I_T - 2Ip))}^{\frac{1}{2}}$$

The onset of translational whirl can be estimated by the equation,

$$N_{\substack{\text{onset} \\ \text{translational}}} = \frac{60}{\pi} \frac{(k_L)^{\frac{1}{2}}}{(\overline{M})}$$

where, N_{onset} = speed of onset of instability

k_L = bearing linear stiffness

k_C = bearing conical stiffness

M = mass of the rotor

l_2 = length of the bearing L/2

Ip = polar inertia of the rotor

I_T = transverse inertia of the rotor

In the prediction for onset of conical whirl, the $2\ Ip$ term in the denominator is a correction for the gyroscopic effect when the shaft is performing conical vibrations whilst rotating. From the prediction, if I_T approaches $2\ Ip$ then the conical whirl speed can be raised above that of the onset for translational whirl. This being the case the shaft system is gyroscopically stable and cannot perform conical vibrations at one half of the rotational speed. The use of discs also overcame this problem by designing them such that $I_T < 2\ Ip$.

The design of the bearing rig is therefore a series of compromises, i.e. having discs large enough to provide the necessary inertia and bucket radius for the turbine drive and positioned such that $I_T < 2\ Ip$.

Further Design Considerations

The supply of water to the bearing was at a pressure which could be varied in order to suppress cavitation. The bearing would then run full and allowances would not have to be made for the extent of the cavitation region.

The bearing was designed so that the bush could be turned thus permitting the use of various lubrication feed directions relative to the direction of loading.

The drainage of water from the bearing was made easier by discarding the use of thrust bearings and instead using carbon points on the ends of the shaft. The carbon points ran against brass pads to provide axial location. The shaft extended out of each end of the bearing so that water exhausting from the bearing could escape easily, be collected in catchers and drained under gravity away from the system as illustrated in Fig. (4a). The discarding of thrust bearings also meant that the measured frictional torque of the bearing was purely journal frictional torque.

Three clearance ratios were used in the prototype bearing to permit the control of operational eccentricities and to permit a wide variation of rotational Reynolds numbers and mass flow rates.

Bearing Parameters

R = 25.4 mm

L = 50.8 mm

radial clearances 1. $2.62\ 10^{-5}$ m

2. $5.92\ 10^{-5}$ m

3. $7.90\ 10^{-5}$ m

Disc Diameter = 176 mm

$I_p = 1.38\ 10^{-2}$ Kg m^2

		1	2	3
Surface Finish of Shaft	=	0.25 micron C.L.A.	0.25 micron C.L.A.	0.25 micron C.L.A.
Surface Finish of Bush	=	0.35 micron C.L.A.		

CHAPTER 5

INSTRUMENTATION

In Chapter 2 mention was made of the deceleration experiments carried out with air bearings. The equation of motion for the decelerating shaft can be expressed as,

$$Ip \frac{d\omega}{dt} = - T_{total}$$

from equation (2:2),

$$Ip \frac{d\omega}{dt} = - \frac{2 \pi R^3 L \mu \omega}{c} - \frac{\dot{m} \omega R^2}{2}$$

The solution of this equation is of the simple form,

$$\omega = \omega_o e^{- t/tc}$$

The timing of the decelerations in this case was easily measured using stop watches.

If the equation of motion of the shaft in the self-acting liquid bearing is now considered,

$$\text{again,} \quad Ip \frac{d\omega}{dt} = - T_{total} \qquad (5:1)$$

With the present experimental investigation, the total torque experienced by the shaft is made up of the frictional torque from the bearing and an extra torque from the windage losses from the discs attached to the shaft. When the shaft is decelerating in the laminar regime,

$$T_{total} = \frac{2 \pi R^3 L \mu \omega}{c} \left(\frac{1}{(1 - \varepsilon^2)^{1/2}} \right) + \text{mass flow torque} + \text{disc drag torque}$$

When the shaft is decelerating in the non-laminar regime,

$$T_{total} = T_{\text{rotor non-laminar}} + \text{mass flow torque} + \text{disc drag torque}$$

If the respective T_{totals} are substituted into equation (5:1), it can be seen that the solutions of these equations are not of a simple form but of a complex nature. This then makes it necessary to obtain point deceleration rates at known speeds. To obtain the point deceleration rates accurately electronic timing equipment was used.

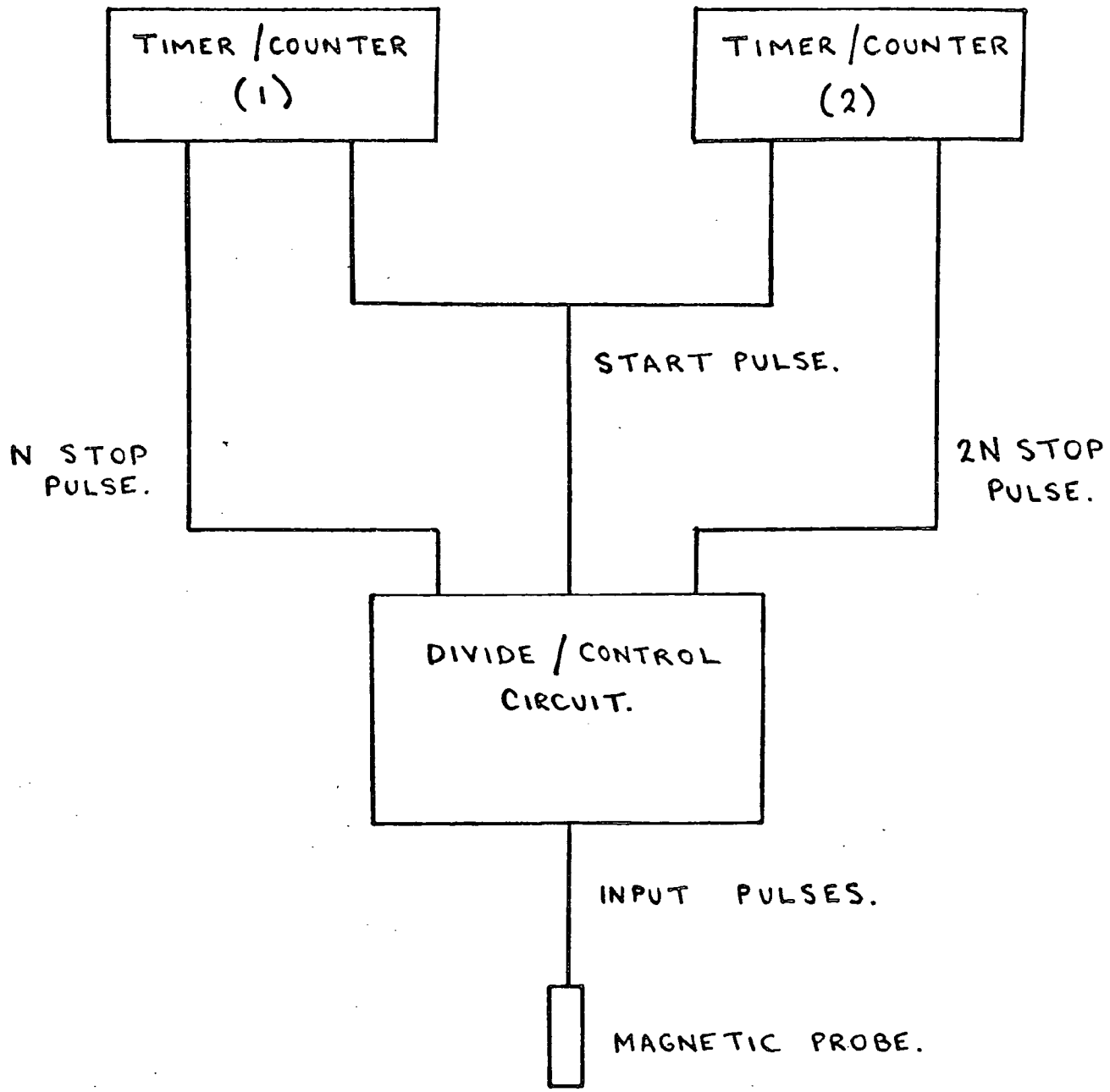

Fig.(5a) Schematic sketch of the deceleration timing circuit.

The Timing Equipment In Brief

The idea of the electronic deceleration circuit was to measure the change in frequency of electric pulses being emitted from a magnetic transducer, positioned close to the machined buckets on the discs. The deceleration can be used to determine the torque on the rotor. Hence the frictional torque which appears in the bearing can be identified.

With reference to the sketch, Fig. (5a), pulses from the magnetic probe are passed into the Control/Divide Unit. When the start button is pressed the Timer/Counters are started simultaneously by a pulse. The Control/Divide Unit divides the following incoming pulses in the ratio of 2:1. Timer/Counter 1 is stopped after N pulses and Timer/Counter 2 is stopped after 2N pulses.

Interpretation of the Measurements

From the description of the circuit operation, the time recorded for 2N pulses is greater than twice the time recorded for N pulses, because the shaft is decelerating.

Consider the Sketch

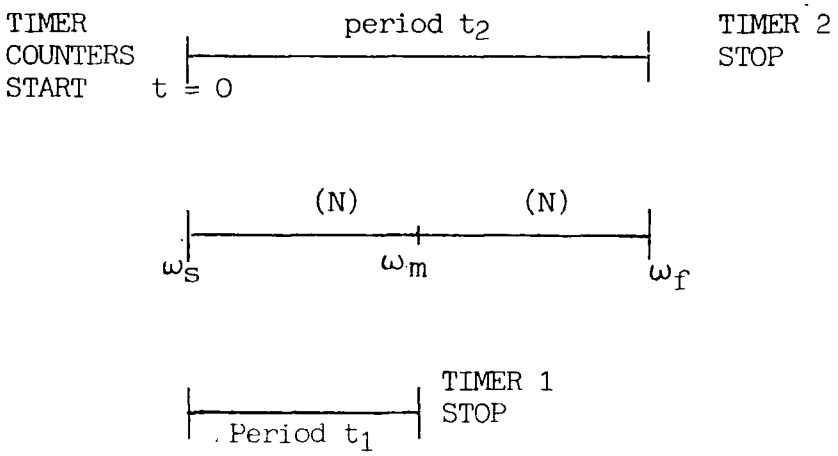

where, α = deceleration rate (assumed constant for small change in ω)

ω_s = initial angular velocity

ω_f = final angular velocity

ω_m = angular velocity after time t_1

N = number of pulses

θ = angle of rotation for N pulses

$\delta = t_2 - 2t_1$

$$\theta = \omega_s t_1 - \tfrac{1}{2}\alpha t_1^2 \qquad (5:2)$$

$$2\theta = \omega_s t_2 - \tfrac{1}{2}\alpha t_2^2$$

equating, $\omega_s t_2 - \tfrac{1}{2}\alpha t_2^2 = 2\omega_s t_1 - \alpha t_1^2$

but, $\omega_m = \omega_s - \alpha t_1 \qquad (5:3)$

substituting, $(\omega_m + \alpha t_1)t_2 - \tfrac{1}{2}\alpha t_2^2 = 2(\omega_m + \alpha t_1)t_1 - \alpha t_1^2$

simplifying, $\omega_m t_2 - 2\omega_m t_1 = \alpha t_1^2 + \tfrac{1}{2}\alpha t_2^2 - \alpha t_1 t_2$

substituting, $\delta = t_2 - 2t_1$,

$$\alpha = \frac{\omega_m \delta}{(t_1^2 + \delta t_1 + \tfrac{1}{2}\delta^2)} \qquad (5:4)$$

and as δ is small compared to t_1

$$\alpha \approx \frac{\delta \omega_m}{t_1^2}$$

From equations, (5:2), (5:3), (5:4)

$$\theta = (\omega_m + \alpha t_1)t_1 - \tfrac{1}{2}\alpha t_1^2$$

$$= \omega_m t_1 + \frac{\alpha t_1^2}{2}$$

transforming and substituting for α ,

$$\omega_m = \frac{\theta}{t_1 + \tfrac{1}{2}\left(\dfrac{\delta t_1^2}{(t_1^2 + \delta t_1 + \delta^2/2)}\right)}$$

again for small δ $\omega_m \approx \dfrac{\theta}{t_1 + \tfrac{1}{2}\delta}$

The average ω over the period $t_2 = \frac{2\theta}{t_2} = \frac{\theta}{t_1 + \frac{1}{2}\delta} \approx \omega_m$

Summarising, $\alpha = \frac{\omega_m \delta}{t_1^2}$

$$\omega_m = \frac{2\theta}{t_2}$$

Although these expressions are only approximations they greatly aid the arithmetic. The maximum error introduced by using these approximations has been calculated to be at worst less than 0.2%

By determining t_1 and t_2 the point speeds and deceleration rates can be found for a given deceleration of a shaft in a bearing. From the equation,

$$Ip \frac{d\omega}{dt} = \text{(Frictional Torque)} + \text{(Angular Momentum Torque)} + \text{(Disc Torque)}$$

if $\frac{d\omega}{dt}$ is determined and the mass flow rate and Disc Torques are known, then the frictional torque in the bearing can be calculated for a given speed of rotation.

Circuit Operation in Detail, Reference Fig. (5b)

In the initial state, that is without the time start switch operated, pulses from the magnetic probe are fed into the Schmitt Trigger (2) and are shaped into logic square wave pulses. The trigger also acts as a filter in that by having a signal pass level, the noise from the probe is filtered out and not shaped as random pulses.

The pulses are passed onto components (1) and (3) and do not proceed further in the circuit until the start switch is in an operated state. The start circuit consists of two components, that is a Nand gate (1) and a J-K flip flop (3). When the start switch is operated the first pulse received by component (1) is not permitted to enter the division part of the circuit, but the second and subsequent pulses are. The reason for this is

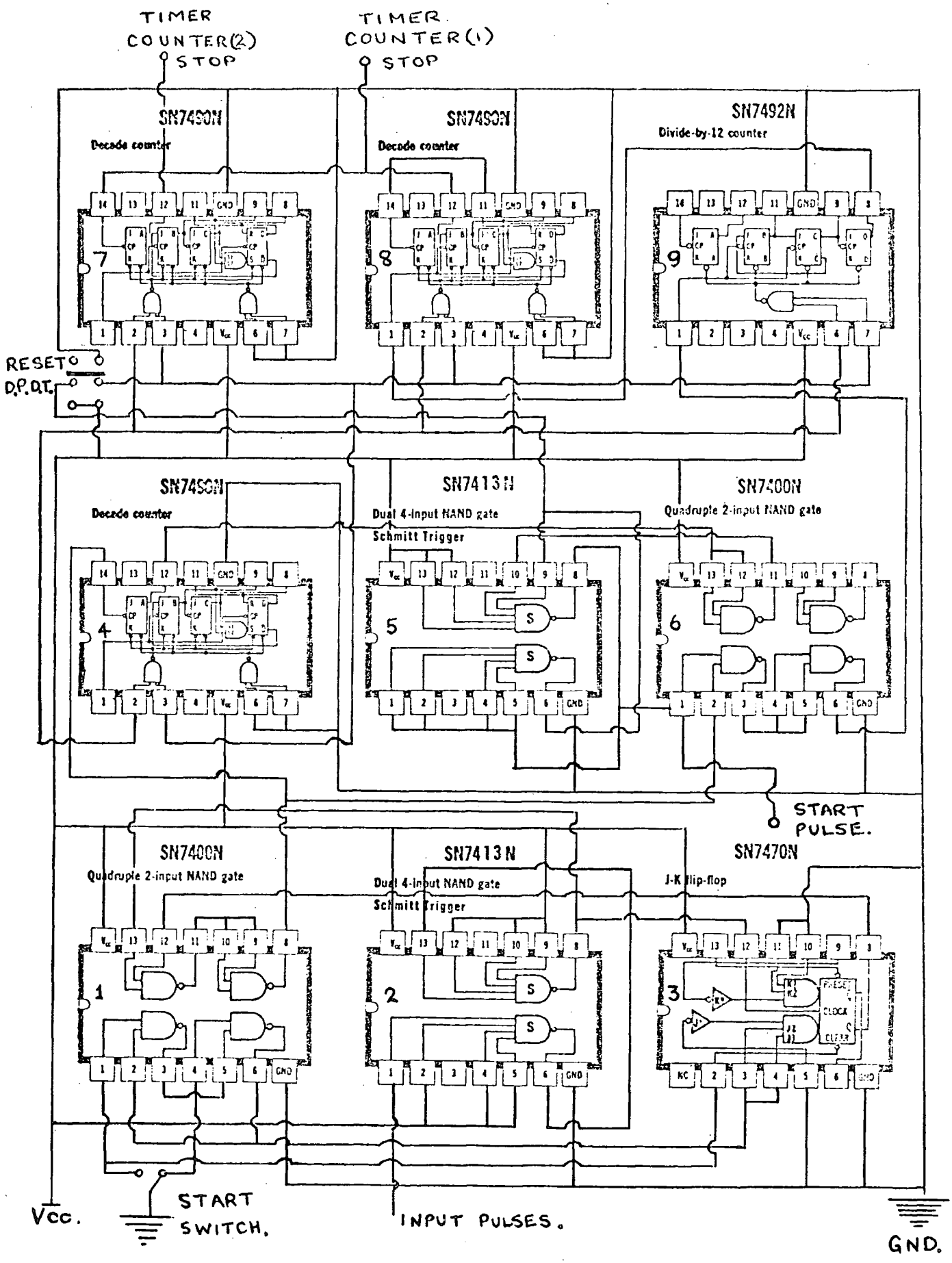

Fig.(5b) Circuit Diagram of the Divide / Control Unit.

to ensure that the division components are started at the leading edge of the second pulse and this excludes the possibility of starting in the middle of the first pulse.

The pulses are then passed on to components (4), (5) and (6), the purpose of these chips is to start the Timer/Counters and to pass on pulses to the division chips. Component (4) ensures with component (6) that the counters receive a simultaneous start pulse when required and also that the start pulse does not register with the following division components as a period pulse. Component (5) is used as a circuit lock so that the Timer/Counters cannot be restarted before the circuit reset cycle is put into operation, thus permitting written recordings of deceleration time periods to be made.

The pulses following the start pulse are fed into component (9) which divides their number by ten, and then passes a pulse to component (8) which again divides by ten. The output pulse from (8) is split into two parts, the first stops the first Timer/Counter and the other is fed into component (7) which divides the input by 2 and then passes a pulse to stop the second timer counter. It can be seen from the above explanation that the Timer/Counters would then display the relevant times for 100 and 200 pulses.

The particular circuit described measures the times for 100 and 200 pulses but the number of pulses timed can be easily varied by adding or subtracting additional division chips, to or from the circuit. At the outset of a series of experimental runs the number of pulses to be timed was selected and the circuit altered accordingly. The method of selection was based on having enough pulses to obtain measurable times, t_1 and t_2 and a measurable difference, $t_2 - 2t_1$. Also the difference had not to be

so large as to invalidate the assumption that the deceleration rate is constant over the time period t_2.

The circuit can be quickly reset with the aid of the start and reset switches and made ready for further deceleration timings.

Comments on Circuit Operation

The circuit was found to be very accurate in operation, so much so that after test runs it was found necessary to start and stop the Timer/Counters on pulses from the same machined bucket on the disc. This was necessary because if starting and stopping were done with different buckets, the circuit easily showed up the machining error of the buckets.

Position Checks of the Shaft and Bearing

The eccentricity of the shaft and its mode of operation were continually monitored using capacitance transducers in conjunction with Wayne-Kerr Distance/Vibration meters and an oscilloscope. The capacitance probes were positioned near the shaft on the opposite sides of the discs to the bearing. The reason for this being to prevent water from the bearing interfering with the operation of the probes. Small droplets of water which may have failed to have been contained by the catchers were prevented from reaching the probes by the throwing action of the discs.

CHAPTER 6

EXPERIMENTS WITH THE 2" DIAMETER RIG

The experimental work with this rig consisted of driving the shaft up to a predetermined speed and then letting it decelerate freely. The decelerations were measured accurately with the aid of the instrumentation described in Chapter 5 and the frictional torque acting on the rotor could then be calculated.

The equation of motion of the decelerating shaft is,

$$Ip \frac{d\omega}{dt} = - T_{total}$$

where, $T_{total} = T_{rotor} + T_{disc\ drag}$

The form of T_{total} depends on the regime in which the bearing is operating, i.e. laminar, transition or turbulent.

It is first necessary to determine the disc drag torque before the decelerations can be interpreted to yield information about the bearing torque.

Disc Drag Torque Determinations

The method by which this was determined was as follows. The shaft and discs were removed from the water bearing and assembled in an externally pressurised air bearing. The drag torque was determined by the deceleration technique.

If we consider the equation of motion of the assembly using the air bearing we have,

$$Ip_{total} \frac{d\omega}{dt} = - T_{total}$$

Using the air bearing the frictional torque T_{total} is made up of two components, firstly the drag on the discs and secondly the frictional torque

in the air bearing. Hence,

$$Ip_{\text{total}} \frac{d\omega}{dt} = - T_{\text{discs}} - T_{\text{air bearing}} \qquad (6:1)$$

From Chapter 2,

$$T_{\text{air bearing}} = \frac{2\pi R^3 L \mu \omega}{c} + \frac{\dot{m} \omega R^2}{2}$$

$$= k_1 \omega \qquad \text{say}$$

If we consider equation (6:1), the drag on the discs determined by this method has to be corrected by a small amount because of the frictional torque from the air bearing. Because of the low viscosity of air, the correction for the frictional torque from the air bearing is very small.

The frictional torque from the air bearing was also determined by the deceleration technique. The shaft with the discs removed was decelerated in the air bearing and the decelerations were timed using stop watches and a stroboscope. The electronic method was not used because of the simple nature of the deceleration and also because of the low viscosity of air which provided a sufficiently large time constant such that timing measurements could be easily taken during the deceleration of the rotor. Also the shaft itself did not have any buckets machined in it, it would not have been easy to obtain pulses from it to trigger the electronic circuitry. A possible solution would have been to use a photo electric pick-up to produce pulses, but one of these was not available. The equation of motion for the shaft alone decelerated in the air bearing is substituting k_1,

$$Ip_{\text{shaft}} \frac{d\omega}{dt} = - k_1 \omega$$

From Chapter 2,

$$\frac{Ip_{\text{shaft}}}{tc} = k_1$$

The value of tc was found experimentally as described above and hence the value of k_1. The necessary information to correct the disc drag torque results was then available.

The deceleration of the assembly, shaft plus discs, was carried out. using the electronic method. The reason why the electronic method was used being the complex nature of the torque from the discs. From the results obtained it was possible to plot the disc drag torque as a function of speed which could be used to interpret the decelerations of the shaft plus discs in the liquid bearing. The complex nature of the torque is borne out by the change in gradient of the experimental plot Fig. (6b), at about 2300 r.p.m., thus confirming the need for electronic timing of the decelerations.

The axial location of the shaft was achieved with the aid of carbon points on the end of the shaft. The points ran on brass pads which were fixed to the base plate. The shaft was not nipped between the pads, but was permitted a few microns end float. The friction which appears on the shaft because of the rubbing of the carbon bushes on the brass pads, although small, is corrected for in the disc drag torque measuring determination because this appears as an extra component in the measured torque.

To interpret the bearing frictional torque fully, it was also necessary to obtain information about eccentricity, mass flow rates, viscosity and polar inertia of the rotating shaft.

Mass Flow Rate Determination

The mass flow rate was determined by using a glass beaker to collect the lubricant and a stop watch. The beaker weight, being known before it was placed in the bearing outlet flow and the stop watch started, was subtracted

from the final weight of the beaker plus water and hence a flow rate was determined. A plot of the speed of rotation versus the mass flow rate for each of the lubricant supply pressures was obtained.

Eccentricity Determination

Plots of eccentricity versus speed were obtained by using capacitance probes in conjunction with Wayne Kerr distance vibration meters. The probes were first 'zeroed' by moving the shaft around the bearing clearance so as to establish its effective clearance circle, as is the usual manner. It was then easy to determine the eccentric running conditions of the shaft at various speeds. The measured displacements were first corrected for shaft curvature before being transposed into eccentricity. The correction curves were supplied by Wayne Kerr.

Viscosity of the Lubricant

The lubricant used in all of the experiments reported in this thesis was distilled water. The distilled water was obtained from a laboratory still. The viscosity of the distilled water, which can vary with degree of purity, was checked using a laboratory viscometer. The determination of the viscosity versus temperature data is described in Appendix (3). The experimentally obtained viscosity was used throughout this reported research.

Polar Inertia

Knowledge of the polar inertia of the shaft plus discs is required so as to relate the total torque and deceleration rates of this rotating mass. The rotating discs and shaft are the energy store which must be dissipated before the shaft will come to rest. The rate of dissipation is a reflection of the frictional torque appearing on the rotating mass. Unfortunately, the equipment available for use to determine the polar inertia experimentally was reported to be very inaccurate. It was decided

that a more accurate method of obtaining the polar inertia of the rotating members was to measure each member accurately and with the use of an experimentally determined value for density, to calculate a value for polar inertia. The density was determined by making a sample block of the materials used and measuring it to obtain the volume and then weighing it to obtain the mass.

Total Torque Measurement

The decelerations with the shaft in the liquid bearing were carried out in the following manner. The shaft was driven up to a predetermined speed and then the air drive was totally disconnected, by removing the supply pipe from the drive system. The shaft was then permitted to decelerate freely. Point deceleration rates were obtained, with the electronic instrumentation previously described whilst the shaft was decelerating.

With these results and a knowledge of the polar inertia it was then possible to determine the total torque by calculation.

Experimental Procedure Comments

Before each deceleration of the shaft was timed a 'dummy' signal was fed into the electronic circuit from a laboratory oscillator to check whether the circuit was dividing exactly in the ratio of 2:1. This was done quickly several times before each deceleration. Agreement of the two six figure displays of the counters was, when the circuit was operating satisfactorily, to the last digit. Inbuilt into the circuit was an important feature which ensured that its divide sequence was not started in the middle of a pulse and that the first pulse only started the two timer counters simultaneously and did not also provide the first count pulse. This made certain that the circuit divided exactly in the ratio of 2:1 to the limit set by the accuracy of the counters, $\pm$ 1 microsecond.

The total pulse division of the circuit was varied when required by the addition and removal of various 'chips'. This permitted the difference in times recorded for N and 2N pulses during a deceleration run to be of a reasonable value, i.e. neither too large nor too small.

In all experiments the shaft was driven up to speed using the air turbine drive. The air supply to the turbine was totally disconnected after the required speed of rotation had been reached. This ensured that the decelerations were carried out without any drive torque being delivered to the shaft.

The accuracy of the timing equipment was found to be so good that it was generally only necessary to time one deceleration. Additional measurements were taken over a small speed range when it was desired to investigate a range of Reynolds numbers of particular interest.

Results and Comments

The determination of the disc drag torque was carried out in the manner described earlier. The correction for the air bearing torque was determined first, the results of which are tabulated in Table (10.1) and sketched in graph Fig. (6a). From Fig. (6a) a time constant of 83 seconds was found. Hence using the calculated value of Ip_{shaft} and tc k_1 was calculated to be $5.87\ 10^{-6}$ Kgm^2 $sec.^{-1}$.

The deceleration of the shaft with discs attached in the air bearing was next carried out. The results of these decelerations are tabulated in Table (10.2). From these results Fig. (6b) was drawn, showing $\frac{dN}{dt}$ versus N, where $\frac{dN}{dt}$ is the deceleration rate after correcting for the air bearing torque. The data has been left in the $\frac{dN}{dt}$ form for easier appreciation and for more convenient use later in the experiments. The

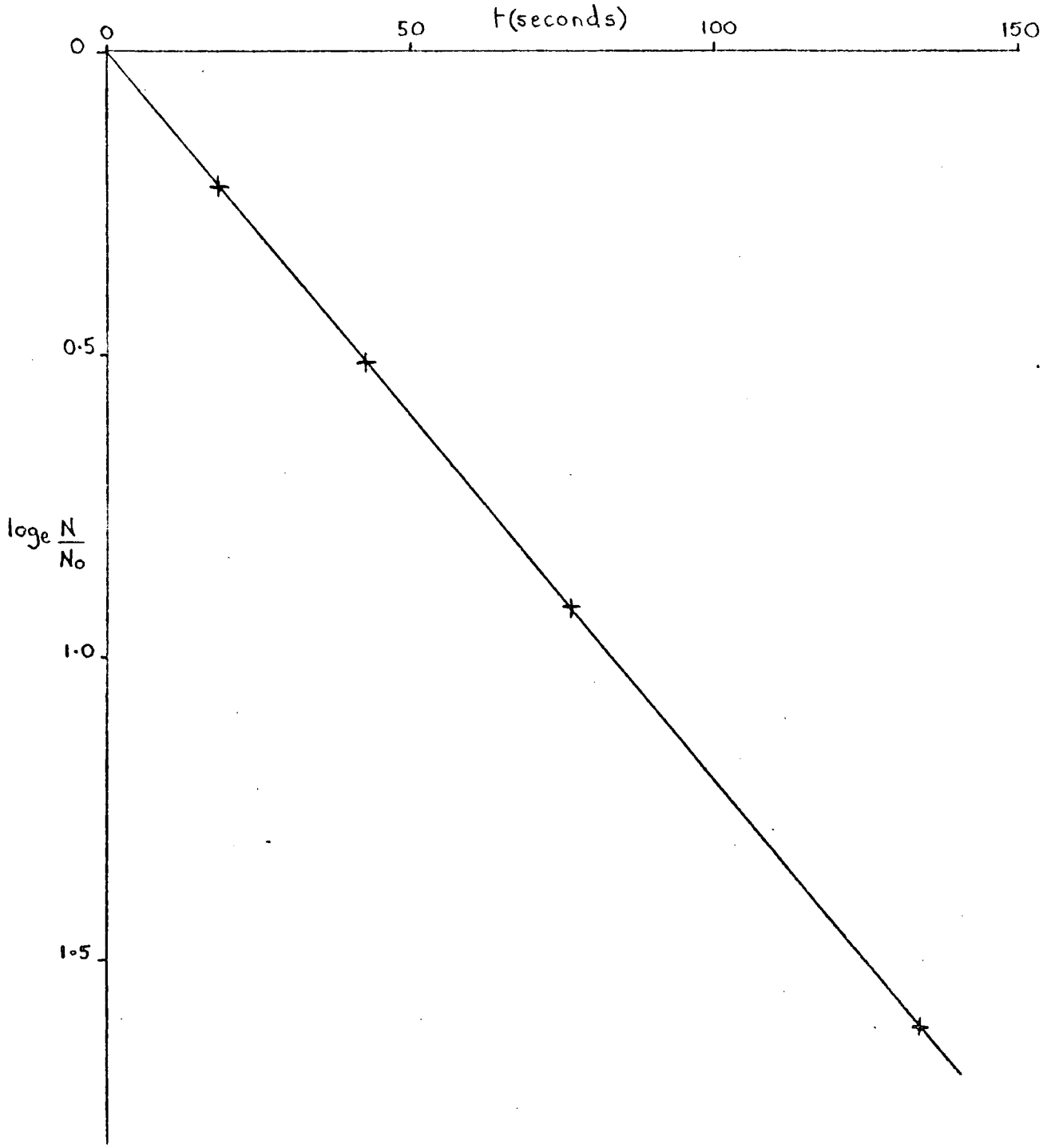

Fig. (6a). Air Bearing Correction Plot $\log_e N/N_o$ versus t.

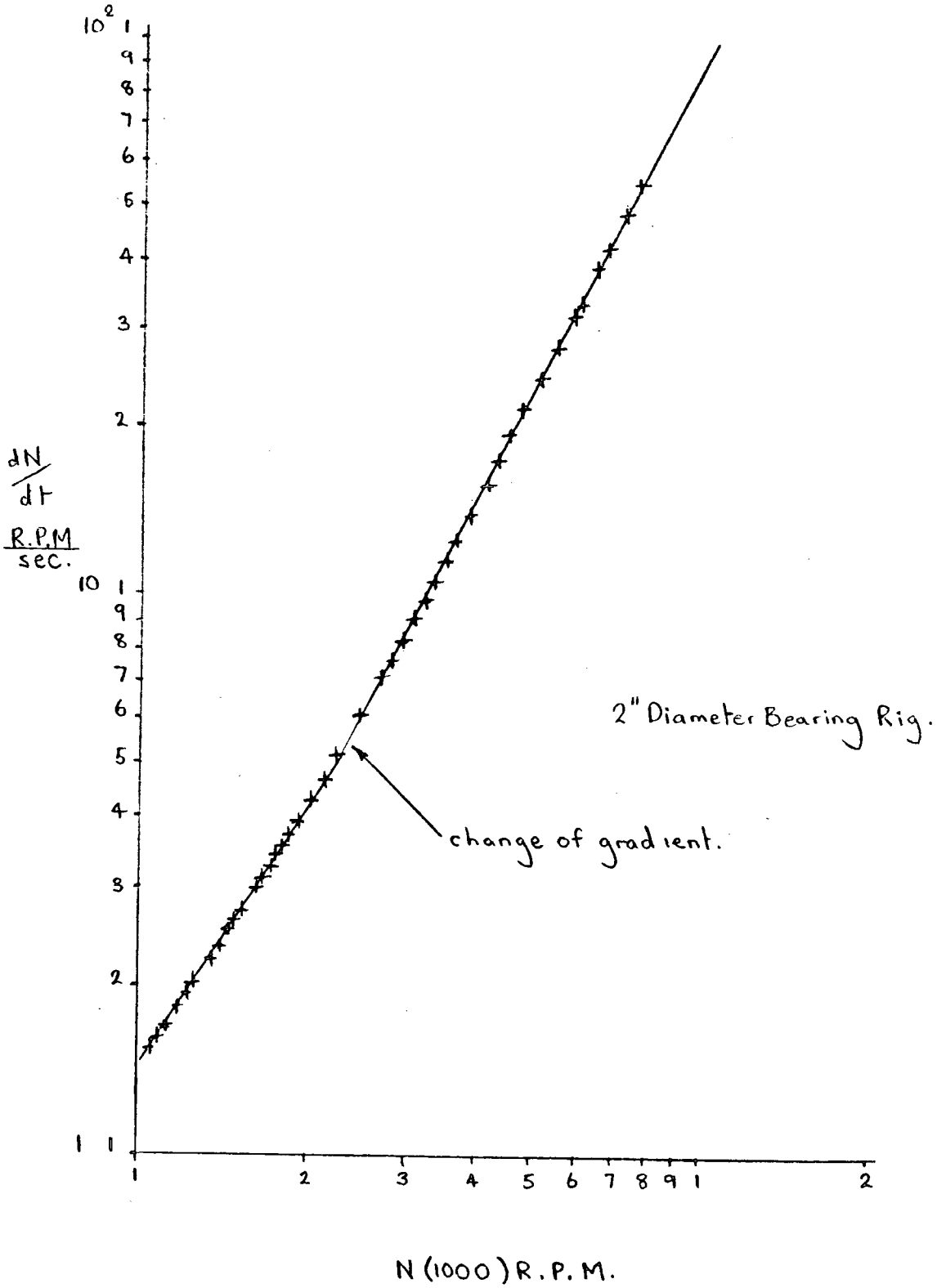

Fig.(6b) Disc Drag. Plot of dN/dt versus N.

results plotted in Fig. (6b) show very little spread and it was found that they were very repeatable.

From past work on windage losses on rotating discs it is apparent that an air jet directed towards the discs in question can cause early onset of turbulent flow over the discs and also increases in friction losses. This is relevant in the disc drag determination in the work reported here since the air escaping from the air bearing can act as a jet to alter the flow over the discs, thus producing incorrect data for windage loss correction in the liquid bearing experiments. This was overcome by using the liquid bearing drain catchers attached to the air bearing to deflect the escaping air from impinging on the rotating discs. This also simulates the experimental layout for the decelerations with the water bearing as closely as possible.

The mass flow rates of water and the eccentricities for given speeds and pressure supplies were obtained as described previously for each bearing clearance. The results obtained can be found in tables (10:3) and (10:4) respectively. These were plotted versus rotational speed in Figs. (6c), (6d), (6e) and (6f). For the 7.90×10^{-5}m clearance the plots of the mass flow rates, Fig. (6c), show a change in gradient indicating the onset of turbulence which causes increased flow restrictions to the lubricant thus decreasing its rate of flow through the bearing.

Three bearing clearances were used as described in Chapter 4, these corresponded roughly to clearance ratios of 0.001, 0.002 and 0.003. For 0.001 clearance ratio, a supply pressure of 2.0 bar gauge was used. For the other two clearance ratios two supply pressures were used, i.e. 1.0 bar and 2.0 bar gauge.

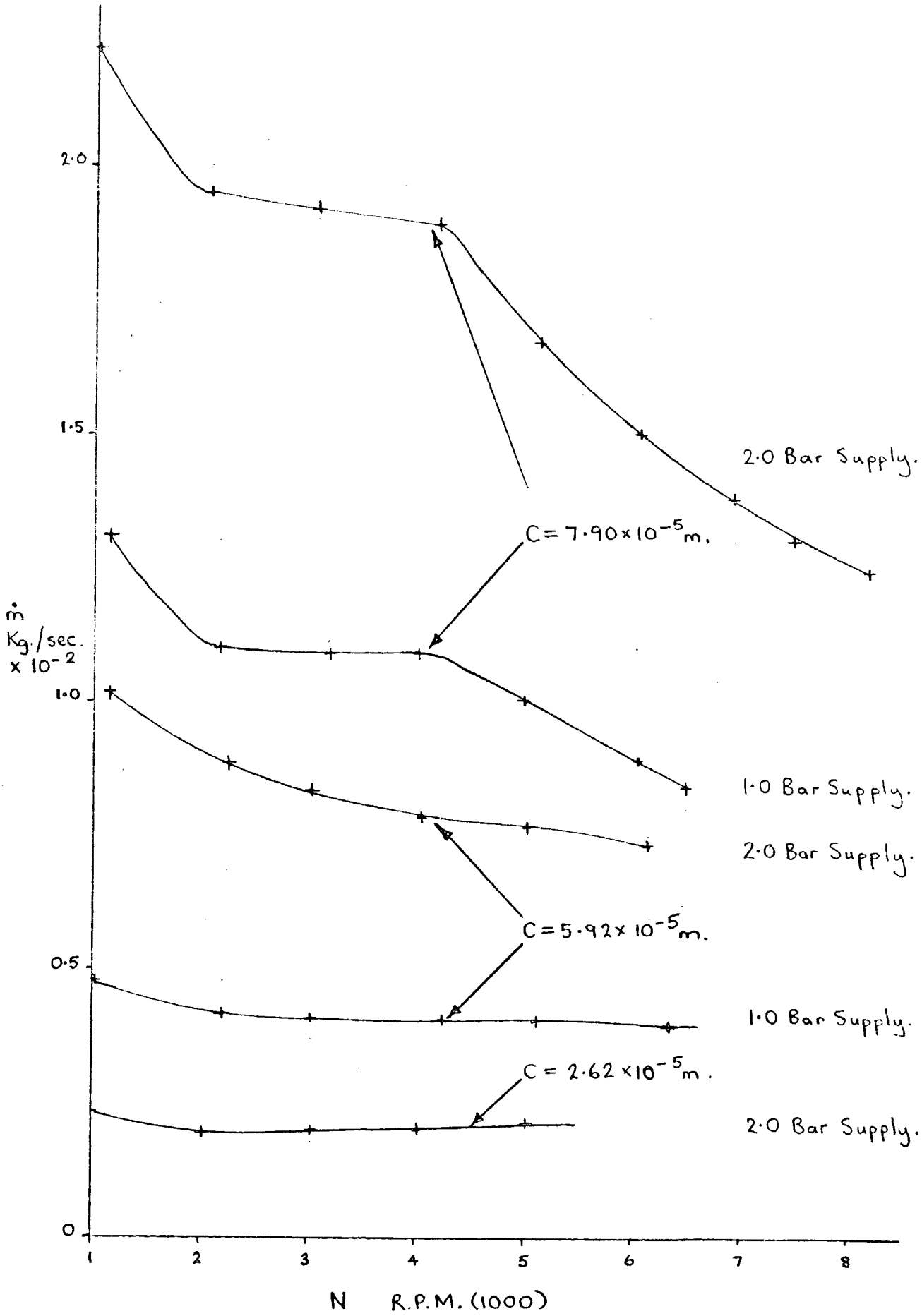

Fig. (6c) 2" Diameter Rig, Mass Flow Rate versus N.

2" Diameter Bearing ($c = 2.62 \times 10^{-5}$ m)

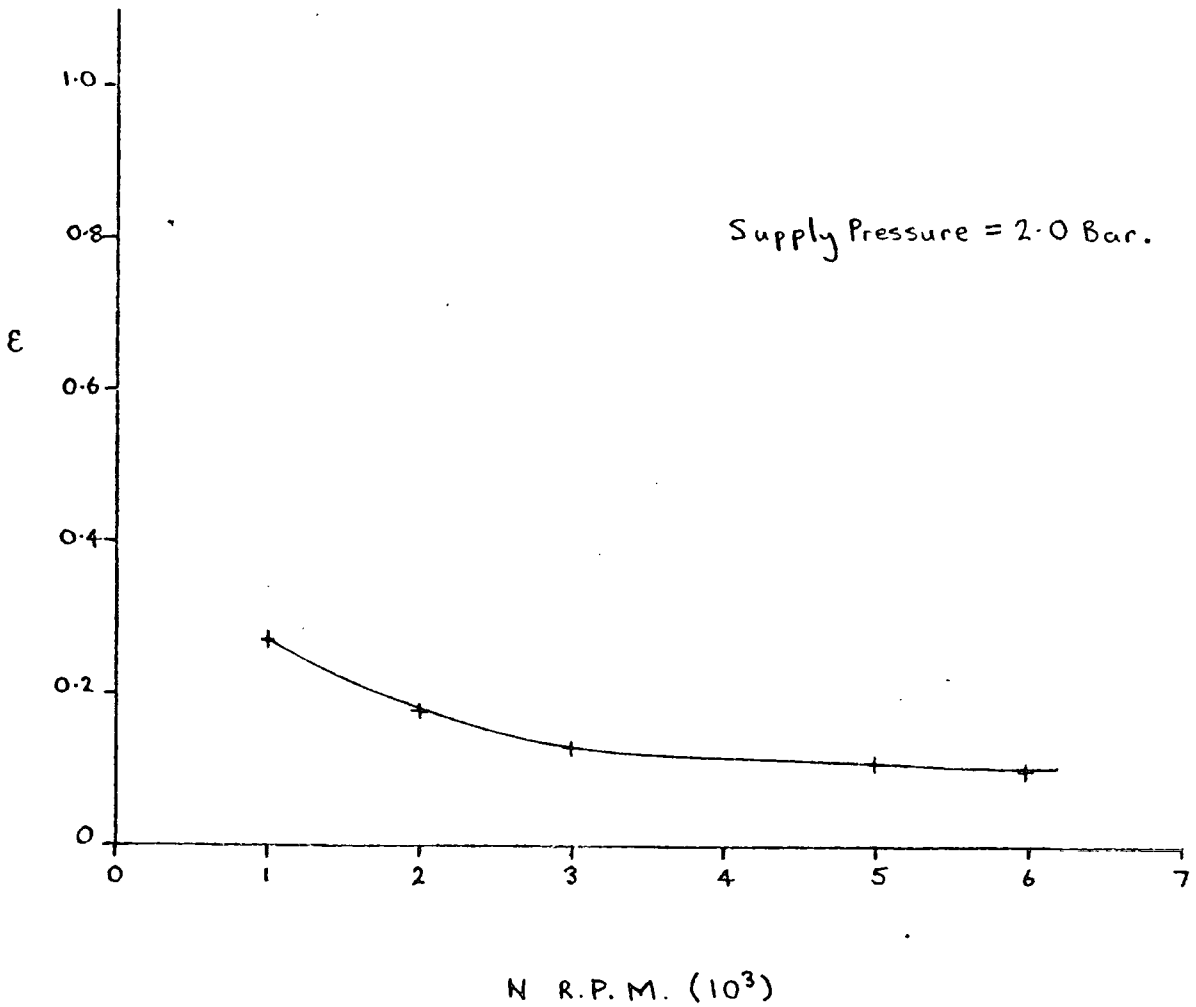

Fig. (6d) Plot of ε versus N.

2" Diameter Bearing ($c = 5.92 \times 10^{-5}$ m)

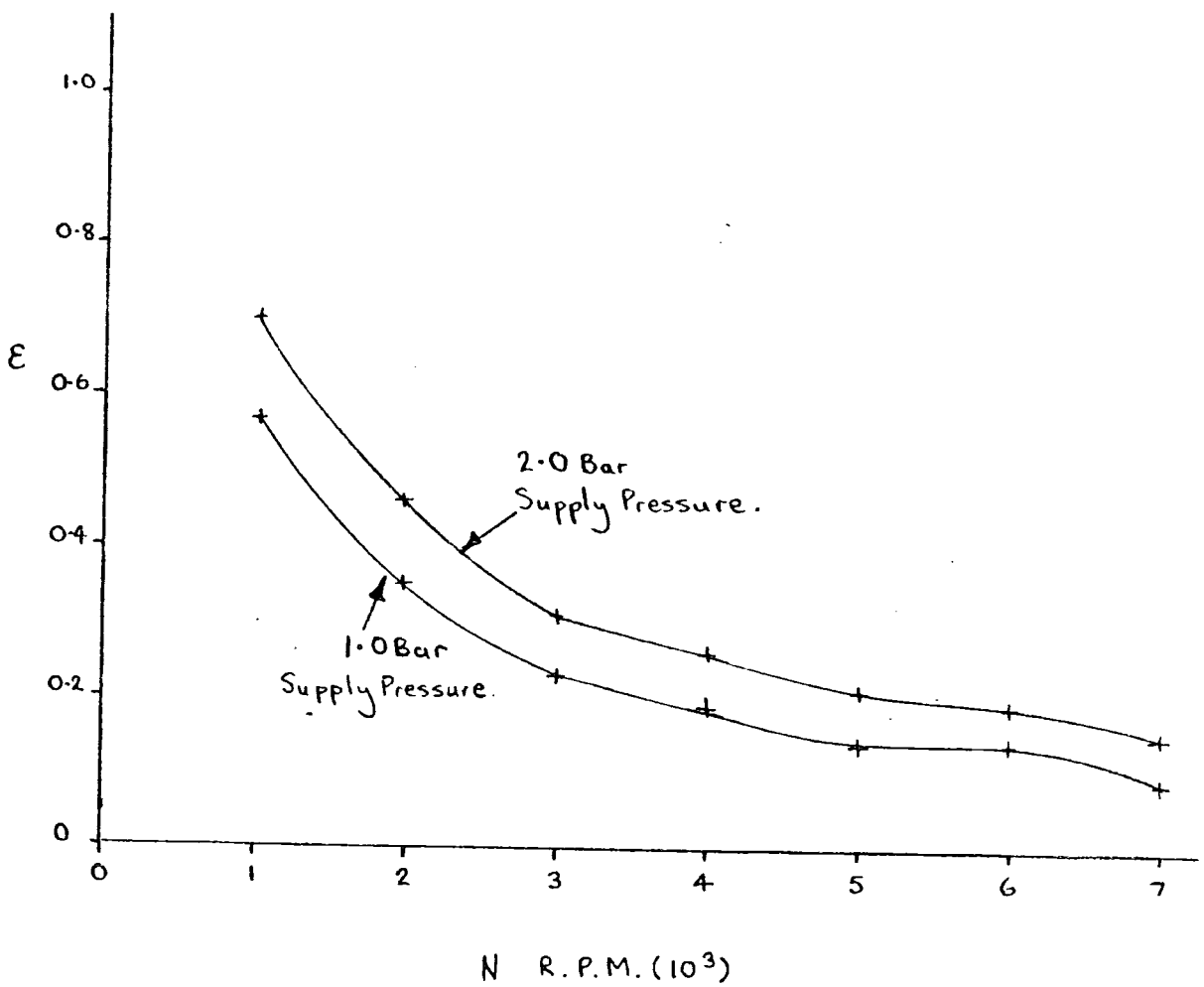

Fig. (6e) Plot of ε versus N.

2" Diameter Bearing ($c = 7.90 \times 10^{-5}$m)

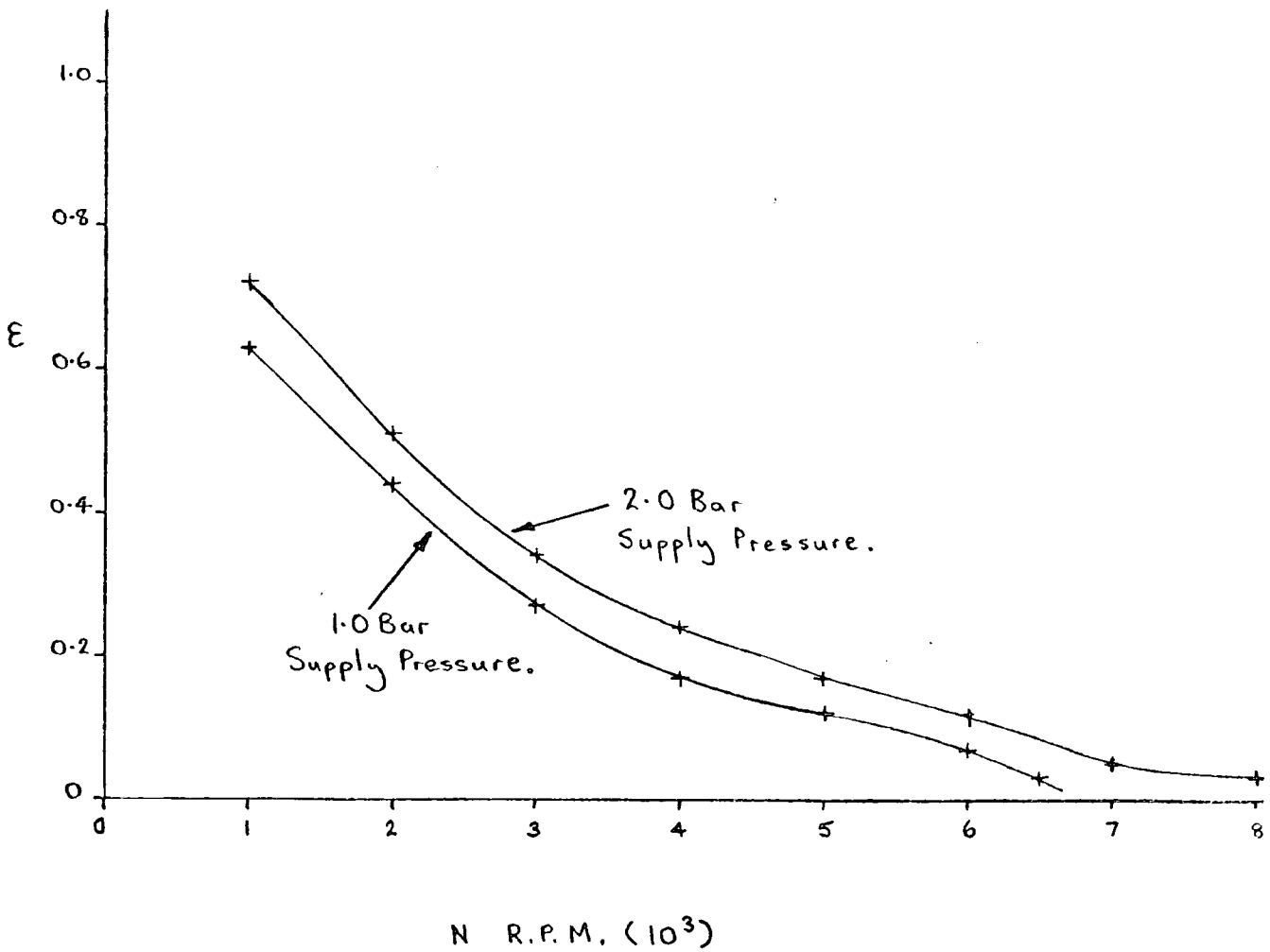

Fig.(6f). Plot of ε versus N.

For each of the clearance ratios total torque decelerations were carried out. The maximum initial speed of each deceleration, and hence Reynolds number, was limited only by the amount of driving torque available from the laboratory air supply. The deceleration times were taken for 10 revolutions and 20 revolutions in each deceleration run at various speeds throughout the run. For each deceleration the inlet and outlet temperature of the water was measured so that the experimental viscosity of the water would be known for a given run. The results obtained from these runs can be found in tables (10:5) - (10:21(a)). Additional shorter runs were made at the high speeds because as the shaft was decelerating quickly the number of points which one could obtain in a given run was limited by the time needed for recording the data.

Discussion of Results

Only a brief discussion of the results will be presented here and a fuller discussion will be presented in Chapter 8. The deceleration runs are plotted in Figs. (6g) and (6h). Fig. (6g) was plotted from the 1.0 bar results and (6h) from the 2.0 bar results. The plots have already been corrected for disc drag. In each graph the upper set of points has not been corrected for momentum torque, but the lower points have been corrected.

With the 2.0 bar supply about 14% of the total rotor torque can be attributed to the throwing of the lubricant. The corresponding percentage for the 1.0 bar supply is around 10%. The angular momentum torque is therefore a significant portion of the total rotor torque.

The departure of the corrected plots from the theoretical Petroff torque can be explained by the eccentric running of the shaft in the bearing. Three graphs Fig. (6i), (6j) and (6k), which are plotted from the

T_{exp}/T_{th} tables in Chapter 10, section 10 (i), indicate the ratio of the experimentally determined torque to that of the theoretical torque for laminar flow corrected for eccentricity. From these graphs, close agreement is apparent between theory and experiment.

It would appear from these results that the use of a pressurised lubricant supply has been successful at suppressing cavitation as there is no difference between the 1.0 and 2.0 bar results and both lie close to the full film theoretical plot.

Decelerations were carried out with two different lubricant feed directions. The first feed position was from the top of the bearing opposite the load and the second 90^{o} displaced in the direction of rotation of the shaft. It was found that the torque measurements for second supply position, did not differ from the measurements reported here, with the supply opposite the load.

The departure of T_{exp}/T_{th} from the predicted plots of unity in graphs Fig. (6j) and (6k) at higher Reynolds numbers indicates the onset of Taylor vortices. The Taylor prediction of onset is indicated on the graphs, using $Re = 41.1 \sqrt{R/c}$, equation (1:1). Fig. (6l) is a plot of the deceleration results, which have been corrected for the angular momentum torque, for the three clearance ratios with 1.0 and 2.0 bar supplies. The onset of turbulence is indicated by the turning of the graph onto a new gradient at the higher Reynolds numbers. It was not possible to investigate this further as the air to drive the turbine was not available to reach higher speeds.

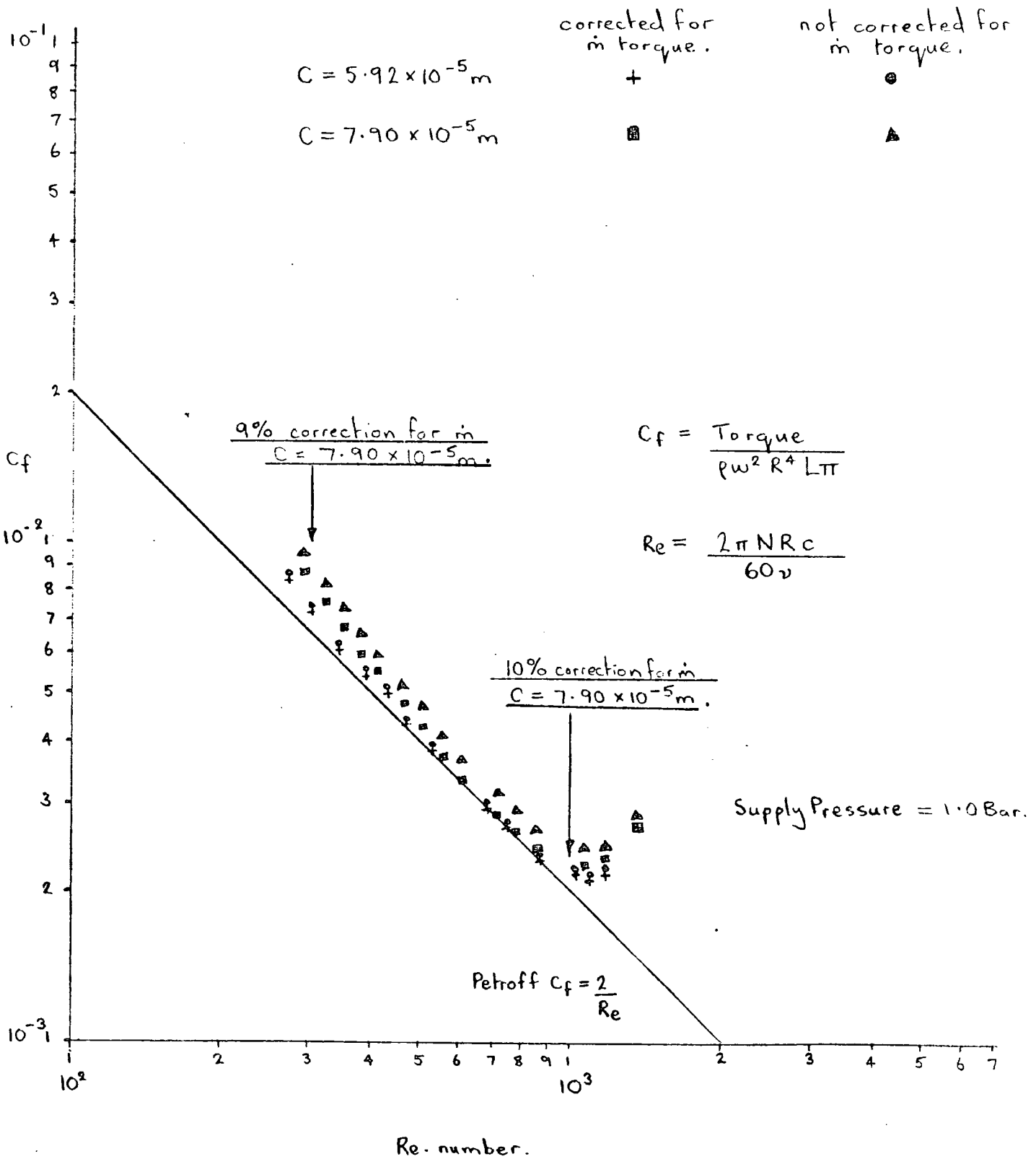

Fig.(6g) Plot of Cf versus Re. number for the 2" Diameter rig.

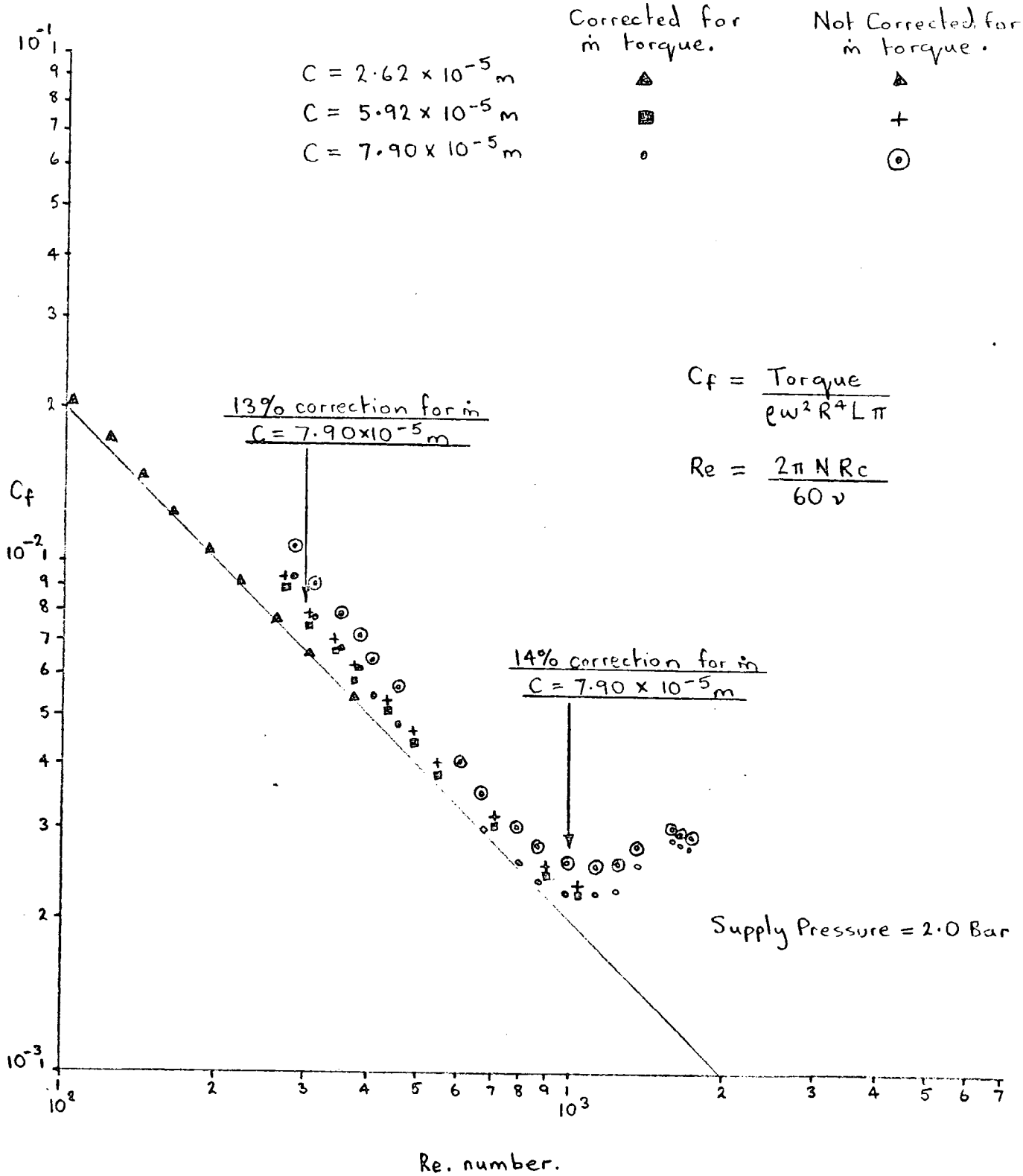

Fig. (6h) Plot of Cf versus Re. number for the 2" Diameter Rig.

2" Diameter Bearing ($c = 2.62 \times 10^{-5}$ m)

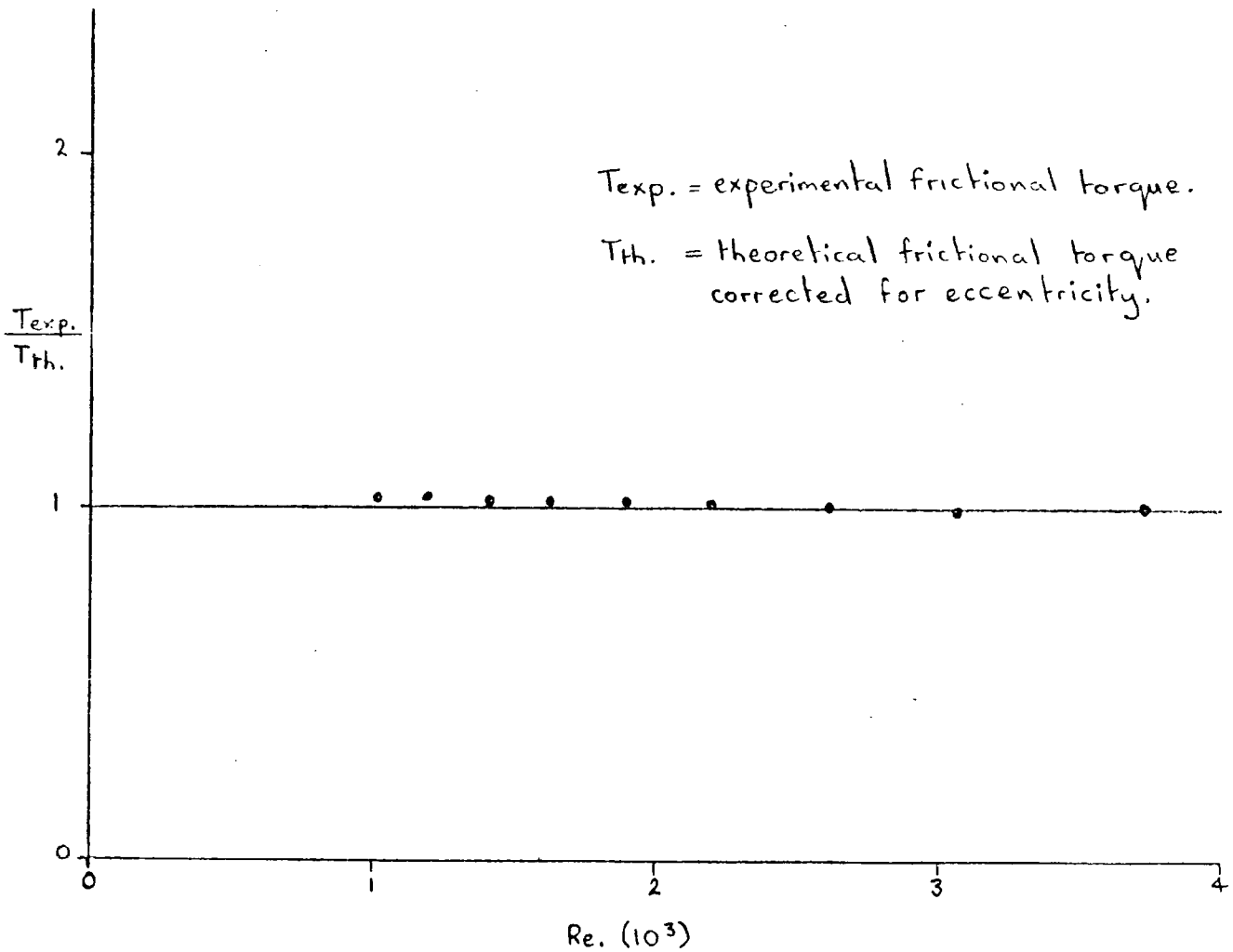

Fig.(6i) Plot of Texp. / TTh. versus Re. number.

2" Diameter Bearing ($c = 5.92 \times 10^{-5}$m)

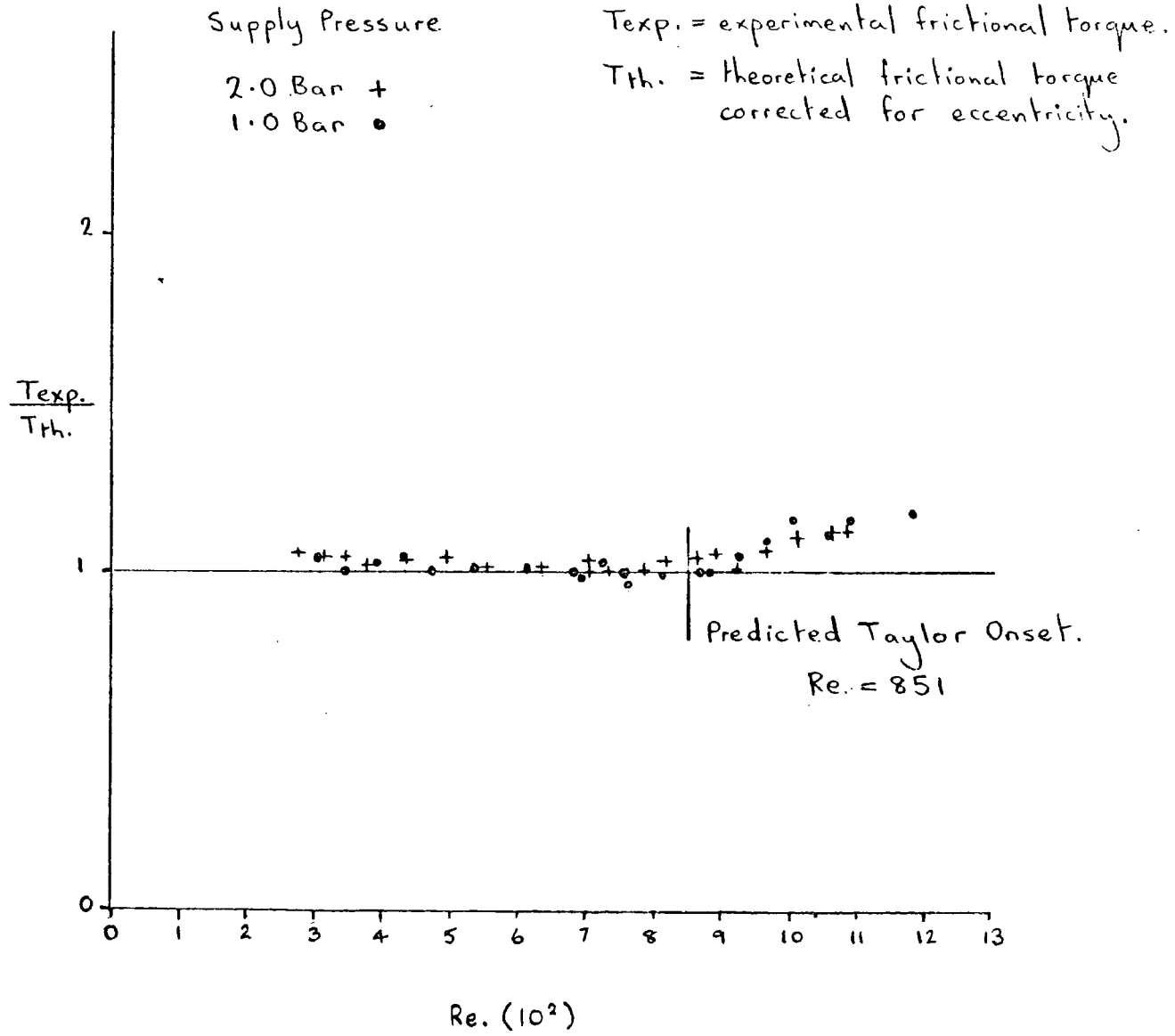

Fig.(6j) Plot of $T_{exp.}/T_{th}$ versus Re. number.

2" Diameter Bearing ($c = 7.90 \times 10^{-5}$m).

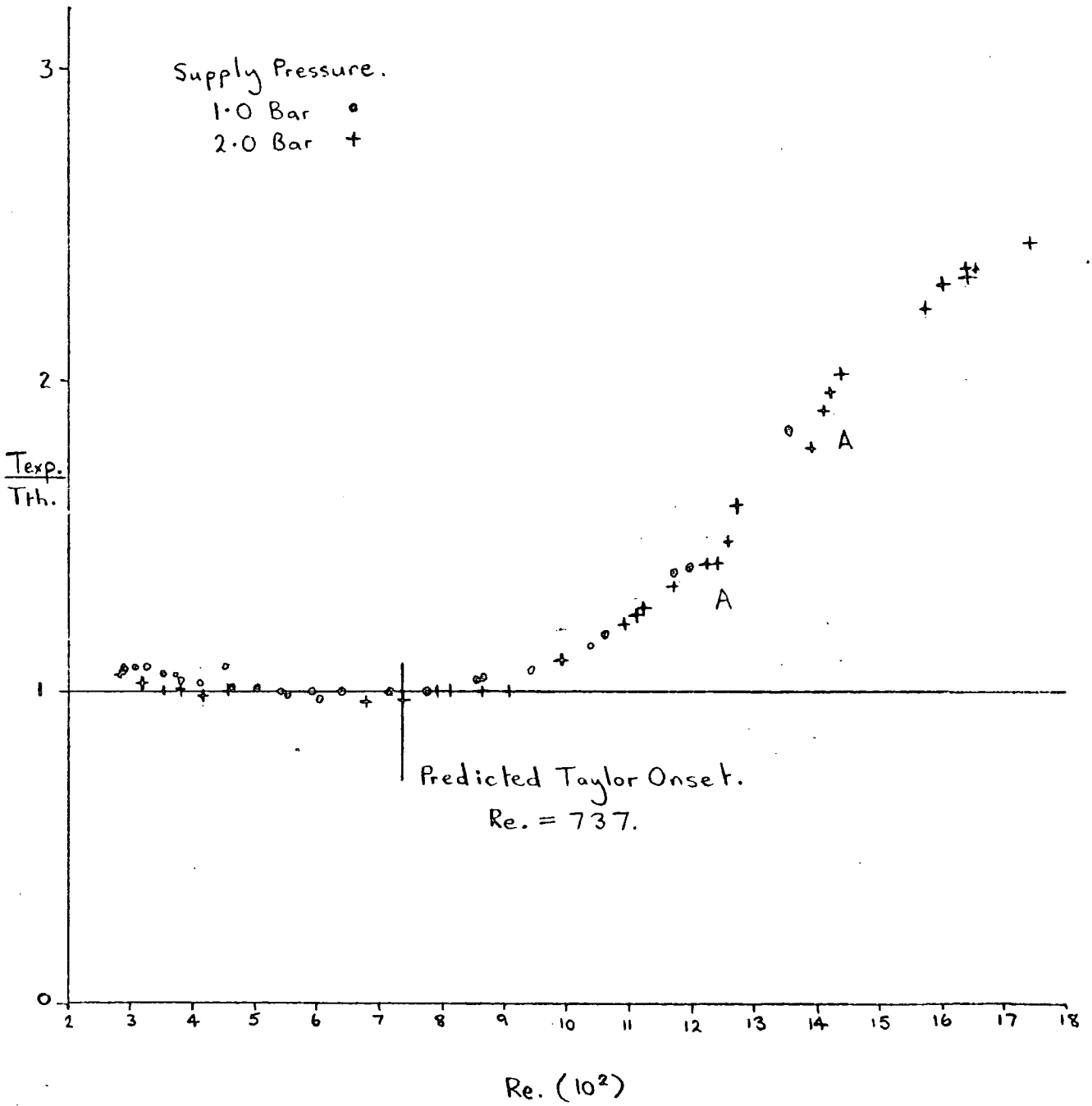

Fig.(6k) Plot of Texp/Tth versus Re. number.

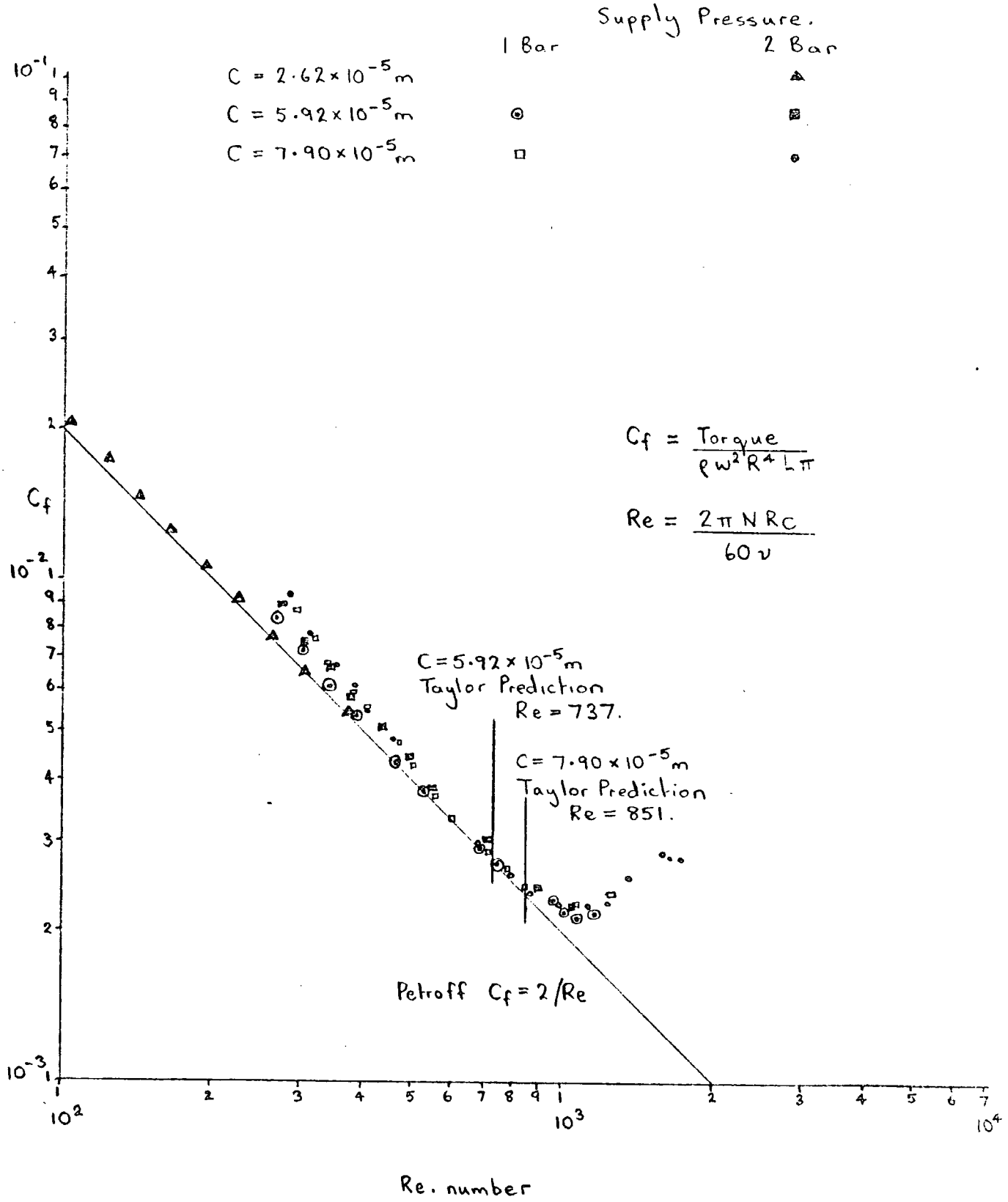

Fig.(61) Plot of C_f versus Re number for the 2" Diameter Rig.
(The results have been corrected for m torque.)

CHAPTER 7

DESIGN OF THE 3" DIAMETER BEARING RIG

The design of the larger rig took the same format as that of the small rig, that was to have discs on the decelerating shaft. The same compromises again had to be made. The discs had to be large enough both to provide sufficient inertia to produce a long deceleration time constant and to ensure that the buckets were at a radius which would enable the shaft to be driven up to speed with an air turbine. Consideration also had to be made of the size and positioning of the discs with a view to shaft stability.

The design of the large rig is illustrated in Fig. (7a). It is similar to the small rig in layout, but a few small changes were made to facilitate easier manufacture and better operation.

The choice of diameter for the bearing of this rig was aided by a computer program. The program is given in Appendix (4). The program is of a fairly simple nature, but because of the large number of variables in the design, it was found to be a great aid to the arithmetic.

Summary of the Computer Program

With reference to Appendix (4):-

The basic parameters of the shaft are fed into the program, i.e. the various radii, lengths and the clearance ratio of the proposed shaft. From these, the program first calculates the polar inertia of the shaft. It then calculates the required diameter of the discs such that the transverse inertia of the rotor is equal to twice the polar inertia in order to inhibit the self excited conical whirl instability of the rotor. After this operation, the program calculates the time constant for deceleration of the shaft plus discs with the bearing operating in the

laminar regime. This gives an estimate of how feasible it is to take measurements from the proposed shaft whilst it is decelerating. The mass of the rotor is then calculated and by using the Ocvirk solution for a short bearing, estimates are made of the eccentricity of the bearing versus speed of rotation of the shaft. The program then proceeds to calculate an estimate of the translational whirl onset speeds, based on an approximate bearing stiffness obtained from the Ocvirk solution to Reynolds equation, the mean rotational Reynolds numbers, the flow rates, the momentum/shear ratios and the stresses set up in the discs during rotation. The disc stresses were calculated in order to determine whether special steel should be used for their manufacture.

The program does not give an exact solution to the bearing design problem but provides a guide to bearing choice for experiments.

Bearing Parameters

R = 38.1 mm

c = 11.48 10^{-5}m

L = 76.2 mm

Ip = 3.93 10^{-2} Kgm^2

Diameter of Discs = 225.4 mm

Surface Finish of Shaft = 0.3 micron C.L.A.

Surface Finish of Bush = 0.8 micron C.L.A.

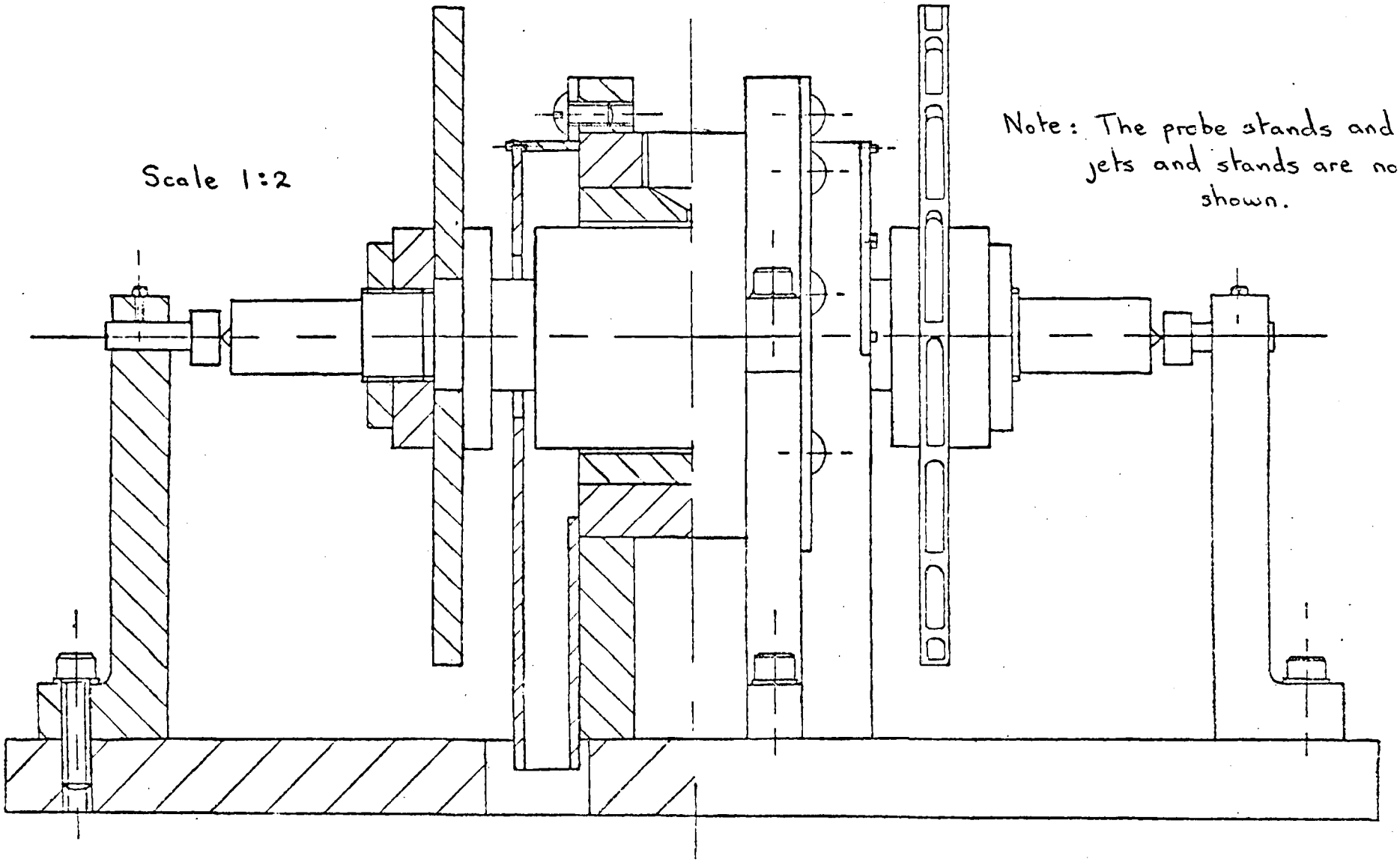

Fig.(7a) Sketch of the 3" Diameter Bearing Rig.

CHAPTER 8

RESULTS AND DISCUSSION

The experiments with the 3" diameter bearing rig took the same form as those reported in Chapter 6 for the 2" diameter rig. Again the total torque was determined using the deceleration technique with electronic timings and this was corrected for windage losses etc., as before. The mass flow rates were measured with beakers and a stop watch and the eccentricities measured using the Wayne-Kerr capacitance probes plus meters. The polar inertia was calculated and the viscosities of water used were those determined experimentally, which are plotted in Appendix (3). Only one radial clearance was used in this series of experiments, 11.48×10^{-5} m, which corresponds roughly to a clearance ratio of 0.003. Again the equation of motion is given by,

$$Ip \frac{d\omega}{dt} = - T_{total}$$

The form of T_{total} this time can be of a very variable nature. As before:

$$T_{total} = T_{rotor} + T_{mass\ flow\ torque} + T_{disc\ drag} \quad (8:1)$$

With the 3" diameter rig the design was such that over the experimental speed range and therefore Reynolds number, the bearing would, at lower speeds, have a laminar film and at higher, a turbulent film. The nature of T_{rotor} with this rig therefore depends on the state of the lubricating film. T_{rotor} was obtained in the same manner as described previously. That was by measuring the total torque and then subtracting from it corrections for disc drag and mass flow rate torques.

Experimental Comments

In the Disc Drag determination the frictional torque on the shaft in the air bearing had to be corrected for a self drive torque which the feed jets in the bush imparted to the shaft. This form of torque was discussed

in Chapter 2. Again during the disc drag determination deflectors were used between the bush and discs to prevent the escaping air from the bearing impinging on the discs and upsetting the boundary layer flow. As with the experiments with the 2" diameter rig, the shaft was driven up to speed by using an air turbine. This was totally disconnected during each deceleration run. Before each deceleration was timed, the satisfactory operation of the electronic timing ciruit was checked by feeding a dummy signal into the circuit from an oscillator. This ensured that the circuit was dividing exactly in the ratio of 2:1.

Results and Comments

The measurements taken during the disc drag determination can be found in Chapter 10, tables (10:22) and (10:23). Graphs, Figs. (8a) and (8b) were plotted from these results. The experimental plot of the disc drag torque, Fig. (8b), is of the same form as that obtained for the 2" diameter rig. The plot shows very little scatter and also a similar distinct gradient change, confirming again the complex nature of the drag torque and the need for electronic timing of the decelerations.

The mass flow rates and eccentricities for the three lubricant supply pressures used, i.e. 1.0 bar 2.0 bar and 2.5 bar, are plotted in Figs. (8c) and (8d). These were plotted from the data in tables (10:24) and (10:25). The change of gradients in these plots indicates a change in lubricating film regime in the bearing. The flow through the bearing is decreased because of the extra flow restriction caused by the turbulent film.

The measurements taken during the deceleration runs can be found in tables (10:26) to (10:34(a)). Fig. (8e) is a plot of the 1.0 bar supply results both corrected and uncorrected for the mass flow rate torque. The angular momentum torque accounts for approximately 14% of the total torque from the bearing when operating with a laminar film.

3" Diameter Bearing Rig.

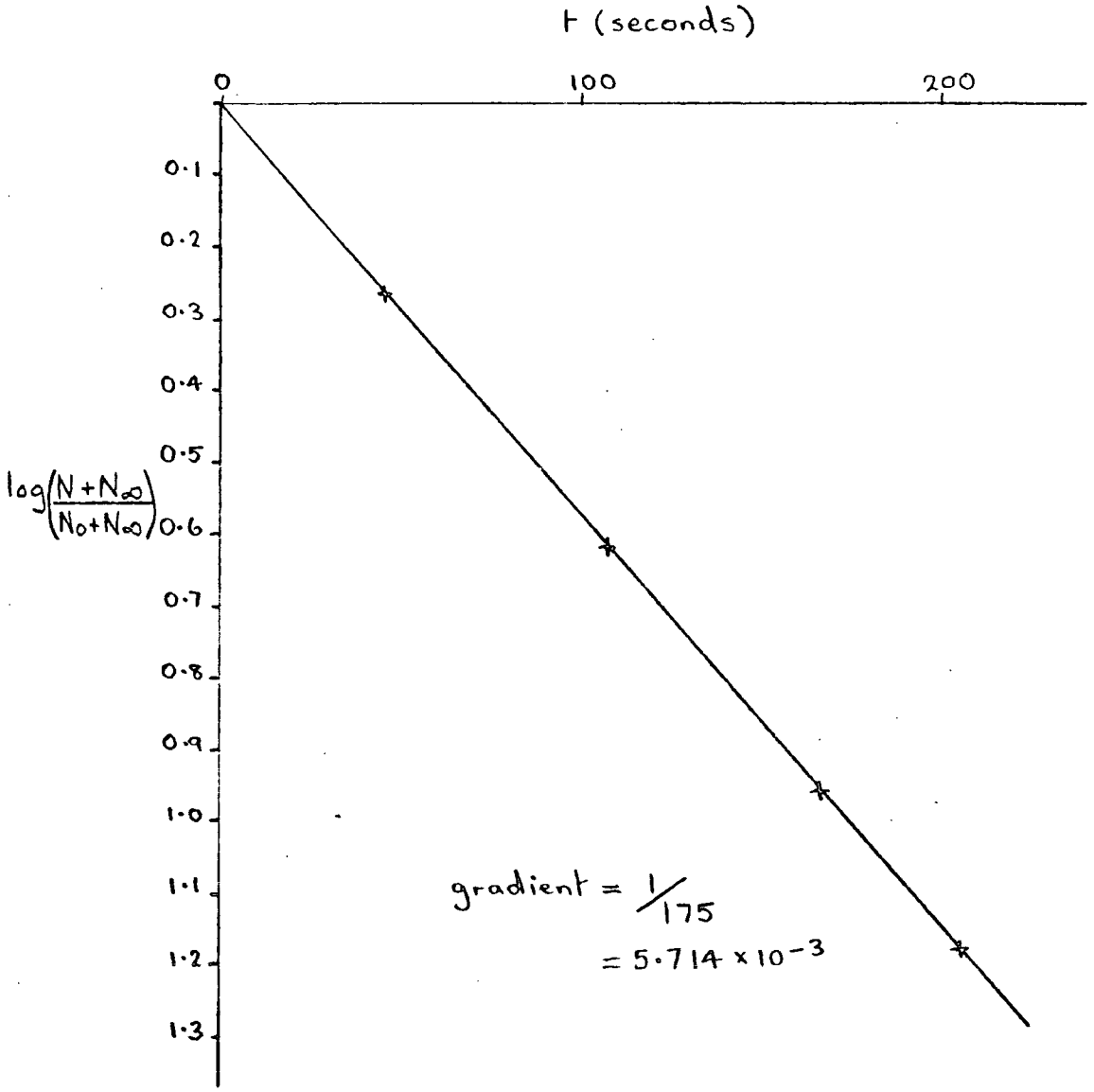

Fig.(8a) Deceleration of the 3" Diameter Shaft in an Air Bearing without Discs.

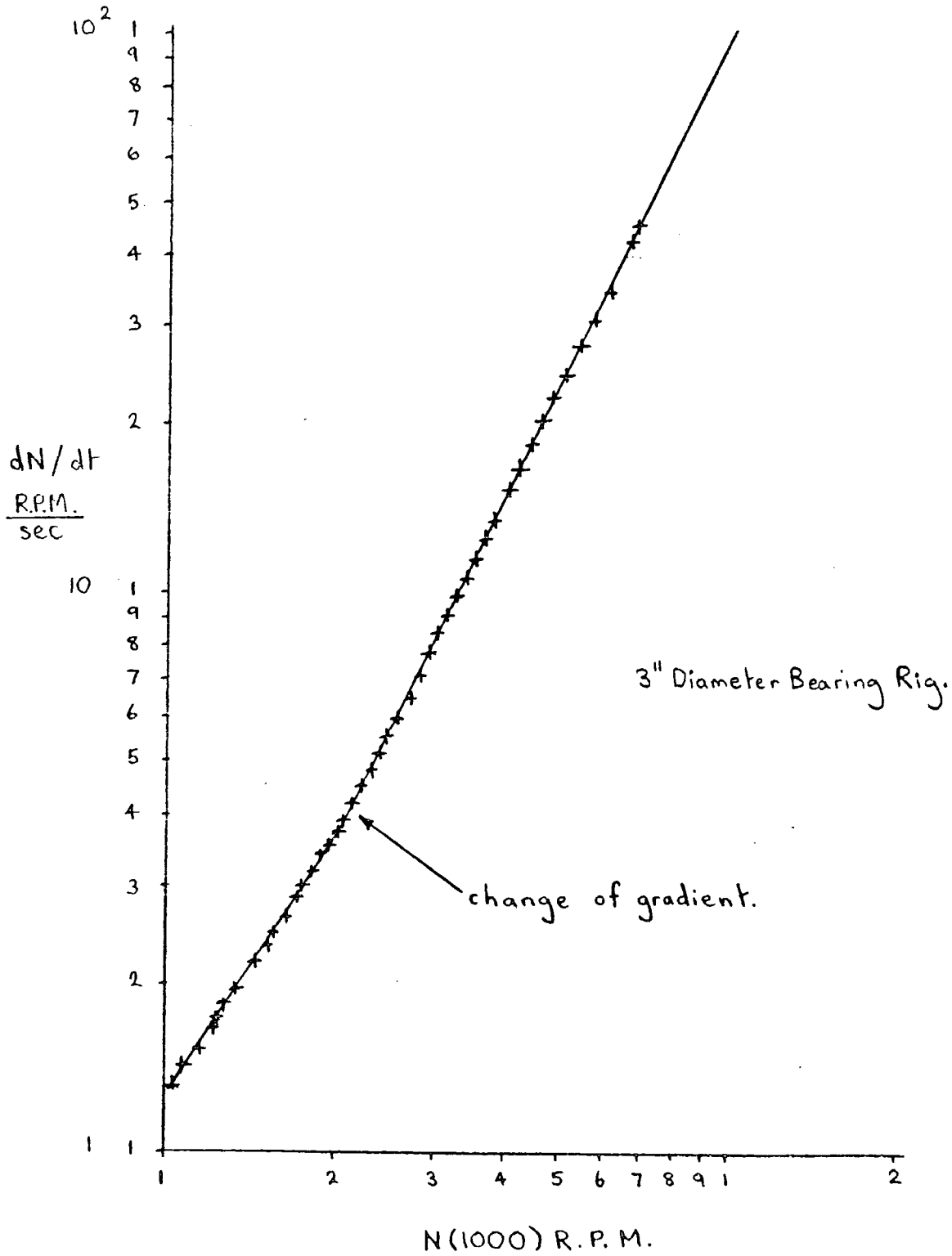

Fig. (8b) Disc Drag. Plot of dN/dt versus N.

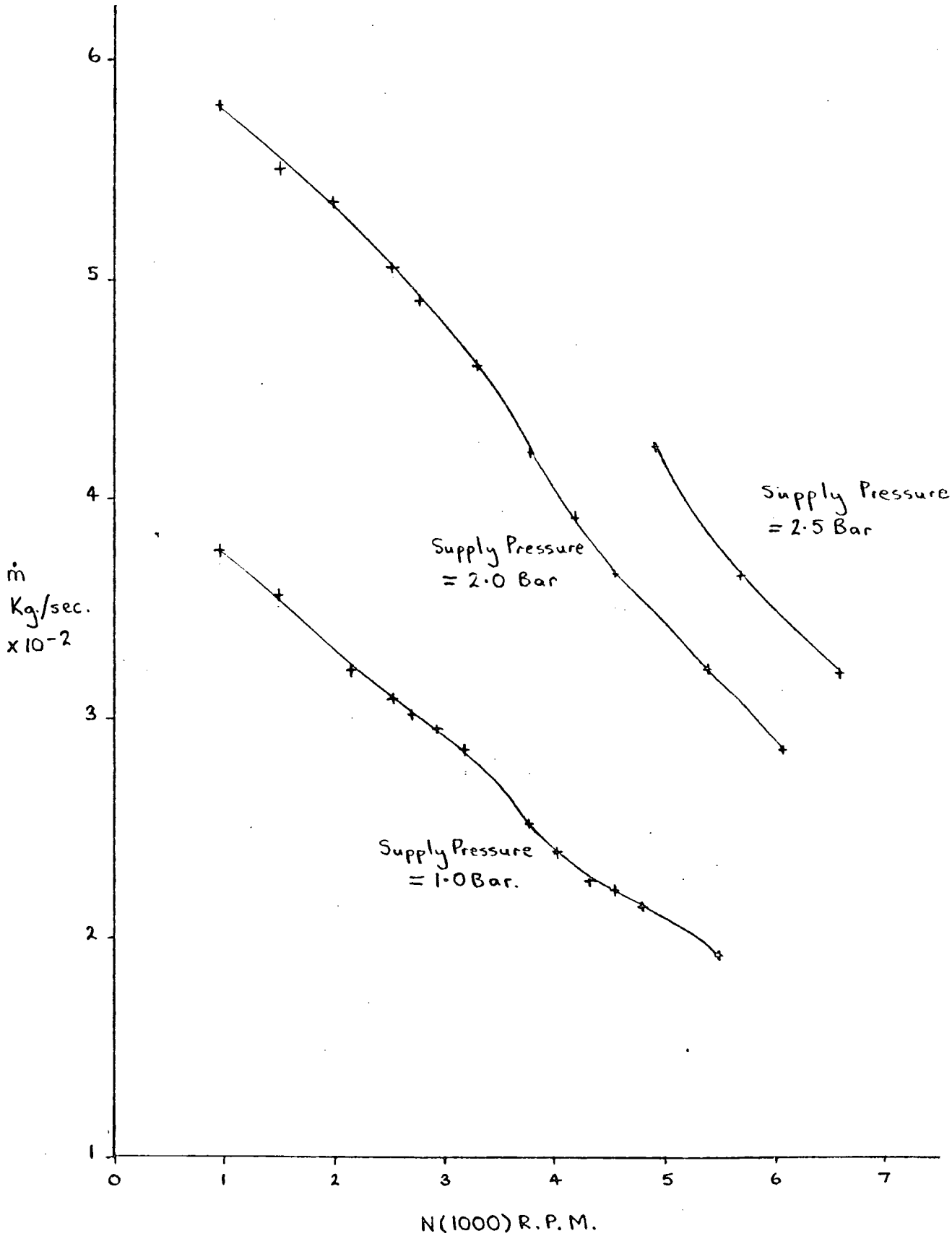

Fig.(8c) Mass flow rate of lubricant versus N for the 3" Diameter Bearing Rig.

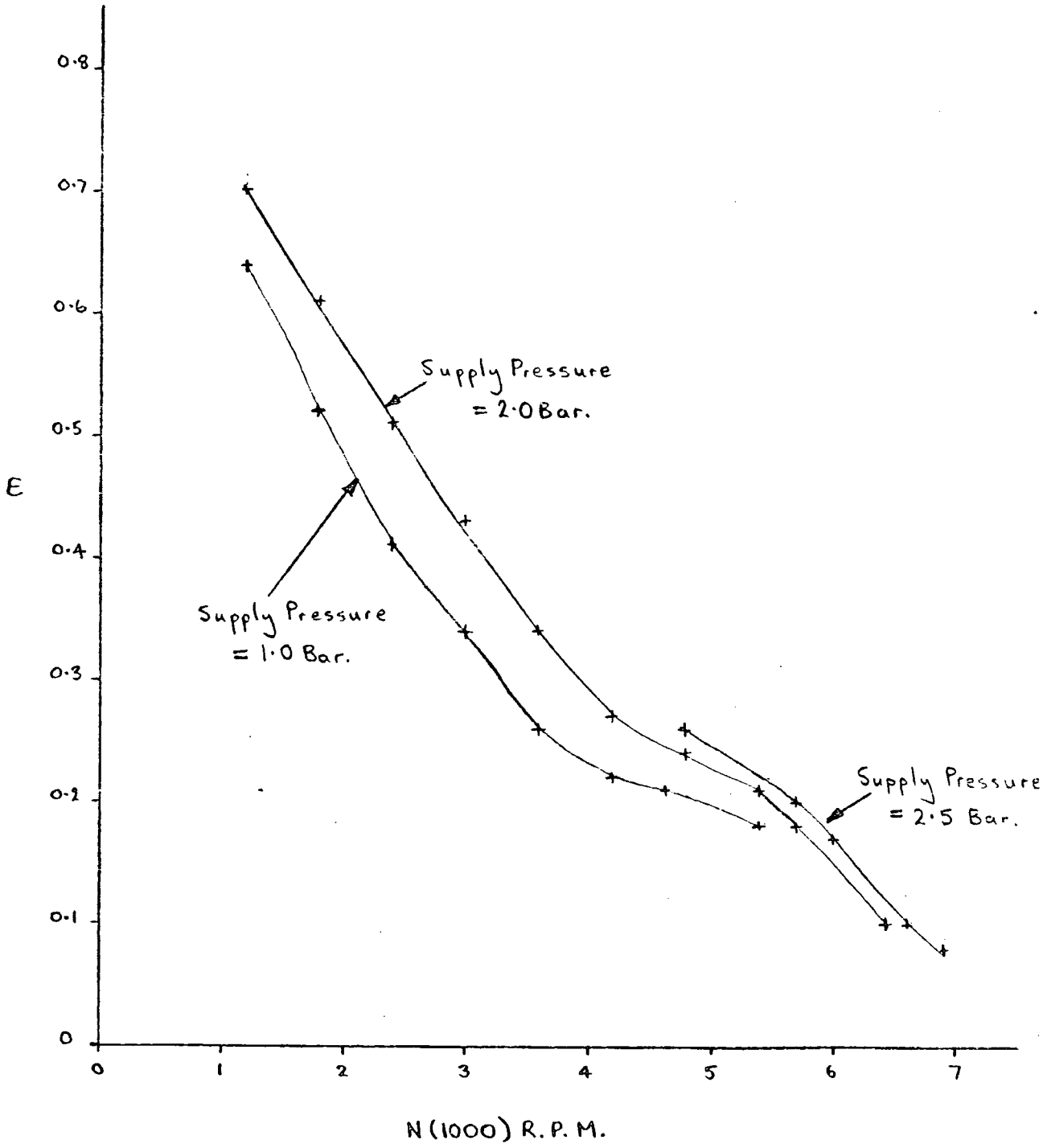

Fig. (8d) Plot of ε versus N for the 3" Diameter Bearing Rig.

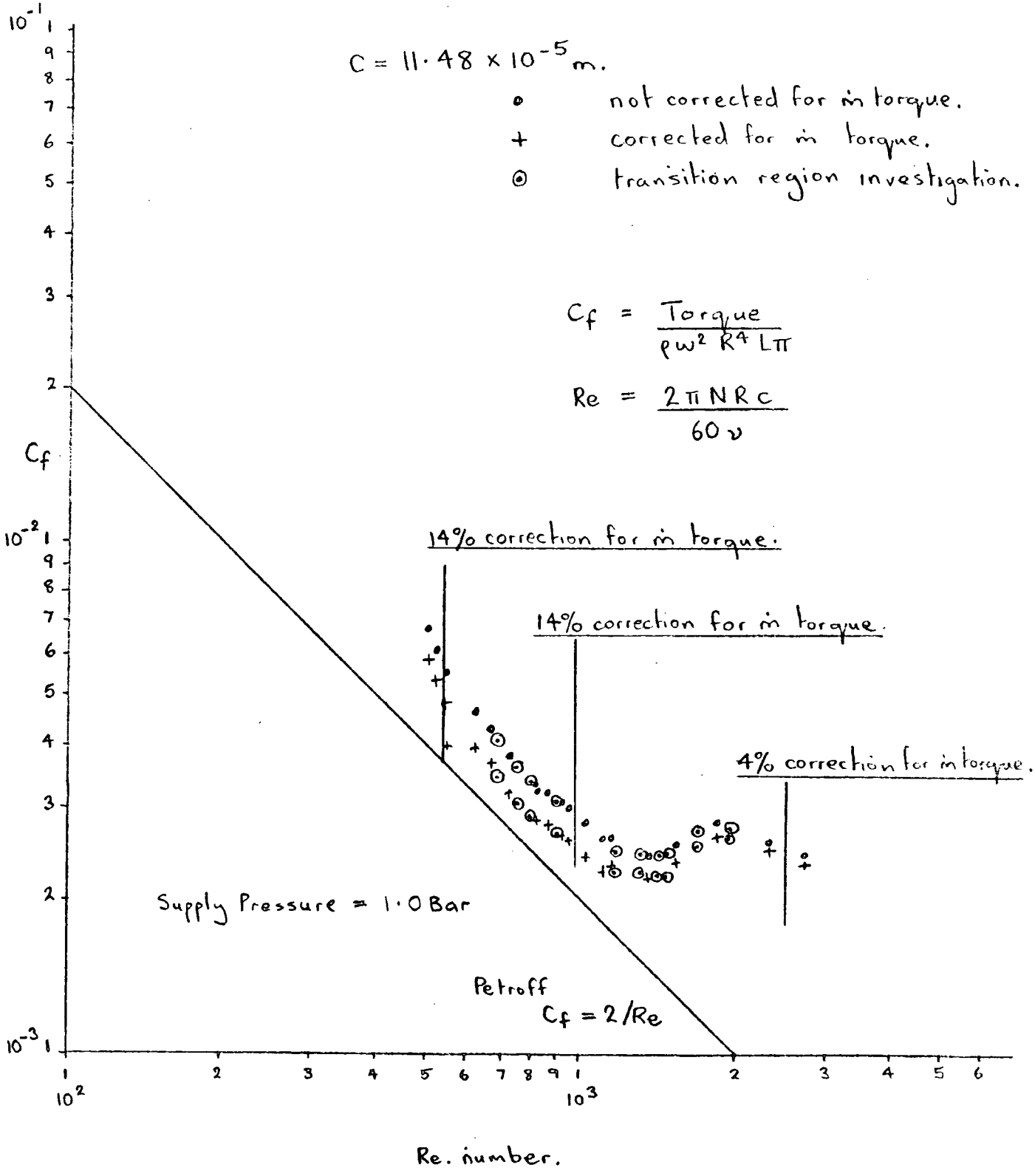

Fig.(8e) Plot of C_f versus Re for the 3" Diameter Bearing Rig.

Fig. (8f) is a plot of the 2.0 bar supply results. This time the angular momentum torque in the laminar regime accounts for approximately 19% of the total frictional torque from the bearing. For both supply pressures the angular momentum torque accounts for approximately 4-5% of the torque when the bearing is running with a turbulent film. Fig. (8g) is a summary plot of the results obtained for the three supply pressures used. Again the plots show very little scatter.

The 2.5 bar supply pressure was used at high Reynolds numbers so as to extend the range of running of the bearing with a turbulent film as far as possible.

The deceleration times recorded for the liquid film bearing are for 10 revolutions and 20 revolutions.

The departure of the 'corrected' results plots in Figs. (8e), (8f), and (8g) from the Petroff theoretical line can be explained at low Reynolds numbers by the eccentricity effect and at high Reynolds numbers by transition and turbulent films causing increased rotational resistance. The plots in Figs. (8h) and (8i) are the ratios of,

$$\frac{T_{\text{experimental}}}{T_{\text{theoretical (laminar torque at a given } \varepsilon)}}$$

i.e.

$$\frac{T_{\text{experimental}}}{\dfrac{2\pi R^3 L \mu \omega}{c\,(1-\varepsilon^2)^{\frac{1}{2}}}}$$

versus rotational Reynolds number. For both supply pressures, the laminar regime, low Reynolds number results, agree well with the theoretical line. The marked departure of the results from the theoretical line show first the onset of Taylor vortices and then the onset of turbulence. It is also evident that the use of a pressurised lubricant supply appears to have suppressed cavitation as the laminar regime results lie slightly above the theoretical plot and not below as would be expected with cavitation.

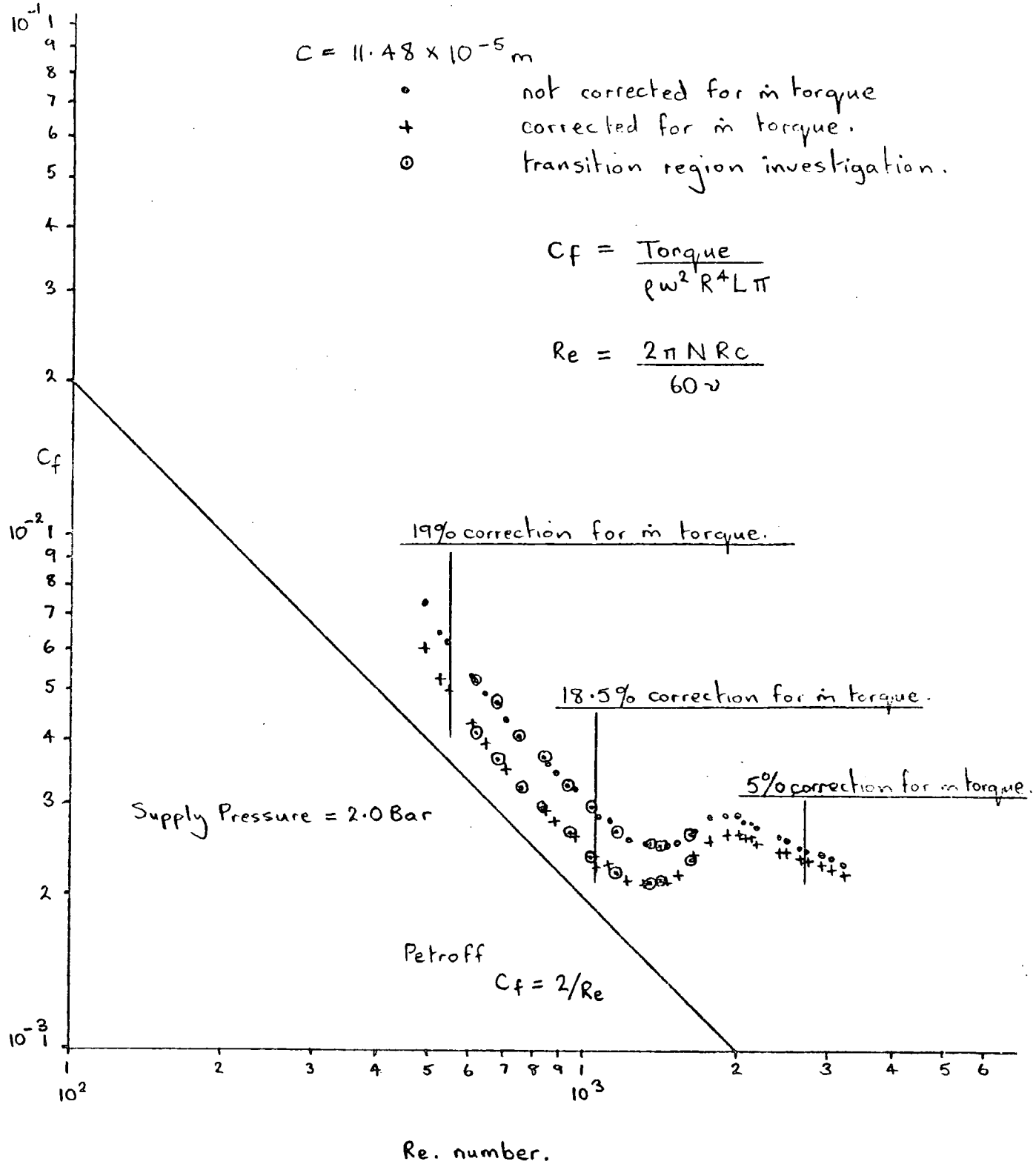

Fig.(8f) Plot of Cf versus Re for the 3" Diameter Bearing Rig.

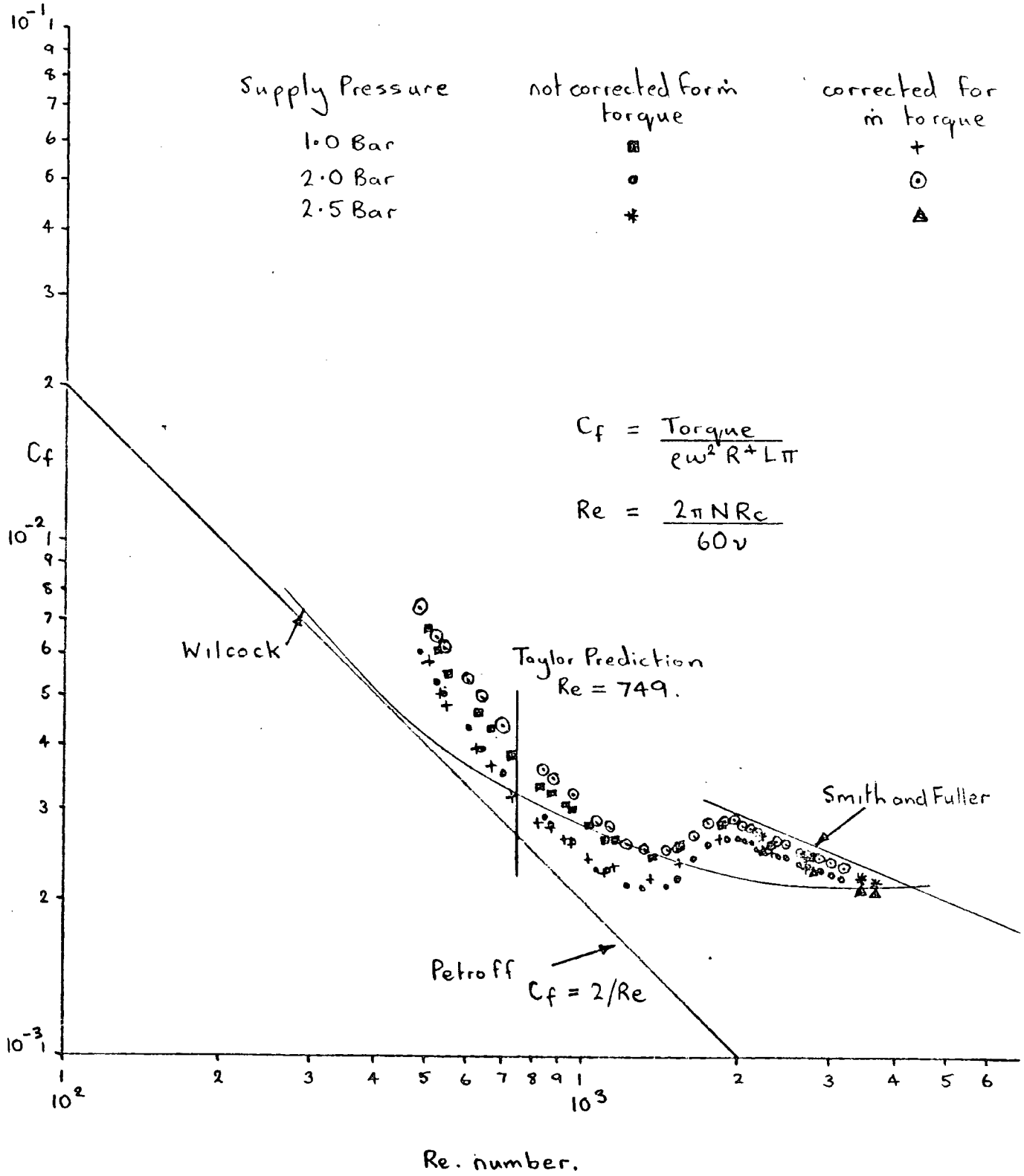

Fig. (8g) Plot of C_f versus Re for the 3" Diameter Bearing Rig.

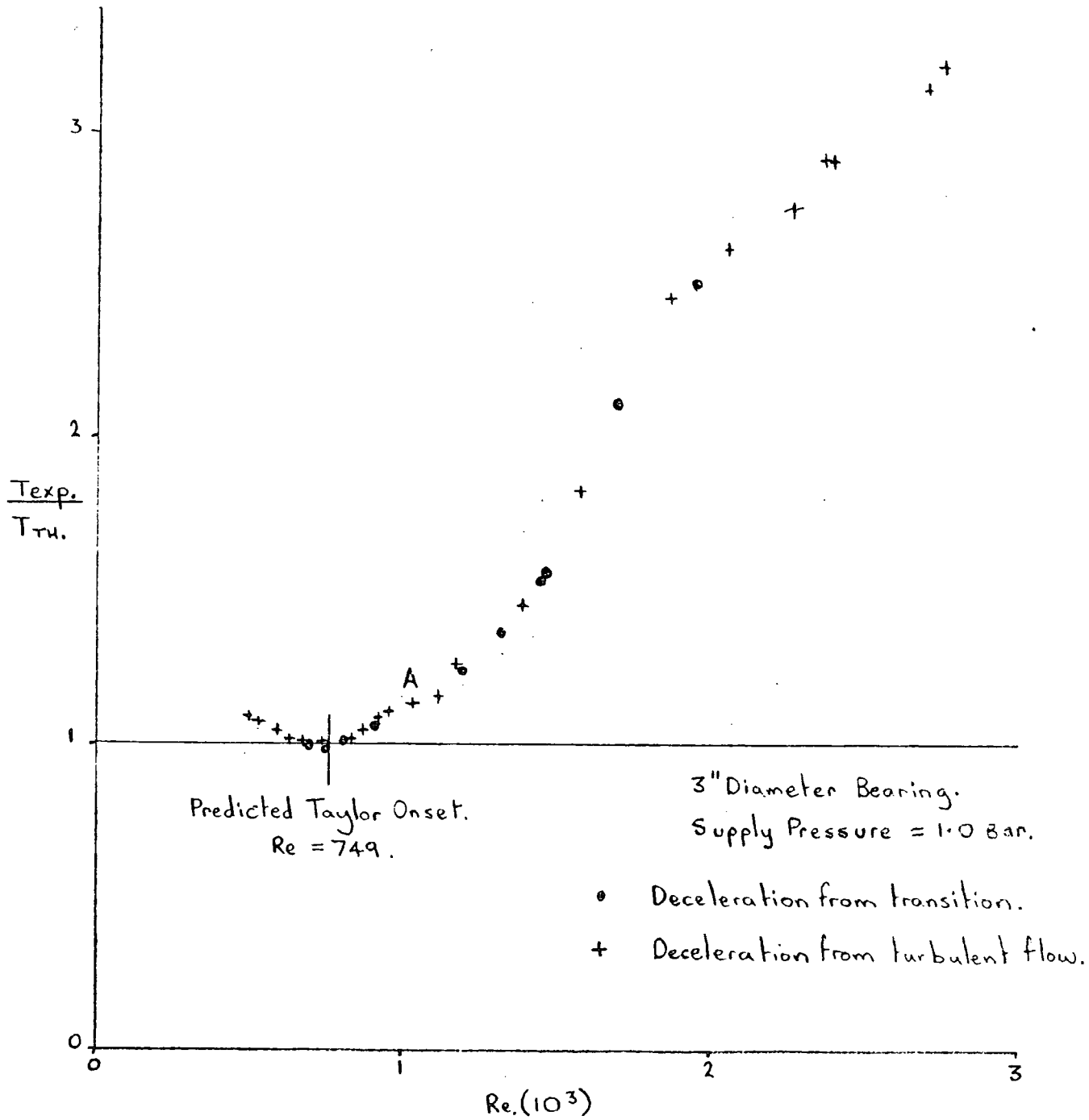

Fig(8h) Plot of Texp./Trh. versus Re.number.

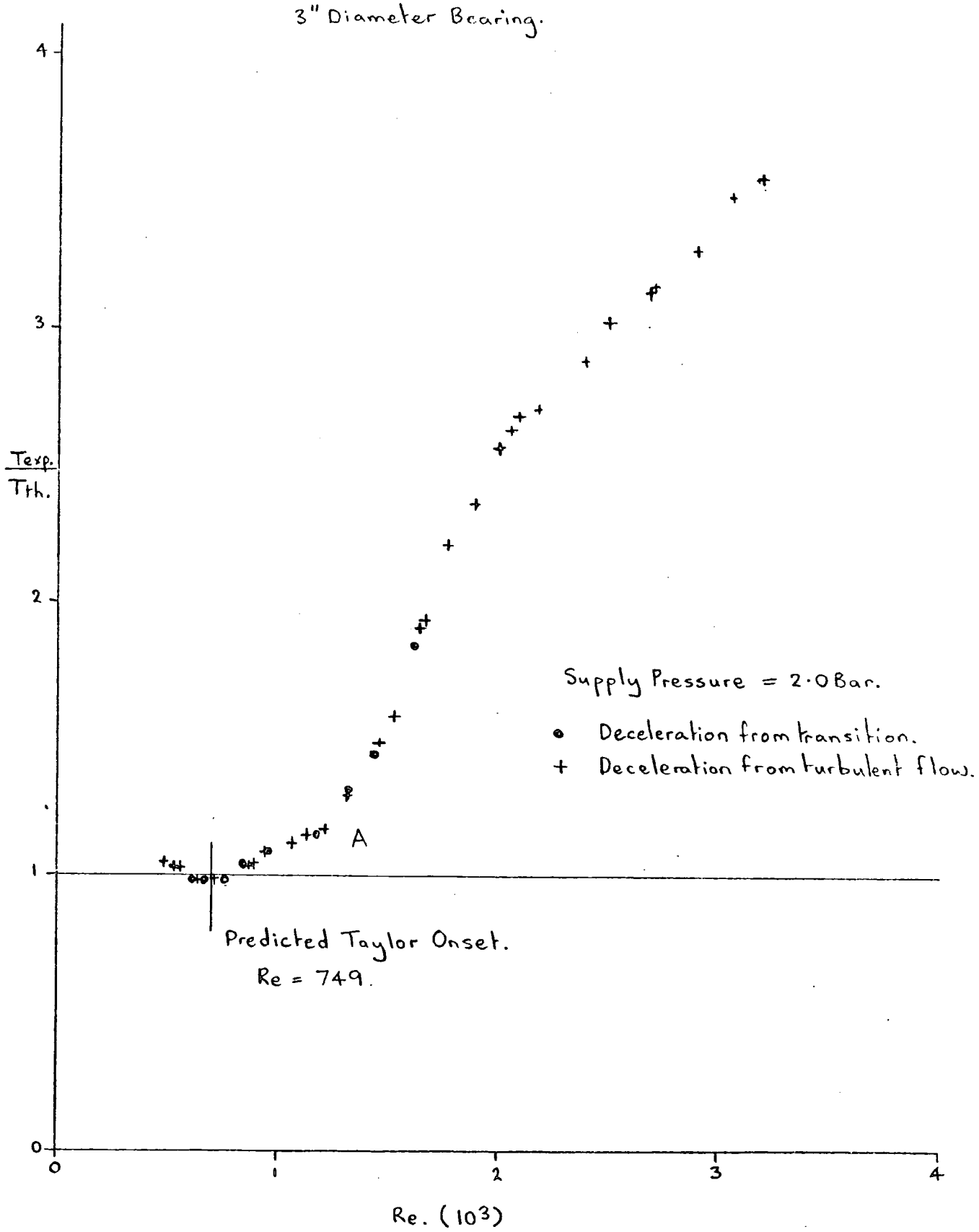

Fig. (8i) Plot of Texp. / Tth. versus Re. number.

In Fig. (8g), the experimental results lie very close to those found by Smith and Fuller (6) in the turbulent regime. As mentioned previously, the 3" diameter bearing used in the experimental work in this thesis was very similar in dimensions to the bearing used by Smith and Fuller. The departure of the results from the Smith and Fuller plot could possibly be explained by the fact that the Smith and Fuller results were not corrected for angular momentum torque. As no details of the drainage system or flow rates were published by Smith and Fuller, it is not possible to discuss this further. However, it was commented that a pressurised feed was used to suppress cavitation which could mean relatively high flow rates and high angular momentum torque. It is also interesting to note that the correction of the results from the present 3" rig also changes the gradient to a small degree in the turbulent regime. This shows that care must be exercised in the extrapolation of turbulent plots which have not been corrected for angular momentum torque.

Taylor Vortices

In Chapter 1 the occurence of Taylor vortices in bearings was discussed in detail. Mention was made of their occurrence, their suppression and delay in formation. The factors which were found to influence the onset of Taylor vortices were eccentricity, clearance ratio, axial flow and annulus length. The only factor of importance as far as the present experimental work is concerned is eccentricity. The effect of axial flow is discounted in these experiments as the maximum Axial Reynolds number encountered is considerably lower than the value of 400 above which the axial flow is found to have significance (Cole (10) (11)). For the 3" bearing rig the order of magnitude of the maximum Axial Reynolds number in the region of transition is given by:

$$Re_{axial} = \frac{\rho V_x 2c}{\mu}$$

$$V_x = \frac{\dot{m}}{2\pi\rho Dc}$$

$$Re_{axial} = \frac{\dot{m}}{\pi D \mu}$$

where Re_{axial} = Axial Reynolds number

c = radial clearance

μ = dynamic viscosity

D = bearing diameter

$\dot{m}$ = lubricant mass flow rate

ρ = lubricant density

V_x = lubricant axial flow velocity

For the 3" bearing rig with a 2 bar lubricant supply pressure, operating in the region of transition:

$D = 7.62 \times 10^{-2}$

$\mu = 10^{-3}$ N sec/m^2

$\dot{m} = 5 \times 10^{-2}$ Kg/sec

substitution gives $Re_{axial} = 209 \ (< 400)$

The other factors, clearance ratio and annulus length, are related to large clearance experimental rigs, such as those used in visual studies of Taylor vortices and are not relevant to the present experimental work.

It is found that there is large scale disagreement in the published experimental results concerned with the effect of eccentricity. Explanations have been presented to account for the spread in the results, but to date no satisfactory solution has been put forward. Generally, but not always, it is found that eccentricity has a stabilising effect on a bearing film and the Reynolds number at which Taylor vortices occur is

found to be greater than the value predicted by the Taylor expression, equation (1:1),

$$Re = 41.1 \sqrt{R/c}$$

The methods commonly used by experimentalists to investigate Taylor vortices are frictional torque measurements and visual observations. The difficulties encountered with these methods are discussed in Chapter 1. The frictional torque measurement technique is generally considered as the most reliable method. With reference to the frictional torque results presented in this thesis, the effect of eccentricity appears to increase the Reynolds number at which Taylor vortices appear or more exactly at which they disappear, when decelerating. With reference to Figs. (6i), (6j), (6k) and Figs. (8h) and (8i), the onsets of Taylor vortices occur at higher Reynolds numbers than the theoretical Taylor vortex predictions indicated on the graphs. The onsets are marked by the departure of the experimental plots from the horizontal zero eccentricity laminar flow lines. The onsets are increased by between 9% and 22% for eccentricities in the range 0.14 to 0.26. It is difficult to determine accurately where the onsets occur as the plots meet the laminar plot tangentially. The discontinuities of the plots in the transition region could possibly be accounted for by various 'wavy modes' superimposed on the Taylor vortices. To investigate Taylor vortices more fully would require a mixture of visual and torque determinations over a short deceleration range. This could be achieved with the aid of an air drive system which could be disconnected and reconnected very quickly with deceleration timings being taken whilst the bearing is not being driven. From graphs, Figs. (6g), (6k) and Figs. (8e), (8f) and (8g) it is evident that if account is not taken of the angular momentum torque then the onset of Taylor vortices detected by frictional torque methods can be confused by the increase caused by the throwing of the lubricant. This possible confusion is probably greater

with large clearance rigs where there is a possibility of large flows and therefore a large angular momentum torque. Also with a large clearance rig, this is made worse by the fact that the Petroff torque will be relatively smaller with the angular momentum torque possibly dominating.

Transition Investigations

It was reported in Chapter 1 that Jackson (12) had investigated a transition discontinuity effect in bearing frictional torque. He noticed that frictional torque measurements taken in the transition region as the speed of the shaft was increased, were different from those taken in the same region as the bearing was slowed down from the turbulent regime. The differences were that discontinuities observed on a torque Reynolds number plot as the speed was increased were not found as the speed was decreased. However it was pointed out by Jackson that this effect was only noticeable at zero eccentricity and that for a small increase in eccentricity the effect disappears,

i.e. for $\varepsilon > 0.1$

During the experimental work with the 3" diameter rig a series of decelerations was timed with the starting Reynolds number at various positions in the transition region. The shaft was not first run into the turbulent regime, but only to a selection of Reynolds numbers in the transition region. The purpose of these experiments was to investigate the relationship of the frictional torque in the bearing to the history of the flow. The results obtained are tabulated in Tables (10:35) to (10:40) and are plotted in Figs. (8e), (8f), (8h) and (8i). These plots indicate that there is no apparent difference in the rotor torques, whether the rotor is first driven into the turbulent regime, or well into the transition region, or only slightly into the transition region.

In other words it does not appear to matter where the deceleration is started, the torque measurements are just the same. This is an important result for the experimental investigations of the transition region frictional torque reported in this thesis. The starting point of a deceleration run, either in the turbulent or transition region does not affect the torque measurements taken.

Discontinuities in the plots of frictional torque in the transition region are in fact apparent indicated as 'A' in Fig. (6k), (8h) and (8i). These may indicate the onset of a wavy mode on the Taylor vortices. The appearance of these discontinuities is not affected by the starting point of the deceleration, whether in the transition region or not, and cannot be attributed to experimental scatter as they are repeatable.

The Angular Momentum Torque

The experiments with the 2" and 3" bearing rigs clearly indicate the magnitude of the angular momentum torque. As much as 19% of the total rotor torque can be attributed to the throwing of the lubricant from the shaft. This effect has not been reported fully before in connection with liquid bearings. It was pointed out in Chapter 3 that the angular momentum torque for a liquid bearing for a given size and flow rate is twice that for an air bearing, i.e. the expression for an air bearing is,

$$T = \frac{\dot{m} R^2 \omega}{2}$$

and for a liquid bearing is, $T = \dot{m} \omega R^2$.

When the total liquid bearing torque measurements are corrected for the angular momentum torque, the experimental plots in Chapters 6 and 8, agree favourably with the theoretical predictions. This indicates that the theoretical prediction for the angular momentum torque is of the right order and is significant.

Turbulence: General Discussion

Very little has been published concerning the change from a transition to a turbulent film. It is generally agreed that turbulence occurs at a Reynolds number equal to twice the critical Reynolds number for the onset of Taylor vortices. That is with the shaft rotating and the bush static. With reference to the experimental work reported in this thesis, the prediction does not appear to be a general criterion for turbulence. Further disagreement is apparent when the 2" rig results are compared with those from the 3" rig. Although the clearance ratio for both rigs is approximately 0.003, the 2" rig indicates an onset to turbulence at a Reynolds number of approximately 1650 and the large rig, around 2000. These values do not appear to be affected by supply pressure, flow rate or eccentricity.

Turbulence: Theoretical Considerations

For laminar film lubrication, Reynolds equation is of the form,

$$\frac{\partial}{\partial x}\left(h^3 \frac{\partial p}{\partial x}\right) + \frac{\partial}{\partial y}\left(h^3 \frac{\partial p}{\partial y}\right) = 6 \mu U \frac{\partial h}{\partial x}$$

The equation is derived from the Navier-Stokes equations of motion and the continuity of flow condition. For the x coordinate direction, the Navier-Stokes equation of motion is,

$$\underbrace{\rho \frac{\partial u}{\partial t} + \rho u \frac{\partial u}{\partial x} + \rho v \frac{\partial u}{\partial y} + \rho w \frac{\partial u}{\partial z}}_{\text{fluid inertia}} = \underbrace{-\frac{\partial p}{\partial x}}_{\text{pressure}} + \underbrace{\mu \frac{\partial^2 u}{\partial z^2}}_{\text{viscous}}$$

where u, v and w are the velocities in the coordinate directions. Body forces have been omitted and the sources of the other terms representing forces per unit volume are indicated. In the derivation of Reynolds equation the main assumption is that the flow takes place in a thin film. The flow is also considered to be laminar and the fluid inertia forces are neglected compared with viscous forces.

At high values of Reynolds number the laminar film can degenerate into turbulence. A transition region exists between the two modes of flow. The Navier-Stokes equations can be adapted for turbulent flow by considering each parameter in them, as having a time mean value, with a fluctuation about this mean value. As such, laminar flow is one in which the fluctuations are negligible compared with the mean overall flow. The turbulent pressure for example can be represented by,

$$p = \bar{p} + p'$$

where p = pressure, $\bar{p}$ = time mean pressure and p' is the pressure fluctuation.

For the x coordinate the equations become,

$$\underbrace{\bar{\rho}\frac{\partial \bar{u}}{\partial t} + \bar{\rho}\bar{u}\frac{\partial \bar{u}}{\partial x} + \bar{\rho}\bar{v}\frac{\partial \bar{u}}{\partial y} + \bar{\rho}\bar{w}\frac{\partial \bar{u}}{\partial z}}_{\text{mean fluid inertia}} = \underbrace{-\frac{\partial \bar{p}}{\partial x}}_{\text{pressure}} + \underbrace{\mu\frac{\partial^2 \bar{u}}{\partial z^2}}_{\text{viscous}} + \underbrace{\frac{\partial}{\partial z}\left(-\bar{\rho}\,\overline{u'w'}\right)}_{\text{turbulent}}$$

In the above equation, the term giving rise to the turbulent stresses derives from the fluctuations connected with fluid inertia. For laminar flow the turbulent stresses and the fluid inertia effects can be neglected in comparison to the viscous stresses. With increasing Reynolds number the fluid inertia stresses start to become significant. In a journal bearing as discussed in Chapter 1, centrifugal inertia can lead to a Taylor vortex flow. For a further increase in Reynolds number the onset of turbulence will be experienced. In this region of transition, little is known about the balance of stresses. In fully established turbulent flow it is generally assumed that turbulent stresses dominate although this is by no means certain. At very high Reynolds numbers, the mean fluid inertia term becomes more significant in comparison with the turbulent stresses. No theoretical analysis of turbulent flow with the effect of mean fluid inertia included, has as yet been published.

Three turbulent lubrication theories are available at the present time. The earliest approach was developed by Constantinescu (1959) (17),

who used the concept of Prandtl's mixing length. Later, Ng and Pan (1965) (18), used the concept of eddy viscosity, to represent the turbulent stresses, in terms of the mean velocity gradient. Hirs (1972) (19), used a more novel approach; he used what he calls a bulk flow approach, which requires no physical representation of the turbulent transport mechanism. The eddy viscosity approach is generally considered to be more preferable.

The first two of the above theories lead to the same form of Reynolds equation, which is,

$$\frac{\partial}{\partial x}\left(\frac{h^3}{k_x \mu}\frac{\partial p}{\partial x}\right) + \frac{\partial}{\partial y}\left(\frac{h^3}{k_y \mu}\frac{\partial p}{\partial y}\right) = \frac{U}{2}\frac{\partial h}{\partial x}$$

where both k_x and k_y are constants related to the Reynolds number by,

$$k_{x,y} = 12 + f(Re)$$

The two theories predict differing values of k_x and k_y. The values obtained by Constantinescu are,

$$k_x = 12 + 0.0260\ (Re)^{0.8265}$$

and $$k_y = 12 + 0.0198\ (Re)^{0.741}$$

Constantinescu also derived a relationship for the shearing stress acting on the surfaces,

$$\tau = -\frac{\mu U}{h}\bar{\tau}_c \pm \frac{h}{2}\frac{\partial p}{\partial x}$$

where $\bar{\tau}_c = 1 + 0.0023\ (Re)^{0.855}$ $\qquad (\bar{\tau}_c = \tau_c h/\mu U)$

where τ = shear stress

τ_c = Couette surface shear stress

The values obtained by Ng and Pan for k_x and k_y are,

$$k_x = 12 + 0.00136\ (Re)^{0.9}$$

$$k_y = 12 + 0.0043\ (Re)^{0.96}$$

The values obtained for $\bar{\tau}_c$ are,

$Re > 10{,}000$

$$\bar{\tau}_c = 1 + 0.00232\ (Re)^{0.86}$$

$$\text{Re onset of turbulence} < Re \leqslant 10{,}000$$

$$\bar{\tau}_c = 1 + 0.00099\,(Re)^{0.96}$$

Turbulence: Comparison of Experimental Results and Theoretical Predictions

Fig. (8j) is a plot of the experimental results obtained with the 3" diameter rig operating with a turbulent film. Also indicated on the plot are the theoretical predictions of Constantinescu and Ng and Pan. Close agreement is apparent between the experimental results from the 3" diameter bearing and the Ng and Pan plot. From the results a value for $\bar{\tau}_c$ was obtained which is,

$$\bar{\tau}_c = 1 + 0.001643\,(Re)^{0.9088}$$

An important point to note is that even though the constant and exponent have values roughly midway between the values obtained by Constantinescu and Ng and Pan, the plot of $\bar{\tau}_c$ is above both of theirs and not a mean value as may be expected.

The turbulent theories rely on the determination of constants, from experiments with flow both in pipes and between stationary and sliding plates, to be used in their equations. The experimental work from which these constants are obtained appears to be limited. However the turbulent theory constants could be obtained from bearing frictional torque measurements derived in the manner described in this thesis. An advantage of this would be that the information would be taken directly from bearings and not have to be derived from general flow situations. This more accurate method of determination would then give more reliable theoretical predictions.

It was intended at the outset of the experimental work with the 3" bearing rig, to investigate the frictional torque in the turbulent regime at higher Reynolds numbers than those actually achieved. The range of Reynolds number investigated was foreshortened, to a degree, by the early

3" Diameter Bearing Rig.

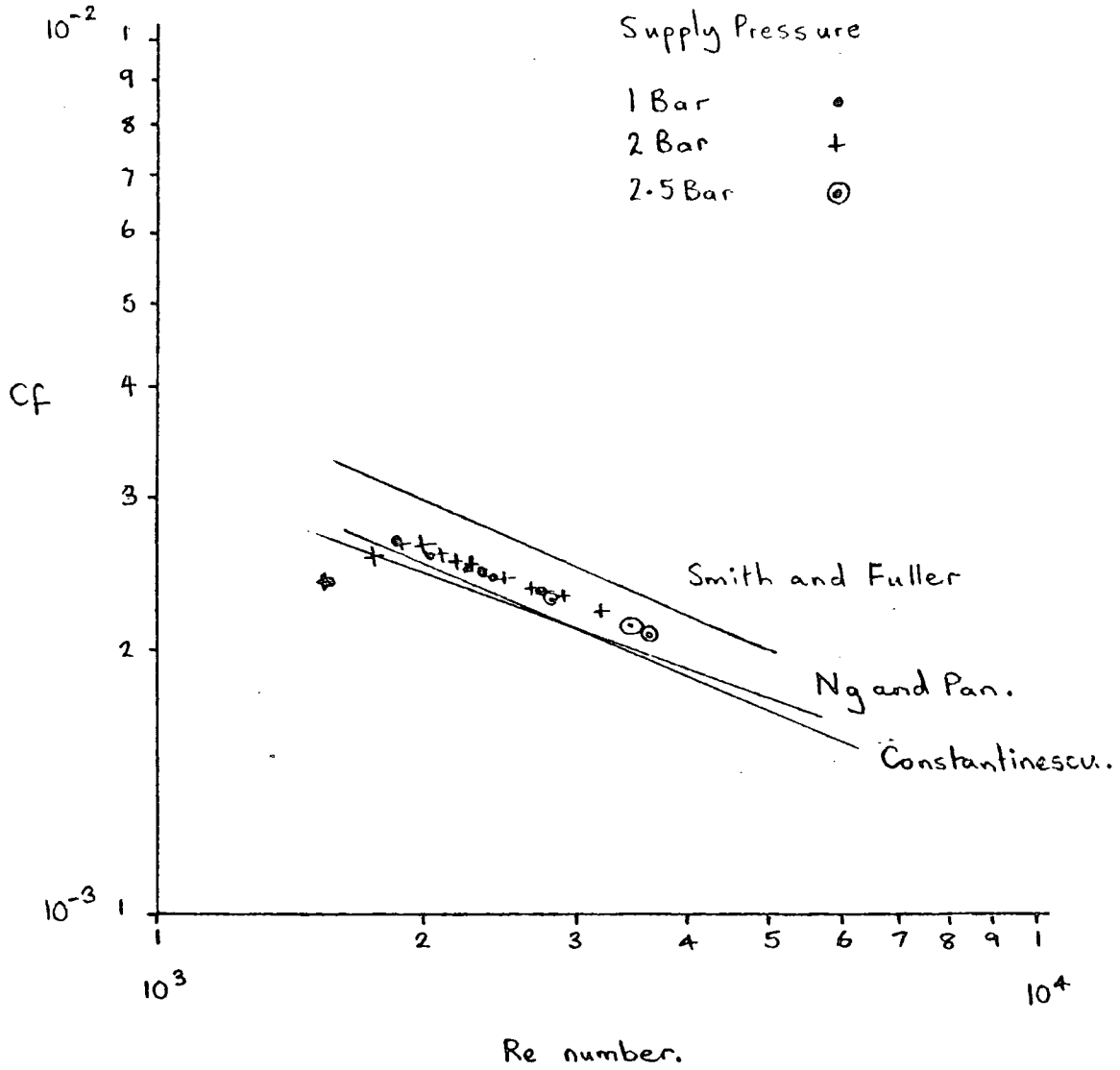

Fig.(8j). Plot of experimental results and theoretical predictions for a turbulent lubricating film.

onset of what appeared to be half speed whirl, at a speed significantly lower than predicted. The whirl of the rotor was not of a conical nature as this had been successfully prevented by gyroscopic stabilization from the discs, reference Chapter 4, but of a translational form. Attempts to suppress this instability were unfortunately unsuccessful. My more recent studies of disc vibration lead me to believe that the instability may actually have been of a more complex form, with possibly a combined instability between disc, shaft and bearing film.

CHAPTER 9

CONCLUSIONS

It has been demonstrated in the experimental work reported in the previous chapters that the electronic timing system, described in Chapter 5, is a very useful tool for investigating the frictional torque in bearings. The circuit consists of only two good timer counters and less than £10 (1976 prices) worth of electronic 'chips'. Although the circuit was designed, built and used between 1974 and 1976, because of the simplicity of the circuit, more recent advances in microprocessors, would not make it any cheaper.

From the experimental work reported, it has been shown that with the aid of the timing circuitry, the frictional torques experienced by a rotating shaft in a journal bearing, can be identified easily and accurately. Direct measurements of rotor torque, such as these, have not been possible in the past.

The usual method of investigating frictional torque in journal bearings, is to measure the torque which appears on the stator. The apparatus generally consists of a rotor, which is mounted in two slave bearings, one at each end, and a centrally positioned 360^{o} liquid bearing. The central bearing is loaded by means of a hydrostatic pad under the bush. The bush, which is otherwise free to rotate, is refrained from doing so by a tension gauge on its periphery. As the rotor is revolved measurements are taken from the restraining tension gauge at different speeds. From these results the bearing frictional torque can be obtained as a function of the rotational speed. Sources of error in this method of determination stem from restrictions to bearing motion, caused by the lubricant supply pipework and misalignments in the hydrostatic pad loading system. Both of these decrease the accuracy of the tension gauge readings. The author's

experience with this form of rig is that it is difficult to obtain reliable results from it.

An important feature of the present experimental work is that it was carried out with bearing rigs having clearance ratios which are commonly found in industry.

The rigs were designed such that cavitation of the lubricant film was suppressed and the bearings would run full. Suppression was achieved with the aid of a pressurised supply of lubricant. The purpose of this was to simplify the experimental work and to eliminate the necessity for correcting the frictional torque measurements for a cavitated region. The close agreement between the experimental plots of the present work and the theoretical predictions for a bearing running full, indicates that suppression has been successful.

In the discussion of previous experimental work (Chapter 1) no mention was made of the magnitude of the angular momentum torque. This is because the effect has not been reported in connection with liquid bearings. The effect has been reported only in connection with experimental work with air bearings, reference Bennett and Marsh (13). The magnitude of the torque for an air bearing is, for a given flow rate and speed, half that for a liquid bearing with the same exhaust radius. The reason for this being that the air, on leaving the air bearing, has a mass averaged tangential velocity of $\frac{\omega R}{2}$, whereas all of the lubricant exiting from a liquid bearing, flows along the shaft and gains the shaft velocty, ωR, before being thrown off. The momentum torque for a liquid bearing is therefore, $\dot{m}\,\omega\,R^2$, as opposed to that for an air bearing, $\dot{m}\,\omega\,R^2/_2$. The velocity of the liquid being thrown from the rotor depends on the radius of the rotor and not only on its rotational frequency. With an air bearing

the exhaust radius of the bearing is of prime importance whereas with a liquid bearing, the radius at which the liquid is thrown from the rotor, which may be greater than the bearing radius, is of more significance. The 'throwing' radius of the rotor can be several times the magnitude of the bearing radius, for example, if discs are present. The magnitude of the angular momentum torque can therefore be greatly magnified by the lubricant being thrown from these larger radii. Throughout the present experimental work steps were taken in initial design, by stepping down the shaft radius, as it leaves the bearing, to ensure that the lubricant was thrown at the bearing radius.

For the 3" diameter rig, operating with a laminar film, approximately 19% of the total frictional torque of the rotor was attributable to the throwing of the lubricant. For a bearing operating at low Reynolds numbers, with a laminar film, the rotor torque plots, when corrected for momentum torque and eccentricity, lie very close to theoretical predictions. The agreement is good for both of the rigs, this indicates that the predicted magnitude of the correction for angular momentum torque is of the right order. The magnitude of the angular momentum torque has also been confirmed by experiments with air bearings as discussed in Chapter 2.

The relative importance of the angular momentum torque is less for oil bearings than it is for water bearings, the reason being that the viscous torque is significantly greater for the higher viscosity of oils. Considering the total torque expression, for a given laminar film bearing, the viscous torque is proportional to the viscosity of the lubricant and the momentum torque is proportional to its density. The density of oils varies little for a large range of different viscosity oils. Therefore for a given flow rate the magnitude of the viscous torque can increase

many fold to that of the momentum torque. With low viscosity lubricants the angular momentum torque contributes more significantly to the total torque on the rotor. Such fluids are being increasingly used in industry. The use of water as a lubricant is also becoming more of an accepted practice and manufacturers of large steam turbines are known to be considering its use. Water is also a popular choice for bearing research rigs. When using low viscosity lubricants in bearings omission of the consideration of the angular momentum torque can lead to large errors in the predicted rotor torque.

From the results obtained from the 2" and 3" rigs the following observations can be made. For a laminar, low Reynolds number film, close agreement is apparent, with the theoretical Petroff predictions, which are indicated on the torque plots by the line, $Cf = 2/Re$. For the turbulent, high Reynolds number film, there is good agreement between the experimental results of Smith and Fuller and those of the present work. In the transition region, the experimental plots indicate that the onset of Taylor vortices is delayed by the eccentric running of the shaft in the bearing. With reference to Chapter 1, many experimental investigations of this phenomenum have been reported and much disagreement is apparent in the published results. Some of this disagreement can be explained by the fact that no account has been taken of the angular momentum torque in the frictional torque determinations of the onset of vortices. If the frictional torque is measured from the stator as described previously in this chapter, the results obtained will be in error for the neglect of the angular momentum torque only if the exhausting lubricant is collected by 'catchers' which are attached directly to the bearing. If the spent lubricant from the bearing is thrown from the rotor and drained from catchers attached directly to the bearing, the

angular momentum, of the lubricant, in this case would be transferred to the catchers and appear as an increased measured total frictional torque. If the catchers, however, are not attached directly to the bearing, the momentum torque will not be transferred to the bearing. This fact was demonstrated by a final year project student at Durham University who carried out experiments using Hampson's rig (16). This rig was of the type mentioned above with frictional torque measurements being taken from the stator. Hampson's measurements were taken with catchers attached to the stator. The student investigated the effect of mounting the catchers independently from the stator and identified a change in the magnitude of the frictional torque.

A series of experiments has been reported in Chapter 8 in connection with the starting point of a deceleration timing run. It was found that whether the deceleration started in the turbulent region or in the transition region, the measured frictional torque was unchanged. The frictional torque on the rotor was independent of the previous operating history of the bearing. A similar investigation was reported by Jackson (12). He reported that in the transition region, discontinuities in the plot of measured torque versus Reynolds number, which were apparent with increasing Reynolds number, were not found with decreasing Reynolds number. Jackson explained the occurrence of these discontinuities by the appearance of the onset of a wavy mode superimposed on the Taylor vortices. It was pointed out, however, that this phenomenon was only observable for a concentrically running bearing and that for only a small increase in eccentricity the effect disappeared.

In Chapter 8 the application of frictional torque measurements to test theories for turbulent lubrication was discussed. Close agreement

was apparent between the theoretical predictions of Ng and Pan and the results from the 3" diameter rig, for the frictional torque for a bearing operating with a turbulent lubricating film. The turbulent theories rely on the experimental determination of constants for substitution into theoretical predictions. The accuracy of determination of these constants greatly effects the validity of the theoretical predictions. The accuracy of the present method of determination of frictional torque constants, can therefore be of significant help in future turbulent lubrication investigations.

Although the work in this thesis describes the use of the deceleration timing circuit applied to frictional torque determination in journal bearings, its use can be easily extended to other experimental fields. Since 1977, when the experimental work reported in this thesis was terminated, the deceleration method has been successfully used in turbomachinery experiments performed at Durham University.

It is hoped that the work reported in this thesis, will aid the designer and the researcher to more accurate measurement and knowledge of friction in journal bearings.

CHAPTER 10

EXPERIMENTAL RESULTS: TABULATIONS

Notation:

t_1	time in seconds for N pulses
t_2	time in seconds for 2N pulses
δ	$(t_2 - 2t_1)$, seconds
N	speed, R.P.M.
N_o	initial speed, R.P.M.
N_∞	self drive equilibrium speed
ReN^o	rotational Reynolds number
$\dot{m}$	lubricant mass flow rate
$\dot{m}_c$	non-dimensional correction for angular momentum torque
c	bearing radial clearance, metres
ϵ	eccentricity
ratio $\frac{T_{exp}}{Tth}$	$\frac{\text{experimentally measured frictional torque}}{\text{theoretical frictional torque corrected for } \epsilon}$

For purposes of convenience the deceleration rates are recorded in R.P.M./sec

For the disc drag determination:

α_T	total deceleration rate including support air bearing drag, for windage losses, R.P.M./sec
α_c	correction for air bearing drag, R.P.M./sec
D	$\alpha_T - \alpha_c$ R.P.M./sec (disc drag)

For the liquid bearings:

dN/dt_1	total deceleration rate including windage and mass flow rate effects R.P.M./sec
DRAG	correction for windage losses R.P.M./sec
dN/dt	deceleration rate for bearing torque + mass flow rate torque R.P.M./sec

Cf_1 non-dimensional frictional torque uncorrected for mass flow rate torque

Cf non-dimensional frictional torque corrected for mass flow rate torque

Generally,

$$\alpha = \frac{N(\text{average})\ \delta}{t_1^2}$$

$$N(\text{average}) = \frac{60 \times \text{Number of revolutions in time } t_2}{t_2}$$

$$Cf = \frac{\text{Torque}}{\rho \omega^2 R^4 L \pi}$$

$$\dot{m}_c = \frac{\dot{m} R \omega^2}{\rho \omega^2 R^4 L \pi}$$

10. i) 2" Diameter Rig

10:1	Air Bearing corrections
10:2	Disc Drag decelerations
10:3	Mass flow rates
10:4	Eccentricities
10:5	Deceleration of 2 " Rig $c = 2.62\ 10^{-5}m$ supply pressure = 2.0 bar gauge
10:5(a)	T_{exp}/T_{th} tabulation for run 10:5
10:6 - 10:11(a)	Decelerations of the 2" Rig $c = 5.92\ 10^{-5}m$ supply pressures = 1.0 and 2.0 bar gauge
10:12 - 10:21(a)	Decelerations of the 2" Rig $c = 7.90\ 10^{-5}m$ supply pressures = 1.0 and 2.0 bar gauge

Table (10:1) Air Bearing Correction:

N R.P.M.	t secs	t secs	t secs	t secs	t_{ave} secs	$\log_e N/N_o$
4000	18.5	18.6	18.6	18.7	18.6	-0.2231
3000	42.3	42.7	42.8	42.8	42.7	-0.5108
2000	76.4	76.1	76.7	76.5	76.4	-0.9160
1000	132.5	133.3	133.6	132.8	133.1	-1.6094

N_o = 5000 R.P.M. Zero running speed 12 R.P.M.

Supply pressure = 4.0 bar gauge

All of the above times were measured with a stop watch. The speeds were measured with a stroboscope which was set to a particular speed, 5000 R.P.M. (accuracy ± ½%).

The theory concerned with the above air bearing correction determination can be found in Chapter 6.

Table (10:2) Disc Drag Decelerations

t_2 (50 revs) 10^{-6} secs	t_1 (25 revs) 10^{-6} secs	∂ 10^{-6}secs	N R.P.M.	α_T R.P.M./sec	α_c R.P.M/sec	DISC DRAG D R.P.M/sec
390506	195110	286	7682	57.72	3.27	54.45
414044	206871	302	7246	51.13	3.08	48.05
440373	220027	319	6812	44.89	2.90	41.99
464302	231980	342	6461	41.06	2.75	38.31
499575	249604	369	6005	35.57	2.55	33.02
508845	254235	375	5896	34.21	2.51	31.70
544435	272016	403	5510	30.01	2.34	27.67
585229	292394	441	5126	26.44	2.18	24.26
626120	312818	484	4791	23.70	2.04	21.66
658997	329244	509	4552	21.38	1.94	19.44
694263	346864	535	4321	19.22	1.84	17.38
727214	363326	562	4125	17.56	1.76	15.80
770717	385060	596	3893	15.65	1.66	13.99
812004	405686	632	3695	14.19	1.57	12.62
851204	425268	668	3524	13.02	1.50	11.52
892862	446078	706	3360	11.92	1.43	10.49
929863	464559	745	3226	11.14	1.37	9.77
970655	484934	787	3091	10.34	1.32	9.02
1017980	508571	838	2947	9.55	1.25	8.30
1066794	532952	890	2812	8.81	1.20	7.61
1111203	555130	943	2700	8.26	1.15	7.11
1213880	606408	1064	2471	7.15	1.05	6.10
1333863	666326	1211	2249	6.14	0.96	5.18
1418620	708648	1324	2115	5.58	0.90	4.68
1490826	744702	1422	2012	5.16	0.86	4.30
1567905	783189	1527	1913	4.76	0.81	3.95
1613159	805786	1587	1860	4.55	0.79	3.76
1667293	832808	1677	1799	4.35	0.77	3.58
1710153	854212	1729	1754	4.17	0.75	3.42
1752566	875387	1792	1712	4.00	0.73	3.27
1803763	900946	1871	1663	3.83	0.71	3.12
1849263	923662	1939	1622	3.69	0.69	3.00
1964640	981259	2122	1527	3.37	0.65	2.72
2013493	1005642	2209	1490	3.26	0.63	2.63
2071040	1034365	2310	1449	3.13	0.62	2.51
2140965	1069275	2415	1401	2.96	0.60	2.36
2225083	1111259	2565	1348	2.80	0.57	2.23
2365056	1181119	2818	1269	2.56	0.54	2.02
2441219	1219126	2967	1229	2.45	0.52	1.93
2516495	1256691	3113	1192	2.35	0.51	1.84
2656231	1326424	3383	1129	2.17	0.48	1.69
2735800	1366128	3544	1097	2.08	0.47	1.61
2818601	1407441	3719	1064	2.00	0.45	1.55

Table (10:3) 2" Diameter Bearing Mass Flow Rates

$c = 2.62 \times 10^{-5}$m Supply Pressure 2 Bar		$c = 5.92 \times 10^{-5}$m Supply Pressure				$c = 7.90 \times 10^{-5}$m Supply Pressure			
		1 Bar		2 Bar		1 Bar		2 Bar	
N R.P.M.	$\dot{m}(10^{-4})$ Kg/sec	N R.P.M.	$\dot{m}(10^{-3})$ Kg/sec	N R.P.M.	$\dot{m}(10^{-3})$ Kg/sec	N R.P.M.	$\dot{m}(10^{-2})$ Kg/sec	N R.P.M.	$\dot{m}(10^{-2})$ Kg/sec
993	7.35	1010	4.78	1160	10.2	1150	1.31	1025	2.22
2010	6.99	2200	4.18	2250	8.87	2160	1.10	2060	1.95
3025	7.00	3020	4.10	3020	8.35	3190	1.09	3060	1.92
4005	7.04	4250	4.08	4050	7.82	4025	1.09	4200	1.89
5008	7.15	5130	4.06	5020	7.66	5020	1.00	5160	1.67
		6350	3.95	6150	7.31	6050	0.89	6070	1.50
						6500	0.84	6950	1.38
								7500	1.30
								7950	1.24

Table (10:4) 2" Diameter Bearing: Eccentricities

$c = 2.62 \times 10^{-5}$m Supply Pressure 2 Bar		$c = 5.92 \times 10^{-5}$m Supply Pressure				$c = 7.90 \times 10^{-5}$m Supply Pressure			
		1 Bar		2 Bar		1 Bar		2 Bar	
N R.P.M.	ε	N R.P.M.	ε	N R.P.M.	ε	N R.P.M.	ε	N R.P.M.	ε
1000	0.27	1010	0.57	1010	0.7	1000	0.63	1000	0.72
2000	0.18	1980	0.35	1980	0.46	2000	0.44	2000	0.51
3000	0.13	3000	0.23	3000	0.31	3000	0.27	3000	0.34
5000	0.11	4000	0.19	4000	0.26	4000	0.17	4000	0.24
6000	0.10	5000	0.14	5000	0.21	5000	0.12	5000	0.17
		6000	0.14	6000	0.19	6000	0.07	6000	0.12
		7000	0.09	7000	0.15	6500	0.03	7000	0.05
								8000	0.03

t_1 (10 revs) 10^{-6} secs	t_2 (20 revs) 10^{-6} secs	N R.P.M.	∂ 10^{-6} secs	dN/dt_1 R.P.M./sec	DRAG R.P.M./sec	dN/dt R.P.M./sec	Re N^o	Cf_1 10^{-3}	$\dot{m}_c$ 10^{-3}	Cf 10^{-3}	ε
Table (10:5) 2" Diameter Bearing Decelerations: c = 2.62 x 10^{-5}m Supply Pressure = 2 Bar											
115299	230850	5198	252	98.54	24.88	73.65	372.2	5.43	0.01	5.42	0.11
140552	281461	4264	357	77.05	16.94	60.10	305.3	6.58	0.02	6.56	0.12
164000	328473	3653	473	64.25	12.27	51.97	261.6	7.75	0.02	7.73	0.12
192174	384984	3117	636	53.68	9.09	44.59	223.2	9.13	0.02	9.11	0.13
224573	450003	2667	857	45.31	6.87	38.45	191.0	10.76	0.02	10.74	0.14
261620	524390	2288	1150	38.45	5.35	33.10	163.9	12.58	0.03	12.55	0.16
304256	610057	1967	1545	32.83	4.10	28.73	140.9	14.76	0.03	14.73	0.18
354559	711206	1687	2088	28.03	3.16	24.86	120.8	17.38	0.04	17.34	0.21
416219	835313	1437	2875	23.84	2.41	21.43	102.9	20.66	0.05	20.61	0.23

Inlet Temperature = 20.05^oC
Outlet Temperature = 21.2^oC
Viscosity = 0.972×10^{-3} N sec/m^2

Re	Re Cf/2	ε (measured)	T_{exp}/T_{th}
2" Diameter Bearing Decelerations $c = 2.62\ 10^{-5}m$			
Table (10:5(a)) Supply Pressure = 2 Bar			
372.2	1.01	0.11	1.00
305.3	1.00	0.12	0.99
261.6	1.01	0.12	1.00
223.2	1.02	0.13	1.01
191.0	1.03	0.14	1.02
163.9	1.03	0.16	1.02
140.9	1.04	0.18	1.02
120.8	1.05	0.21	1.03
102.9	1.06	0.23	1.03

t_1 (10 revs) 10^{-6} secs	t_2 (20 revs) 10^{-6} secs	N R.P.M.	δ 10^{-6} secs	dN/dt_1 R.P.M./sec	DRAG R.P.M./sec	dN/dt R.P.M./sec	Re N^o	Cf_1 10^{-3}	$\dot{m}_c$ 10^{-3}	Cf 10^{-3}	ϵ
Table (10:6) 2" Diameter Bearing Decelerations: $c = 5.92\ 10^{-5}$m Supply Pressure = 1 Bar											
92886	185885	6456	113	84.55	37.61	46.94	1004	2.24	0.06	2.18	0.12
107183	214502	5594	136	66.23	28.74	37.48	870	2.38	0.07	2.31	0.14
123277	246725	4864	171	54.73	21.95	32.78	756	2.76	0.08	2.68	0.15
136818	273837	4382	201	47.05	17.94	29.12	681	3.02	0.09	2.93	0.16
173568	347438	3454	302	34.62	11.02	23.60	537	3.94	0.11	3.83	0.20
195515	391402	3066	372	29.84	8.80	21.04	476	4.45	0.12	4.33	0.23
215070	430596	2787	456	27.47	7.43	20.04	433	5.14	0.14	5.00	0.25
235551	471635	2544	533	24.44	6.38	18.06	396	5.55	0.15	5.40	0.28
267713	536094	2238	668	20.86	5.15	15.71	348	6.24	0.17	6.07	0.32
301015	602898	1990	868	19.07	4.17	14.90	309	7.48	0.20	7.28	0.36
338939	678983	1767	1105	17.00	3.40	13.60	275	8.66	0.23	8.43	0.40

Inlet Temperature = 20.1^oC
Outlet Temperature = 20.4^oC
Viscosity = $1.01\ 10^{-3}$ N sec/m^2

t_1 (10 revs) 10^{-6} secs	t_2 (20 revs) 10^{-6} secs	N R.P.M.	δ 10^{-6} secs	dN/dt_1 R.P.M./sec	DRAG R.P.M./sec	dN/dt R.P.M./sec	Re N^o	Cf_1 10^{-3}	$\dot{m}_c$ 10^{-3}	Cf 10^{-3}	ε
Table (10:7) 2" Diameter Bearing Decelerations: c = 5.92 10^{-5}m Supply Pressure = 1 Bar											
80862	161822	7416	98	111.14	48.57	62.57	1181	2.24	0.05	2.19	0.07
89852	179812	6674	108	89.28	40.18	49.09	1063	2.19	0.06	2.13	0.11
102750	205629	5836	129	71.31	31.16	40.15	929	2.35	0.06	2.29	0.14
117127	234408	5119	154	57.47	24.17	33.29	814	2.53	0.07	2.46	0.14
131490	263170	4560	190	50.11	19.44	30.67	726	2.94	0.08	2.86	0.15

Inlet Temperature = 21.1°C Viscosity = 0.986 10^{-3} N sec/m^2
Outlet Temperature = 21.3°C

Table (10:8) 2" Diameter Bearing Decelerations: c = 5.92 10^{-5}m Supply Pressure = 1 Bar											
87515	175135	6852	105	93.94	42.37	51.57	1091	2.19	0.05	2.14	0.10
98749	197622	6072	124	77.22	33.59	43.62	967	2.35	0.06	2.29	0.14
105128	210389	5704	133	68.64	29.84	38.80	882	2.37	0.07	2.30	0.14
124125	248418	4831	168	52.67	21.71	30.96	769	2.64	0.08	2.56	0.15
137580	275360	4358	200	46.05	17.72	28.33	694	2.97	0.09	2.88	0.16
153060	306361	3917	241	40.29	14.15	26.14	624	3.39	0.10	3.29	0.18

Inlet Temperature = 21.1°C
Outlet Temperature = 21.3°C
Viscosity = 0.986 N sec/m^2

Re	Re Cf/2	ε (measured)	T_{exp}/T_{th}	Re	Re Cf/2	ε (measured)	T_{exp}/T_{th}

2" Diameter Bearing Decelerations $c = 5.92\ 10^{-5}m$

Table (10:6(a)) Supply Pressure = 1 Bar

1004	1.09	0.12	1.08	1181	1.29	0.07	1.29
870	1.01	0.14	1.00	1063	1.13	0.11	1.12
756	1.01	0.15	1.00	929	1.06	0.14	1.05
681	1.00	0.16	0.99	814	1.00	0.14	0.99
537	1.03	0.20	1.01	726	1.04	0.15	1.03
476	1.03	0.23	1.00				
433	1.08	0.25	1.05				
396	1.07	0.28	1.03				
348	1.06	0.32	1.00				
309	1.13	0.36	1.05				
275	1.16	0.40	1.06				

Table (10:7(a)) Supply Pressure = 1 Bar

Table (10:8(a)) Supply Pressure = 1 Bar

1091	1.17	0.1	1.16
967	1.11	0.14	1.10
882	1.01	0.14	1.00
769	0.98	0.15	0.97
694	1.00	0.16	0.99
624	1.03	0.18	1.01

t_1 (10 revs) 10^{-6} secs	t_2 (20 revs) 10^{-6} secs	N R.P.M.	δ 10^{-6} secs	dN/dt_1 R.P.M./sec	DRAG R.P.M./sec	dN/dt R.P.M./sec	Re N^o	Cf_1 10^{-3}	$\dot{m}_c$ 10^{-3}	Cf 10^{-3}	ε
Table (10:9) 2" Diameter Bearing Decelerations: $c = 5.92 \times 10^{-5}$m Supply Pressure = 2 Bar											
91667	183448	6541	114	88.75	38.60	50.15	1012	2.34	0.10	2.24	0.17
104108	208353	5760	137	72.80	30.40	42.41	891	2.55	0.12	2.43	0.20
132090	264382	4539	202	52.55	19.25	33.30	702	3.22	0.16	3.06	0.23
167745	335786	3574	296	37.59	11.74	25.85	553	4.03	0.21	3.82	0.28
187072	374512	3204	368	33.69	9.53	24.17	496	4.69	0.24	4.45	0.30
212303	425068	2823	462	28.94	7.59	21.35	437	5.34	0.28	5.06	0.34
244835	490269	2448	599	24.46	5.99	18.47	379	6.14	0.33	5.81	0.38
269602	539942	2223	738	22.57	5.09	17.48	344	7.05	0.37	6.68	0.41
297735	596369	2012	899	20.41	4.25	16.16	311	7.95	0.42	7.53	0.45
338531	678239	1769	1177	18.17	3.41	14.76	274	9.39	0.50	8.89	0.50

Inlet Temperature = 20.0°C
Outlet Temperature = 20.1°C
Viscosity = 1.015×10^{-3} N sec/m^2

t_1 (10 revs) 10^{-6} secs	t_2(20 revs) 10^{-6} secs	N R.P.M.	δ 10^{-6} secs	dN/dt_1 R.P.M./sec	DRAG R.P.M./sec	dN/dt R.P.M./sec	Re N^{o}	Cf_1 10^{-3}	$\dot{m}_c$ 10^{-3}	Cf 10^{-3}	ε
Table (10:10) 2" Diameter Bearing Decelerations: $c = 5.92\ 10^{-5}$m Supply Pressure = 2 Bar											
89980	180070	6664	110	90.54	40.07	50.47	1061	2.26	0.10	2.16	0.17
103447	207024	5796	130	70.42	30.76	39.65	923	2.35	0.12	2.23	0.20
116422	233004	5150	160	60.80	24.45	36.34	820	2.73	0.14	2.59	0.21
129966	260121	4613	189	51.62	19.93	31.69	734	2.96	0.16	2.80	0.23
142203	284626	4216	220	45.87	16.61	29.26	671	3.28	0.17	3.11	0.24

Inlet Temperature = 21.1^{o}C Viscosity = 0.986×10^{-3} N sec/m^2
Outlet Temperature = 21.3^{o}C

Table (10:11) 2" Diameter Bearing Decelerations: $c = 5.92\ 10^{-5}$m Supply Pressure = 2 Bar

88003	176112	6814	106	93.26	41.95	51.31	1085	2.20	0.10	2.10	0.16
98607	197338	6081	124	77.55	33.69	43.86	968	2.36	0.11	2.25	0.18
110127	220401	5445	147	65.99	27.30	38.69	867	2.60	0.13	2.47	0.20
121134	242436	4950	168	56.67	22.65	34.02	788	2.76	0.14	2.62	0.22
135487	271176	4425	202	48.70	18.30	30.39	705	3.09	0.16	2.93	0.23
150694	301631	3978	243	42.57	14.71	27.87	634	3.50	0.18	3.32	0.25

Inlet Temperature = 21.1^{o}C
Outlet Temperature = 21.3^{o}C
Viscosity = 0.986×10^{-3} N sec/m^2

Re	Re Cf/2	ε (measured)	T_{exp}/T_{th}	Re	Re Cf/2	ε (measured)	T_{exp}/T_{th}

2" Diameter Bearing Decelerations $c = 5.92\ 10^{-5}m$

Table (10:9(a)) Supply Pressure = 2 Bar

1012	1.13	0.17	1.11
891	1.08	0.20	1.06
702	1.07	0.23	1.04
553	1.06	0.28	1.02
496	1.10	0.30	1.05
437	1.11	0.34	1.04
379	1.10	0.38	1.02
344	1.15	0.41	1.05
311	1.17	0.45	1.05
274	1.22	0.50	1.06

Table (10:10(a)) Supply Pressure = 2 Bar

1061	1.15	0.17	1.13
923	1.03	0.20	1.01
820	1.06	0.21	1.04
734	1.03	0.23	1.00
671	1.04	0.24	1.01

Table (10:11(a)) Supply Pressure = 2 Bar

1085	1.14	0.16	1.13
968	1.09	0.18	1.07
867	1.07	0.20	1.05
788	1.03	0.22	1.01
705	1.03	0.23	1.00
634	1.05	0.25	1.02

t_1 (10 revs) 10^{-6} secs	t_2 (20 revs) 10^{-6} secs	N R.P.M.	δ 10^{-6} secs	dN/dt_1 R.P.M./sec	DRAG R.P.M./sec	dN/dt R.P.M./sec	Re N^o	Cf_1 10^{-3}	$\dot{m}_c$ 10^{-3}	Cf 10^{-3}	ε
Table (10:12) 2" Diameter Bearing Decelerations c = 7.90 x 10^{-5}m Supply Pressure = 1 Bar											
90518	181162	6624	126	101.86	39.59	62.28	1360	2.83	0.12	2.71	0.03
104711	209558	5726	136	71.03	30.06	40.97	1176	2.49	0.15	2.34	0.08
115997	232143	5169	149	57.24	24.62	32.62	1061	2.44	0.18	2.26	0.11
143130	286455	4189	195	39.88	16.41	23.46	860	2.67	0.24	2.43	0.16
157996	316217	3795	225	34.21	13.26	20.94	779	2.90	0.27	2.63	0.19
170995	842247	3506	257	30.82	11.34	19.48	720	3.16	0.29	2.87	0.22
202351	405040	2963	338	24.46	8.21	16.24	608	3.69	0.34	3.35	0.28
220534	441466	2718	398	22.24	7.09	15.15	558	4.09	0.37	3.72	0.32
243698	487885	2460	489	20.25	6.04	14.21	505	4.69	0.41	4.28	0.35
264977	530530	2262	576	18.56	5.25	13.31	464	5.19	0.45	4.74	0.39
291827	584356	2054	702	16.93	4.41	12.51	422	5.92	0.50	5.42	0.42
316899	634624	1891	826	15.55	3.86	11.69	388	6.53	0.56	5.97	0.45
345661	692317	1733	995	14.43	3.30	11.13	356	7.40	0.63	6.77	0.48
375514	752219	1595	1191	13.47	2.89	10.59	328	8.30	0.70	7.60	0.51
417116	835712	1436	1480	12.21	2.41	9.81	294	9.49	0.80	8.69	0.55

Inlet Temperature = 19.9°C
Outlet Temperature = 19.9°C
Viscosity = 1.02 x 10^{-3} N sec/m^2

t_1 (10 revs) 10^{-6} secs	t_2 (20 revs) 10^{-6} secs	N R.P.M.	δ 10^{-6} secs	dN/dt_1 R.P.M./sec	DRAG R.P.M./sec	dN/dt R.P.M./sec	Re N^o	Cf_1 10^{-3}	$\dot{m}_c$ 10^{-3}	Cf 10^{-3}	ε
Table (10:13) 2" Diameter Bearing Decelerations c = 7.90 10^{-5}m Supply Pressure = 1 Bar											
90481	181088	6627	126	101.99	39.62	62.37	1360	2.83	0.12	2.71	0.03
102540	205213	5848	133	73.97	31.28	42.69	1200	2.49	0.15	2.34	0.08
117701	235552	5094	150	55.16	23.95	31.21	1046	2.39	0.18	2.21	0.11
130171	260513	4606	171	46.49	19.86	26.62	946	2.50	0.21	2.29	0.14
142045	284283	4221	193	40.38	16.65	23.73	867	2.65	0.24	2.41	0.16
157600	315426	3804	226	34.62	13.33	21.29	781	2.93	0.27	2.66	0.19
172516	345292	3475	260	30.36	11.15	19.21	714	3.17	0.29	2.88	0.22
190231	380771	3152	309	26.91	9.26	17.65	647	3.54	0.32	3.22	0.26
205988	412330	2910	354	24.28	7.95	16.33	598	3.84	0.35	3.49	0.28
224617	449651	2669	417	22.06	6.88	15.18	548	4.24	0.38	3.86	0.32
244902	490293	2448	489	20.00	5.99	13.97	503	4.64	0.41	4.23	0.35
271234	543102	2210	634	19.04	5.04	14.00	454	5.71	0.46	5.25	0.40
297639	596013	2013	735	16.70	4.25	12.45	413	6.11	0.52	5.59	0.43
326038	652963	1838	887	15.34	3.65	11.68	377	6.88	0.58	6.30	0.46
360484	722064	1662	1096	14.02	3.09	10.93	341	7.88	0.66	7.22	0.50
394559	790450	1518	1332	12.99	2.65	10.34	312	8.92	0.75	8.17	0.53

Inlet Temperature = 19.9°C
Outlet Temperature = 19.9°C
Viscosity = 1.02×10^{-3} N sec/m^2

Re	Re Cf/2	ε (measured)	T_{exp}/T_{th}	Re	Re Cf/2	ε (measured)	T_{exp}/T_{th}
2" Diameter Bearing Decelerations $c = 7.9\ 10^{-5}m$							
Table (10:12(a)) Supply Pressure = 1 Bar				Table (10:13(a)) Supply Pressure = 1 Bar			
1360	1.84	0.03	1.84	1360	1.84	0.03	1.84
1176	1.38	0.08	1.38	1200	1.40	0.08	1.40
1061	1.20	0.11	1.19	1046	1.16	0.11	1.15
860	1.05	0.16	1.04	946	1.08	0.14	1.07
779	1.02	0.19	1.00	867	1.05	0.16	1.04
720	1.03	0.22	1.00	781	1.04	0.19	1.02
608	1.02	0.28	0.98	714	1.03	0.22	1.01
558	1.04	0.32	0.99	647	1.04	0.26	1.00
505	1.08	0.35	1.01	598	1.04	0.28	1.00
464	1.10	0.39	1.01	548	1.06	0.32	1.00
422	1.14	0.42	1.03	503	1.06	0.35	0.99
388	1.16	0.45	1.04	454	1.19	0.40	1.09
356	1.21	0.48	1.06	413	1.15	0.43	1.04
328	1.25	0.51	1.08	377	1.19	0.46	1.06
294	1.28	0.55	1.07	341	1.23	0.50	1.07
				312	1.28	0.53	1.08

t_1 (10 revs) 10^{-6} secs	t_2 (20 revs) 10^{-6} secs	N R.P.M.	δ 10^{-6} secs	dN/dt_1 R.P.M./sec	DRAG R.P.M./sec	dN/dt R.P.M./sec	Re N^o	Cf_1 10^{-3}	$\dot{m}_c$ 10^{-3}	Cf 10^{-3}	ε
Table (10:14) 2" Diameter Bearing Decelerations: c = 7.90 10^{-5}m Supply Pressure = 2 Bar											
76528	153167	7835	111	148.49	55.38	93.11	1644	2.99	0.15	2.84	0.03
78448	157011	7643	115	142.82	52.64	90.18	1603	3.04	0.16	2.88	0.04
113192	226534	5297	150	62.02	25.78	36.24	1112	2.55	0.29	2.26	0.15
126881	253934	4726	172	50.49	20.98	29.51	992	2.60	0.35	2.25	0.19
144563	289330	4148	204	40.49	16.08	24.41	869	2.80	0.42	2.38	0.23
158535	317305	3782	235	35.36	13.17	22.19	794	3.06	0.47	2.59	0.26
185285	370873	3235	303	28.56	9.71	18.84	679	3.55	0.55	3.00	0.31
273520	547682	2191	642	18.80	4.96	13.84	460	5.68	0.82	4.86	0.46
299065	598901	2004	771	17.27	4.22	13.06	420	6.41	0.91	5.50	0.51
325570	652062	1840	922	16.01	3.66	12.35	386	7.18	1.00	6.18	0.53
352582	706253	1699	1089	14.88	3.20	11.69	357	7.98	1.20	6.78	0.56
385481	772286	1554	1324	13.85	2.76	11.08	326	9.05	1.22	7.83	0.59
434440	870616	1378	1736	12.68	2.26	10.42	289	10.81	1.41	9.40	0.63

Inlet Temperature = 20.8°C
Outlet Temperature = 20.8°C
Viscosity = 0.998 x 10^{-3} N sec/m^2

t_1 (10 revs) 10^{-6} secs	t_2 (20 revs) 10^{-6} secs	N R.P.M.	δ 10^{-6} secs	dN/dt_1 R.P.M./sec	DRAG R.P.M./sec	dN/dt R.P.M./sec	Re N^o	Cf_1 10^{-3}	$\dot{m}_c$ 10^{-3}	Cf 10^{-3}	ε
Table (10:15) 2" Diameter Bearing Decelerations: $c = 7.90\ 10^{-5}$m Supply Pressure = 2 Bar											
86623	173369	6922	123	113.46	43.14	70.32	1441	2.99	0.19	2.80	0.06
97964	196063	6121	135	86.10	34.13	51.97	1274	2.76	0.23	2.53	0.11
111156	222458	5394	146	63.74	26.84	36.90	1123	2.52	0.28	2.26	0.15
125782	251734	4767	170	51.22	21.27	29.95	992	2.62	0.34	2.28	0.19
138528	277248	4328	192	43.31	17.45	25.85	901	2.71	0.40	2.37	0.22
152805	305832	3924	222	37.31	14.21	23.09	817	2.98	0.45	2.53	0.25
168703	337663	3554	257	32.09	11.62	20.47	740	3.22	0.50	2.72	0.28
183687	367675	3264	301	29.12	9.88	19.23	679	3.59	0.55	3.04	0.33
206362	413094	2905	370	25.24	7.93	17.32	605	4.08	0.61	3.47	0.36

Inlet Temperature = 20.4°C
Outlet Temperature = 20.4°C
Viscosity = 1.006×10^{-3} N sec/m^2

t_1 (10 revs) 10^{-6} secs	t_2 (20 revs) 10^{-6} secs	N R.P.M.	δ 10^{-6} secs	dN/dt_1 R.P.M./sec	DRAG R.P.M./sec	dN/dt R.P.M./sec	Re N^{o}	Cf_1 10^{-3}	$\dot{m}_c$ 10^{-3}	Cf 10^{-3}	ε
Table (10:16) 2" Diameter Bearing Decelerations: c = 7.90 10^{-5}m Supply Pressure = 2 Bar											
76481	153073	7839	111	148.76	55.43	93.33	1645	3.02	0.15	2.87	0.03
88890	177905	6745	125	106.71	41.09	65.62	1415	2.87	0.19	2.68	0.07
102433	205001	5854	135	75.32	31.34	43.98	1228	2.55	0.24	2.31	0.12
114534	229219	5235	151	60.26	25.22	35.05	1098	2.55	0.29	2.26	0.16
Inlet Temperature = 20.8°C Outlet Temperature = 20.8°C Viscosity = 0.998 x 10^{-3} N sec/m^2											
Table (10:17) 2" Diameter Bearing Decelerations: c = 7.90 10^{-5}m Supply Pressure = 2 Bar											
79788	159692	7515	116	136.93	51.15	85.78	1577	3.07	0.16	2.91	0.04
87809	175742	6828	124	109.81	42.11	67.70	1433	2.93	0.19	2.74	0.07
Inlet Temperature = 20.8°C Outlet Temperature = 20.8°C Viscosity = 0.998 x 10^{-3} N sec/m^2											
Table (10:18) 2" Diameter Bearing Decelerations: c = 7.90 10^{-5}m Supply Pressure = 2 Bar											
90281	180687	6641	125	101.85	39.80	62.06	1393	2.77	0.20	2.57	0.08
101296	202725	5919	133	76.73	31.99	44.73	1242	2.52	0.24	2.28	0.12
115223	230598	5204	152	59.58	24.94	34.64	1092	2.52	0.30	2.22	0.16
Inlet Temperature = 20.8°C Outlet Temperature = 20.8°C Viscosity = 0.998 x 10^{-3} N sec/m^2											

t_1 (10 revs) 10^{-6} secs	t_2 (20 revs) 10^{-6} secs	N R.P.M.	δ 10^{-6} secs	dN/dt_1 R.P.M./sec	DRAG R.P.M./sec	dN/dt R.P.M./sec	Re N^o	Cf_1 10^{-3}	$\dot{m}_c$ 10^{-3}	Cf 10^{-3}	ε
Table (10:19) 2" Diameter Bearing Decelerations: c = 7.90 10^{-5}m Supply Pressure = 2 Bar											
72040	144183	8323	103	165.18	62.25	102.93	1746	2.93	0.13	2.80	0.03
90275	180674	6642	124	101.06	39.80	61.26	1394	2.74	0.20	2.54	0.08
107050	214242	5601	142	69.41	28.81	40.59	1175	2.55	0.26	2.29	0.14
Inlet Temperature = 20.8°C Outlet Temperature = 20.8°C Viscosity = 0.998 x 10^{-3} N sec/m^2											
Table (10:20) 2" Diameter Bearing Decelerations: c = 7.90 10^{-5}m Supply Pressure = 2 Bar											
72170	144444	8308	104	165.88	62.09	103.80	1743	2.96	0.13	2.83	0.03
90718	181562	6609	126	101.19	39.41	61.78	1387	2.79	0.20	2.59	0.08
101766	203667	5892	135	76.81	31.72	45.09	1236	2.56	0.24	2.32	0.12
112569	225286	5327	148	62.21	26.09	36.12	1118	2.51	0.29	2.22	0.15
Inlet Temperature = 20.8°C Outlet Temperature = 20.8°C Viscosity = 0.998 x 10^{-3} N sec/m^2											
Table (10:21) 2" Diameter Bearing Decelerations: c = 7.90 10^{-5}m Supply Pressure = 2 Bar											
75862	151834	7903	110	151.06	56.15	94.92	1658	2.99	0.15	2.84	0.03
88006	176137	6813	125	109.96	41.94	68.01	1430	2.89	0.19	2.70	0.07
99781	199695	6009	133	80.27	32.90	47.37	1261	2.59	0.23	2.36	0.12
Inlet Temperature = 20.8°C Outlet Temperature = 20.8°C Viscosity = 0.998 x 10^{-3} N sec/m^2											

Re	Re Cf/2	ε (measured)	T_{exp}/T_{th}	Re	Re Cf/2	ε (measured)	T_{exp}/T_{th}

2" Diameter Bearing Decelerations $c = 7.9\ 10^{-5}m$

Table (10:14(a)) Supply Pressure = 2 Bar

1644	2.33	0.03	2.33
1603	2.31	0.04	2.31
1112	1.26	0.15	1.25
992	1.12	0.19	1.10
869	1.03	0.23	1.00
794	1.03	0.26	1.00
679	1.02	0.31	0.97
460	1.12	0.46	1.00
420	1.15	0.51	0.99
386	1.19	0.53	1.01
357	1.21	0.56	1.00
326	1.28	0.59	1.03
289	1.36	0.63	1.06

Table (10:15(a)) Supply Pressure = 2 Bar

1441	2.02	0.06	2.02
1274	1.61	0.11	1.60
1123	1.28	0.15	1.27
992	1.13	0.19	1.11
901	1.02	0.22	1.00
817	1.03	0.25	1.00
740	1.01	0.28	0.97
679	1.03	0.33	0.97
605	1.05	0.36	0.98

Table (10:16(a)) Supply Pressure = 2 Bar

1645	2.36	0.03	2.36
1415	1.90	0.07	1.90
1228	1.42	0.12	1.41
1098	1.24	0.16	1.22

Re	Re Cf/2	ε (measured)	T_{exp}/T_{th}	Re	Re Cf/2	ε (measured)	T_{exp}/T_{th}

2" Diameter Bearing Decelerations $c = 7.90\ 10^{-5}m$

Table (10:17(a)) Supply Pressure = 2 Bar

1577	2.30	0.04	2.30
1433	1.96	0.07	1.96

Table (10:18(a)) Supply Pressure = 2 Bar

1393	1.79	0.08	1.78
1242	1.42	0.12	1.41
1092	1.21	0.16	1.19

Table (10:19(a)) Supply Pressure = 2 Bar

1746	2.44	0.03	2.44
1394	1.77	0.08	1.76
1175	1.35	0.14	1.34

Table (10:20(a)) Supply Pressure = 2 Bar

1743	2.47	0.03	2.47
1387	1.80	0.08	1.80
1236	1.43	0.12	1.42
1118	1.24	0.15	1.23

Table (10:21(a)) Supply Pressure = 2 Bar

1658	2.35	0.03	2.35
1430	1.93	0.07	1.93
1261	1.49	0.12	1.48

10. ii) 3" Diameter Rig

10:22	Air Bearing corrections
10:23	Disc Drag decelerations
10:24	Mass flow rates
10:25	Eccentricities
10:26 - 10:34(a)	Decelerations of the 3" Rig $c = 11.48\ 10^{-5}m$ supply pressures = 1.0, 2.0 and 2.5 bar gauge
10:35 - 10:40(a)	Decelerations of the 3" Rig. Decelerations started in the transition region. $c = 11.48\ 10^{-5}m$ supply pressures = 1.0 and 2.0 bar gauge.

Table (10:22) 3 " Diameter Shaft Deceleration in the Air Bearing:

N R.P.M.	N_∞ R.P.M.	$N + N_\infty$ R.P.M.	$\log_e \frac{N + N_\infty}{N_o + N_\infty}$	t secs
3000	346	3346	-0.2615	45.4
2000	346	2346	-0.6165	107.75
1333	346	1679	-0.9511	166.6
1000	346	1346	-1.1721	205.8

Supply Pressure = 4.0 bar gauge

All Runs started at 4000 R.P.M.

Shaft driven against self drive torque

The above times were measured with a stop watch. The speeds were measured with a stroboscope set at a particular speed, 4000 R.P.M. (accuracy $\pm$ ½%). The air bearing was found because of a machining error to possess a self drive torque. The equations of motion for the shaft decelerating after being driven against the self drive torque are,

$$Ip \frac{dN}{dt} = - kN - kN_\infty$$

$$\text{where } k = \frac{2 \pi R^3 L \mu}{c} + \frac{\dot{m} R^2}{2}$$

$$\frac{dN}{(N + N_\infty)} = - \frac{kdt}{Ip}$$

$$\int \frac{dN}{(N + N_\infty)} = - \int \frac{kdt}{Ip}$$

$$\log_e (N + N_\infty) = - \frac{kt}{Ip} + \text{constant}$$

when $t = 0$

$N = N_o$

$\therefore \log_e (N_o + N_\infty) = \text{constant}$

$$\log_e \frac{(N + N_\infty)}{(N_o + N_\infty)} = - \frac{kt}{Ip}$$

From this expression the frictional torque from the air bearing was found and taken into account in the disc drag determination.

Table (10:23) Disc Drag Decelerations

t_2 (50 revs) 10^{-6} secs	t_1 (25 revs) 10^{-6} secs	∂ 10^{-6} secs	N R.P.M.	α_T R.P.M./sec	α_c R.P.M/sec	DISC DRAG D R.P.M./sec
215590	431508	328	6952	48.99	3.36	45.63
223945	448232	342	6693	45.57	3.23	42.34
244426	489226	374	6132	38.39	3.76	34.63
259145	518689	399	5784	34.36	3.55	30.81
274880	550184	424	5453	30.60	2.80	27.80
291393	583236	450	5144	27.26	2.65	24.61
306618	613713	477	4888	24.80	2.53	22.27
320753	642006	500	4673	22.71	2.42	20.29
335943	672413	527	4462	20.83	2.32	18.51
352992	706540	556	4246	18.95	2.22	16.73
370450	741488	588	4046	17.34	2.13	15.21
391040	782702	622	3833	15.59	2.02	13.57
406901	814452	650	3684	14.46	1.95	12.51
423204	847083	675	3542	13.35	1.88	11.47
439227	879160	706	3412	12.49	1.82	10.67
456266	913268	736	3285	11.61	1.75	9.86
472363	945488	762	3173	10.84	1.70	9.14
488683	978156	790	3067	10.15	1.65	8.50
507650	1016119	819	2952	9.38	1.59	7.79
529272	1059395	851	2832	8.60	1.53	7.07
554762	1110426	902	2702	7.92	1.47	6.45
577232	1155412	948	2597	7.39	1.42	5.97
600288	1201572	996	2497	6.90	1.37	5.53
620958	1242955	1039	2414	6.50	1.33	5.17
645683	1292463	1097	2321	6.11	1.29	4.82
671143	1343447	1161	2233	5.76	1.25	4.51
697444	1396113	1225	2149	5.41	1.20	4.21
719090	1439457	1277	2084	5.15	1.18	3.97
743327	1487996	1342	2016	4.90	1.14	3.76
770981	1543380	1418	1944	4.64	1.11	3.53
789671	1580819	1477	1898	4.49	1.08	3.41
821214	1643996	1568	1825	4.24	1.05	3.19
852237	1706134	1660	1758	4.02	1.02	3.00
879691	1761129	1747	1704	3.85	0.99	2.86
925073	1852042	1896	1620	3.59	0.95	2.64
962851	1927724	2022	1556	3.39	0.91	2.48
991373	1984858	2112	1511	3.25	0.90	2.35
1036212	2074704	2280	1446	3.07	0.87	2.20
1119303	2241198	2592	1339	2.77	0.81	1.96
1159679	2322118	2760	1292	2.65	0.79	1.86
1208861	2420678	2956	1239	2.51	0.77	1.74
1246161	2495439	3117	1202	2.41	0.74	1.67
1313174	2629742	3394	1141	2.25	0.72	1.53
1370620	2744915	3675	1093	2.14	0.70	1.44
1475778	2955748	4192	1015	1.95	0.65	1.30

Table (10:24) 3" Diameter Bearing Mass Flow Rates

Supply Pressure = 1.0 Bar		Supply Pressure = 2.0 Bar		Supply Pressure = 2.5 Bar	
N R.P.M.	$\dot{m}(10^{-2})$ Kg/sec	N R.P.M.	$\dot{m}(10^{-2})$ Kg/sec	N R.P.M.	$\dot{m}(10^{-2})$ Kg/sec
960	3.77	961	5.78	6600	3.21
1500	3.56	1500	5.5	5700	3.65
2160	3.22	1980	5.35	4920	4.23
2520	3.09	2520	5.05		
2700	3.02	2760	4.90		
2940	2.95	3300	4.60		
3180	2.86	3780	4.21		
3770	2.52	4200	3.91		
4020	2.39	4560	3.66		
4321	2.26	5400	3.22		
4560	2.22	6075	2.86		
4800	2.14				
5500	1.92				

Table (10:25) 3" Diameter Bearing: Eccentricities

Supply Pressure = 1.0 Bar		Supply Pressure = 2.0 Bar		Supply Pressure = 2.5 Bar	
N R.P.M.	ε	N R.P.M.	ε	N R.P.M.	ε
1200	0.64	1200	0.70	4800	0.26
1800	0.52	1800	0.61	5700	0.20
2400	0.41	2400	0.51	6000	0.17
3000	0.34	3000	0.43	6600	0.10
3600	0.26	3600	0.34	6900	0.08
4200	0.22	4200	0.27		
4620	0.21	4800	0.24		
5400	0.18	5400	0.21		
		5700	0.18		
		6420	0.10		

t_1 (10 revs) 10^{-6} secs	t_2 (20 revs) 10^{-6} secs	N R.P.M.	δ 10^{-6} secs	dN/dt_1 R.P.M./sec	DRAG R.P.M./sec	dN/dt R.P.M./sec	Re N^o	Cf_1 10^{-3}	$\dot{m}_c$ 10^{-3}	Cf 10^{-3}	ε
Table (10:26) 3" Diameter Bearing Decelerations: c = 11.48 x 10^{-5}m Supply Pressure = 1 Bar											
110411	221115	5427	293	130.4	27.5	102.9	2368	2.60	0.10	2.50	0.18
139626	279648	4291	396	87.16	17.0	70.16	1872	2.84	0.15	2.69	0.21
165640	331716	3618	436	57.49	12.0	45.49	1579	2.59	0.20	2.39	0.26
187647	375767	3194	473	42.91	9.20	33.71	1394	2.46	0.25	2.21	0.31
223827	448250	2677	596	31.85	6.35	25.50	1168	2.65	0.31	2.34	0.38
236326	473274	2536	622	28.24	5.70	22.54	1106	2.61	0.33	2.28	0.40
255260	511236	2347	716	25.79	4.90	20.89	1024	2.82	0.37	2.45	0.42
274396	549602	2183	810	23.48	4.25	19.23	952	3.01	0.41	2.60	0.45
282888	566633	2118	857	22.68	4.08	18.60	924	3.09	0.42	2.67	0.47
302969	606902	1977	964	20.76	3.65	17.11	862	3.26	0.46	2.80	0.49
316696	634427	1891	1035	19.51	3.40	16.11	825	3.36	0.49	2.87	0.51
355136	711598	1686	1326	17.73	3.10	14.63	736	3.83	0.56	3.27	0.54
391928	785455	1528	1599	15.91	2.40	13.51	667	4.31	0.63	3.68	0.57
414507	830828	1444	1814	15.25	2.20	13.05	630	4.66	0.68	3.98	0.58
467212	936839	1281	2415	14.17	1.85	12.32	559	5.59	0.78	4.81	0.62
493439	989660	1213	2782	13.86	1.68	12.18	529	6.16	0.83	5.33	0.64
519905	1042987	1151	3177	13.53	1.55	11.98	502	6.74	0.88	5.86	0.66

Inlet Temperature = 18.2^{o}C
Outlet Temperature = 18.7^{o}C
Viscosity = 1.05 x 10^{-3} N sec/m2

Re	Re Cf/2	ε (measured)	T_{exp}/T_{th}

3" Diameter Bearing Decelerations

Table (10:26(a) Supply Pressure = 1 Bar

2368	2.96	0.18	2.91
1872	2.52	0.21	2.46
1579	1.89	0.26	1.83
1394	1.54	0.31	1.46
1168	1.37	0.38	1.27
1106	1.26	0.40	1.16
1024	1.26	0.42	1.14
952	1.24	0.45	1.11
924	1.23	0.47	1.09
862	1.21	0.49	1.05
825	1.18	0.51	1.02
736	1.20	0.54	1.01
667	1.23	0.57	1.01
630	1.25	0.58	1.02
559	1.34	0.62	1.05
529	1.41	0.64	1.08
502	1.47	0.66	1.10

t_1 (10 revs) 10^{-6} secs	t_2 (20 revs) 10^{-6} secs	N R.P.M.	δ 10^{-6} secs	dN/dt_1 R.P.M./sec	DRAG R.P.M./sec	dN/dt R.P.M./sec	Re N^o	Cf_1 10^{-3}	$\dot{m}_c$ 10^{-3}	Cf 10^{-3}	ε
Table (10:27) 3" Diameter Bearing Decelerations: c = 11.48×10^{-5}m Supply Pressure = 1 Bar											
99649	199549	6014	251	152.02	34.00	118.02	2760	2.43	0.08	2.35	0.12
108338	216959	5531	283	133.36	28.70	104.66	2401	2.55	0.10	2.45	0.17
133566	267499	4486	367	92.29	18.30	73.99	2059	2.74	0.14	2.60	0.21

Inlet Temperature = 20.8°C
Outlet Temperature = 20.8°C
Viscosity = 0.998×10^{-3} N sec/m^2

Table (10:28) 3" Diameter Bearing Decelerations: c = 11.48×10^{-5}m Supply Pressure = 1 Bar											
101862	203908	5885	256	145.30	32.00	113.30	2701	2.44	0.09	2.35	0.13
121003	242326	4952	320	108.23	22.5	85.73	2273	2.60	0.12	2.48	0.20

Inlet Temperature = 20.8°C
Outlet Temperature = 20.8°C
Viscosity = 0.998×10^{-3} N sec/m^2

Re	Re Cf/2	ϵ (measured)	T_{exp}/T_{th}
	3" Diameter Bearing Decelerations		
	Table (10:27(a)) Supply Pressure = 1 Bar		
2760	3.24	0.12	3.22
2401	2.94	0.17	2.90
2059	2.68	0.21	2.62
	Table (10:28(a)) Supply Pressure = 1 Bar		
2701	3.17	0.13	3.14
2273	2.81	0.20	2.75

t_1 (10 revs) 10^{-6} secs	t_2 (20 revs) 10^{-6} secs	N R.P.M.	δ 10^{-6} secs	dN/dt_1 R.P.M./sec	DRAG R.P.M./sec	dN/dt R.P.M./sec	Re N^o	Cf_1 10^{-3}	$\dot{m}_c$ 10^{-3}	Cf 10^{-3}	ε
Table (10:29) 3" Diameter Bearing Decelerations: c = 11.48×10^{-5} m Supply Pressure = 2 Bar											
100772	201810	5946	266	155.75	33.5	122.25	2499	2.58	0.14	2.44	0.16
125475	251308	4775	358	108.58	21.0	87.58	2006	2.87	0.21	2.66	0.24
150700	301809	3976	409	71.61	14.5	57.11	1672	2.69	0.28	2.41	0.30
171396	343231	3496	439	52.24	11.0	41.24	1469	2.51	0.35	2.16	0.36
222309	445238	2695	620	33.81	6.4	27.41	1133	2.81	0.51	2.30	0.47
235703	472088	2542	682	31.20	5.8	25.4	1068	2.93	0.54	2.39	0.48
261815	524451	2288	821	27.40	4.58	22.82	962	3.25	0.62	2.63	0.52
283212	567369	2115	945	24.92	4.05	20.87	889	3.48	0.68	2.80	0.55
293582	588183	2040	1019	24.12	3.82	20.30	857	3.63	0.71	2.92	0.56
353800	709062	1692	1462	19.76	2.85	16.91	711	4.40	0.88	3.52	0.62
389692	781167	1536	1783	18.03	2.40	15.63	646	4.93	0.99	3.94	0.64
412739	827520	1450	2042	17.38	2.22	15.16	609	5.37	1.06	4.31	0.66
458215	919034	1306	2604	16.20	1.90	14.3	549	6.24	1.19	5.05	0.68
472097	946976	1267	2782	15.82	1.80	14.02	532	6.50	1.23	5.27	0.68
511301	1025998	1170	3396	15.20	1.60	13.60	491	7.40	1.34	6.06	0.70

Inlet Temperature = 16.9^oC
Outlet Temperature = 16.9^oC
Viscosity = 1.09×10^{-3} N sec/m^2

Re	Re Cf/2	ε (measured)	T_{exp}/T_{th}
	3" Diameter Bearing Decelerations		
	Table (10:29(a)) Supply Pressure = 2 Bar		
2499	3.05	0.16	3.01
2006	2.67	0.24	2.59
1672	2.02	0.30	1.93
1469	1.59	0.36	1.48
1133	1.30	0.47	1.15
1068	1.28	0.48	1.12
962	1.27	0.52	1.08
889	1.25	0.55	1.04
857	1.25	0.56	1.03
711	1.25	0.62	0.99
646	1.27	0.64	0.98
609	1.31	0.66	0.99
549	1.39	0.68	1.03
532	1.40	0.68	1.03
491	1.49	0.70	1.05

t_1 (10 revs) 10^{-6} secs	t_2 (20 revs) 10^{-6} secs	N R.P.M.	δ 10^{-6} secs	dN/dt_1 R.P.M./sec	DRAG R.P.M./sec	dN/dt R.P.M./sec	Re N^o	Cf_1 10^{-3}	$\dot{m}_c$ 10^{-3}	Cf 10^{-3}	ε
Table (10:30) 3" Diameter Bearing Decelerations: c = 11.48 x 10^{-5}m Supply Pressure = 2 Bar											
92054	184343	6510	235	180.54	39.50	141.04	2687	2.48	0.11	2.37	0.09
117654	235636	5092	328	120.70	24.00	96.70	2101	2.78	0.18	2.60	0.23
121842	244026	4918	342	113.30	22.50	90.80	2067	2.80	0.19	2.61	0.24
130014	260400	4608	372	101.41	19.60	81.81	1902	2.87	0.22	2.65	0.25
142315	285033	4210	403	83.77	16.40	67.37	1770	2.83	0.25	2.58	0.27
150319	301047	3986	409	72.15	14.50	57.65	1645	2.70	0.28	2.42	0.30
164886	330197	3635	425	56.82	12.00	44.82	1528	2.53	0.33	2.20	0.34
186455	373390	3214	480	44.38	9.25	35.13	1326	2.53	0.40	2.13	0.40
203387	407307	2946	533	37.96	7.80	30.16	1216	2.59	0.45	2.14	0.44
230831	462308	2596	646	31.47	5.98	25.49	1071	2.82	0.53	2.29	0.48

Inlet Temperature = 16.5°C
Outlet Temperature = 16.5°C
Viscosity = 1.11 x 10^{-3} N sec/m^2

t_1 (10 revs) 10^{-6} secs	t_2 (20 revs) 10^{-6} secs	N R.P.M.	δ 10^{-6} secs	dN/dt_1 R.P.M./sec	DRAG R.P.M./sec	dN/dt R.P.M./sec	Re N^o	Cf_1 10^{-3}	$\dot{m}_c$ 10^{-3}	Cf 10^{-3}	ε
Table (10:31) 3" Diameter Bearing Decelerations: c = 11.48×10^{-5}m Supply Pressure = 2 Bar											
85819	171846	6983	208	197.21	45.80	151.41	3205	2.31	0.10	2.21	0.05
94772	189783	6323	239	168.25	37.40	130.85	2902	2.44	0.12	2.32	0.11
114548	229402	5231	306	121.99	25.50	96.49	2401	2.63	0.17	2.46	0.23

Inlet Temperature = 20.8°C
Outlet Temperature = 20.8°C
Viscosity = $0.998\ 10^{-3}$ N sec/m^2

Table (10:32) 3" Diameter Bearing Decelerations: c = 11.48×10^{-5}m Supply Pressure = 2 Bar											
89979	180180	6660	222	182.01	41.60	141.01	3057	2.37	0.11	2.28	0.07
101564	203389	5900	261	149.28	32.70	116.58	2708	2.49	0.14	2.35	0.16
125246	250836	4784	344	104.91	21.20	83.71	2196	2.72	0.20	2.52	0.24

Inlet Temperature = 20.8°C
Outlet Temperature = 20.8°C
Viscosity = $0.998\ 10^{-3}$ N sec/m^2

Re	Re Cf/2	ε (measured)	T_{exp}/T_{th}	Re	Re Cf/2	ε (measured)	T_{exp}/T_{th}

3" Diameter Bearing Decelerations

Table (10:30(a)) Supply Pressure = 2 Bar

2687	3.49	0.09	3.12
2101	2.73	0.23	2.66
2067	2.70	0.24	2.62
1902	2.52	0.25	2.44
1770	2.28	0.27	2.20
1645	1.79	0.30	1.90
1528	1.68	0.34	1.58
1326	1.41	0.40	1.29
1216	1.30	0.44	1.17
1071	1.23	0.48	1.08

Table (10:31(a)) Supply Pressure = 2 Bar

3205	3.54	0.05	3.54
2902	3.37	0.11	3.34
2401	2.95	0.23	2.87

Table (10:32(a)) Supply Pressure = 2 Bar

3057	3.48	0.07	3.47
2708	3.18	0.16	3.14
2196	2.77	0.24	2.69

t_1 (10 revs) 10^{-6} secs	t_2 (20 revs) 10^{-6} secs	N R.P.M.	δ 10^{-6} secs	dN/dt_1 R.P.M./sec	DRAG R.P.M./sec	dN/dt R.P.M./sec	Re N^o	Cf_1 10^{-3}	$\dot{m}_c$ 10^{-3}	Cf 10^{-3}	ε
Table (10:33) 3" Diameter Bearing Decelerations: c = 11.48 x 10^{-5}m Supply Pressure = 2.5 Bar											
79213	158612	7566	186	224.30	54.00	170.30	3473	2.22	0.10	2.12	0.01
99179	198612	6042	254	156.00	34.50	121.50	2773	2.48	0.16	2.32	0.16
122744	245826	4882	338	109.53	22.00	87.53	2241	2.74	0.24	2.50	0.26

Inlet Temperature = 20.8°C
Outlet Temperature = 20.8°C
Viscosity = 0.998 10^{-3} N sec/m^2

Table (10:34) 3" Diameter Bearing Decelerations: c = 11.48 x 10^{-5}m Supply Pressure = 2.5 Bar											
75972	152121	7889	177	241.93	59.00	182.93	3621	2.19	0.09	2.10	0.01
97891	196030	6122	248	158.44	35.20	123.24	2810	2.45	0.15	2.30	0.15
124107	248561	4828	347	108.77	21.80	80.97	2216	2.78	0.25	2.53	0.26

Inlet Temperature = 20.8°C
Outlet Temperature = 20.8°C
Viscosity = 0.998 10^{-3} N sec/m^2

Re	Re Cf/2	ε (measured)	T_{exp}/T_{th}	Re	Re Cf/2	ε (measured)	T_{exp}/T_{th}

3" Diameter Bearing Decelerations

Table (10:33(a)) Supply Pressure = 2 Bar				Table (10:34(a)) Supply Pressure = 2 Bar			
3473	3.68	0.00	3.68	3621	3.80	0.00	3.80
2773	3.22	0.16	3.18	2810	3.23	0.15	3.19
2241	2.80	0.26	2.70	2216	2.80	0.26	2.70

(Decelerations started in the Transition Region)

t_1 (10 revs) 10^{-6} secs	t_2 (20 revs) 10^{-6} secs	N R.P.M.	δ 10^{-6} secs	dN/dt_1 R.P.M./sec	DRAG R.P.M./sec	dN/dt R.P.M./sec	Re N°	Cf_1 10^{-3}	$\dot{m}_c$ 10^{-3}	Cf 10^{-3}	ε
Table (10:35) 3" Diameter Bearing Decelerations: c = 11.48 x 10^{-5}m Supply Pressure = 2 Bar											
259966	520758	2304	826	28.16	4.75	23.41	959.5	3.28	0.62	2.66	0.53
295056	591156	2030	1044	24.34	3.8	20.54	845.4	3.71	0.72	2.99	0.57
328715	658704	1822	1274	21.48	3.35	18.13	758.8	4.07	0.82	3.25	0.60
364843	731257	1641	1571	19.37	2.7	16.67	683.4	4.61	0.92	3.69	0.63
402635	807200	1487	1930	17.70	2.33	15.37	619.3	5.18	1.03	4.15	0.65
Inlet Temperature = 17.0°C Outlet Temperature = 17.0°C Viscosity = 1.1 10^{-3} N sec/m^2											
Table (10:36) 3" Diameter Bearing Decelerations: c = 11.48 x 10^{-5}m Supply Pressure = 2 Bar											
187012	374508	3204	484	44.34	9.2	35.14	1334	2.55	0.40	2.15	0.40
212783	426142	2816	576	35.83	7.2	28.63	1173	2.69	0.48	2.21	0.45
235725	472133	2542	683	32.25	5.8	25.45	1059	2.93	0.54	2.39	0.48
Inlet Temperature = 17.0°C Outlet Temperature = 17.0°C Viscosity = 1.1 10^{-3} N sec/m^2											
Table (10:37) 3" Diameter Bearing Decelerations: c = 11.48 x 10^{-5}m Supply Pressure = 2 Bar											
153152	306714	3912	410	68.38	14.0	54.38	1629	2.65	0.28	2.37	0.30
173838	348122	3447	446	50.87	10.7	40.17	1436	2.52	0.36	2.16	0.37
Inlet Temperature = 17.0°C Outlet Temperature = 17.0°C Viscosity = 1.1 x 10^{-3} N sec/m^2											

(Decelerations started in the Transition Region)

t_1 (10 revs) 10^{-6} secs	t_2 (20 revs) 10^{-6} secs	N R.P.M.	δ 10^{-6} secs	dN/dt_1 R.P.M./sec	DRAG R.P.M./sec	dN/dt R.P.M./sec	Re N^{o}	Cf_1 10^{-3}	$\dot{m}_c$ 10^{-3}	Cf 10^{-3}	ε
Table (10:38) 3" Diameter Bearing Decelerations: c = 11.48 x 10^{-5}m Supply Pressure = 1 Bar											
155248	310921	3860	425	68.07	13.50	54.57	1700	2.73	0.18	2.55	0.24
179121	358691	3346	449	46.83	10.2	36.63	1474	2.44	0.23	2.21	0.29
200108	400718	2995	502	37.55	8.0	29.55	1319	2.45	0.27	2.28	0.34
Inlet Temperature = 18.8°C Outlet Temperature = 19.1°C Viscosity = 1.04 10^{-3} N sec/m^2											
Table (10:39) 3" Diameter Bearing Decelerations: c = 11.48 x 10^{-5}m Supply Pressure = 1 Bar											
129461	259280	4628	358	98.85	20.0	78.85	1963	2.74	0.13	2.61	0.21
175493	351425	3415	439	48.68	10.7	37.98	1449	2.43	0.22	2.21	0.29
Inlet Temperature = 18.2°C Outlet Temperature = 18.7°C Viscosity = 1.08 10^{-3} N sec/m^2											
Table (10:40) 3" Diameter Bearing Decelerations: c = 11.48 x 10^{-5}m Supply Pressure = 1 Bar											
212985	426511	2814	541	33.56	7.2	26.36	1193	2.48	0.24	2.24	0.37
280345	561526	2137	836	27.73	4.15	18.58	906	3.03	0.39	2.64	0.46
311742	624501	1922	1017	20.11	3.5	16.61	815	3.35	0.48	2.87	0.50
336927	675036	1778	1182	18.51	3.1	15.41	754	3.63	0.56	3.07	0.52
368250	737917	1626	1417	16.99	2.55	14.44	690	4.07	0.59	3.48	0.55
Inlet Temperature = 18.2°C Outlet Temperature = 18.7°C Viscosity = 1.08 10^{-3} N sec/m^2											

Re	Re Cf/2	ε (measured)	T_{exp}/T_{th}	Re	Re Cf/2	ε (measured)	T_{exp}/T_{th}
3" Diameter Bearing Decelerations started in the Transition Region							
Table (10:35(a)) Supply Pressure = 2 Bar				Table (10:36(a)) Supply Pressure = 2 Bar			
959.5	1.28	0.53	1.09	1334	1.43	0.4	1.31
845.4	1.26	0.57	1.04	1173	1.30	0.45	1.16
758.8	1.23	0.60	0.98	1059	1.27	0.48	1.11
683.4	1.26	0.63	0.98				
619.3	1.29	0.65	0.98				
Table (10:37(a)) Supply Pressure = 2 Bar				Table (10:38(a)) Supply Pressure = 1 Bar			
1629	1.93	0.30	1.84	1700	2.17	0.24	2.11
1436	1.55	0.37	1.44	1474	1.63	0.29	1.56
				1319	1.46	0.34	1.37
Table (10:39(a)) Supply Pressure = 1 Bar				Table (10:40(a)) Supply Pressure = 1 Bar			
1963	2.56	0.21	2.50	1193	1.34	0.37	1.25
1449	1.60	0.28	1.54	906	1.20	0.46	1.07
				815	1.17	0.50	1.01
				754	1.16	0.52	0.99
				690	1.20	0.55	1.00

APPENDIX 1

6th International
GAS BEARING SYMPOSIUM
March 27-29, 1974
University of Southampton

THE FRICTIONAL TORQUE IN EXTERNALLY PRESSURISED BEARINGS

J. Bennett, B.Sc.
and
H. Marsh, S.M., M.A., Ph.D.
University of Durham, U.K.

Summary

The total frictional torque in an externally pressurised bearing consists of two parts, one being that predicted from the Petroff formula and the other being associated with the change in the angular momentum of the lubricant. The analysis is fully confirmed by experiments with an air-lubricated journal bearing. It is shown that if all other parameters are specified, then the minimum total frictional torque is obtained when the clearance is chosen such that 25 per cent of the total torque is required for changing the angular momentum of the lubricant.

Held at the University of Southampton, England.
Symposium organised and sponsored by BHRA Fluid Engineering, Cranfield, Bedford
in conjunction with the Gas Bearing Advisory Service of the University of Southampton.

Nomenclature

A, B	constants,
c	radial clearance,
D	diameter,
I_p	polar inertia,
L	bearing length,
$\dot{m}$	lubricant mass flow rate,
p_s	supply pressure,
p_a	ambient pressure,
R	bearing radius,
T	torque,
t	time,
t_c	time constant for decelerating rotor,
μ	viscosity,
ω	angular velocity,
ω_o	initial angular velocity.

Introduction

Although the viscosity of a gas is low in comparison with liquid lubricants, there are many situations in which is is necessary to estimate the frictional torque and power requirements of a gas bearing. The simplest method for estimating the frictional torque in a journal bearing is that due to Petroff and is based on approximating the journal bearing to two concentric cylinders, so that for laminar flow,

$$T_1 = \frac{2 \pi R^3 L \mu \omega}{c} \qquad (1)$$

This formula for the frictional torque, often with a modification for eccentricity ratio, is to be found in any textbook on lubrication theory.

In the course of research with a lightly loaded externally pressurised journal bearing, it was found that the frictional torque was dependent on the supply pressure. The research bearing operated with a very small load and the variation of frictional torque was not caused by a change in the eccentricity ratio. Further investigation showed that the frictional torque of an externally pressurised journal bearing could be regarded as having two components, one being the frictional torque T_1 predicted from the Petroff equation, and the other torque T_2 being associated with the change of angular momentum for the lubricant passing through the bearing.

In an externally pressurised journal bearing of conventional design, the lubricant enters the bearing clearance through small radial supply jets, which may be plain or recessed, and it leaves from the two ends of the bearing. At inlet to the bearing clearance, the lubricant has no net angular momentum, but on passing through the bearing clearance, it acquires angular momentum. This change of angular momentum for the lubricant requires a torque and the experimental results reported in this paper show that this torque is supplied by the rotor. This additional torque on the rotor can lead to a significant increase in the total frictional torque and power loss in both gas and oil lubricated bearings.

The prediction of the frictional torque

If the lubricant enters the bearing clearance through radial supply holes, then it has no initial angular momentum. At the two ends of the journal bearing, the lubricant leaves the bearing with a mean tangential velocity, so that it has acquired angular momentum while flowing through the bearing clearance. For laminar flow, the mass averaged tangential velocity of the lubricant leaving the bearing is $(\omega R/2)$, so that the change of angular momentum per unit mass is $(\omega R^2/2)$. The lubricant acquires the tangential velocity profile soon after leaving the supply holes and the change of angular momentum is therefore caused by viscous forces in the neighbourhood of the supply holes.

The torque which is required to produce the change of angular momentum is

$$T_2 = \frac{\dot{m} \omega R^2}{2} \qquad (2)$$

where $\dot{m}$ is the mass flowrate of the lubricant. This torque is the sum of the additional torques supplied by the rotor and the bearing,

$$T_2 = T_R + T_B \qquad (3)$$

Experiments with gas bearings having tilted supply jets have shown that the torques on the rotor and bearing are approximately in the same ratio as the relative tangential velocities between the incoming gas and the two surfaces, so that

$$\frac{T_B}{T_R} = \frac{0}{\omega R} \tag{4}$$

On this basis, the change of angular momentum for the lubricant requires an additional torque on the rotor which is given by

$$T_R = T_2 = \frac{\dot{m}\ \omega\ R^2}{2} \tag{5}$$

Although this torque is associated with the change of angular momentum, it is caused by viscous forces and it is a frictional force.

The total frictional force acting on the rotor is the sum of that given by the Petroff formula and that required to change the angular momentum of the lubricant,

$$T_{total} = \frac{2\ \pi\ R^3\ L\ \mu\ \omega}{c} + \frac{\dot{m}\ \omega\ R^2}{2} \tag{6}$$

The total frictional torque acting on the bearing remains that given by the Petroff formula, since from equation (4), there is no additional bearing torque associated with the change of angular momentum.

Experiments with a decelerating rotor

If a rotor is supported in a journal bearing, then the governing equation for deceleration with no applied torque is

$$I_p \frac{d\omega}{dt} = - T_{total} \tag{7}$$

or, substituting from equation (6),

$$I_p \frac{d\omega}{dt} + \left[\frac{2\ \pi\ R^3\ L\ \mu}{c} + \frac{\dot{m}\ R^2}{2}\right]\ \omega = 0 \tag{8}$$

The angular velocity of the rotor is then related to the initial angular velocity, ω_o, by

$$\omega = \omega_o\ e^{-t/t_c} \tag{9}$$

where the reciprocal of the time constant is given by

$$\frac{1}{t_c} = \frac{1}{I_p}\left[\frac{2\ \pi\ R^3\ L\ \mu}{c} + \frac{\dot{m}\ R^2}{2}\right] \tag{10}$$

This relationship between the mass flow rate of the lubricant and the time constant, t_c, suggests that experiments with a decelerating rotor may provide a simple test for this new approach to bearing friction.

A series of experiments have been performed with a rotor and bearing having the following dimensions and polar inertia,

$R = 25.4$ mm, $\quad c = 45.2\ \mu$ m

$L = 66.0$ mm, $\quad I_p = 4.237_{10}{-4}$ kg m^2

The bearing was supplied with air at 20°C through two rows of 12 plain jets situated at 0.25L from each end of the bearing.

The variation of the mass flow rate with supply pressure was measured by the weighing method described in Reference (1). The whole bearing apparatus and a cylinder of compressed air were mounted on a balance and by using a nulling technique, the time to consume a known mass of air was determined. Figure 1 shows the mass flow rate as a function of pressure.

The deceleration of the rotor is characterised by the time constant t_c. The time constant was determined by setting a stroboscope to a fixed frequency, driving the rotor to a higher frequency and then measuring the time taken to decelerate from the fixed frequency to various fractions of this frequency. These deceleration tests were carried out at several supply pressures. The reciprocal of the time constant is shown as a function of the air mass flow rate in Figure 2 where the experimental results may be compared with those predicted from equation (10). It is seen that the experimental results fully confirm the theory. For this simple bearing system, there is a large increase in the frictional torque with supply pressure. With a supply pressure of 0.7 MN/m^2 the total frictional torque is 65% greater than that predicted from the Petroff formula.

A minimum friction design

The total frictional torque in an externally pressurised journal bearing is given by

$$T_{total} = \frac{2\pi R^3 L \mu \omega}{c} + \frac{\dot{m} \omega R^2}{2}$$

For a given supply gauge pressure and gauge pressure ratio and a bearing of given radius and length, the mass flow rate of the lubricant is proportional to the cube of the radial clearance. The total frictional torque can then be written as

$$T_{total} = \frac{A}{c} + B c^3 \qquad (11)$$

where A and B are constants. The minimum total frictional torque is obtained when the clearance is given by

$$\frac{dT}{dc} = 0 = \frac{-A}{c^2} + 3 B c^2$$

or $$c^4 = \frac{A}{3B} \qquad (12)$$

For this minimum friction design, the total frictional torque on the rotor is

$$T_{total} = \frac{A}{C}\left[1 + \frac{B c^4}{A}\right]$$

$$= \frac{4}{3}\frac{A}{C} \qquad (13)$$

which may be compared with the Petroff equation,

$$T_1 = \frac{A}{C} \qquad (14)$$

If a bearing is designed for minimum frictional torque, then this analysis shows that one quarter of the total torque is required for changing the angular momentum of the lubricant. It follows that the torque predicted by the Petroff equation is

then three times that required to change the angular momentum of the lubricant,

$$\frac{2\pi R^3 L \mu \omega}{c} = \frac{3}{2} \dot{m} \omega R^2 \qquad (15)$$

$$\dot{m} = \frac{4}{3} \frac{\pi R L \mu}{c}$$

or $$\frac{\dot{m} L}{D} = \frac{2}{3} \frac{\pi \mu L^2}{c} \qquad (16)$$

This variation of mass flow rate with clearance is shown in Figure 3 for several values of L^2, the lubricant being air. Figure 3 also shows the design curves for mass flow rate for a gauge pressure factor of 0.4 and zero eccentricity ratio, these curves being taken from the work of Shires (Reference 2). The intersection of the lines of constant gauge pressure and those given by equation (16) defines the radial clearance of a bearing designed for minimum total frictional torque. For example, if the bearing parameters are

$L = 66.0$ mm $\qquad\qquad$ $R = 25.4$ mm

$p_o - p_a = 0.35$ MN/m^2

then the corresponding clearance for minimum total friction is $c = 45$ μm, this being the bearing used in the experiments.

Conclusions

The analysis presented in this paper shows that in an externally pressurised bearing, the total frictional torque on the rotor consists of two parts, the first being that predicted by the Petroff formula and the other being associated with the change of angular momentum for the lubricant. The additional torque required to change the angular momentum of the lubricant is supplied by the rotor and it is caused by viscous effects close to the supply holes. Experiments with an externally pressurised air bearing (and also with an oil bearing) have confirmed the analysis and it has been shown that the change in the angular momentum of the lubricant can significantly increase the power requirements of a gas bearing.

The equation derived for the total frictional torque on the rotor has been used to develop a method for designing bearings with the minimum total frictional torque. A simple analysis shows that if the bearing length, the radius, the gauge pressure factor and the gauge pressure are specified, then the minimum total frictional torque on the rotor is obtained when the radial clearance is chosen such that 25% of the rotor torque is required for changing the angular momentum of the lubricant. By combining this result with the design curves of Shires, a simple design method is obtained for bearings with the minimum total frictional torque, or minimum power requirement.

Acknowledgement

The authors would like to thank the Science Research Council for a grant to support research on gas lubricated bearings.

References

1. Marsh, H., Drive systems for gas bearings, Proc. 5th Gas Bearing Symposium, Southampton, 1971
2. Shires, G.L., The design of externally pressurised bearings, Chapter 4 in Gas Lubricated Bearings, ed. by N.S. Grassam and J.W. Powell, Butterworths, 1964

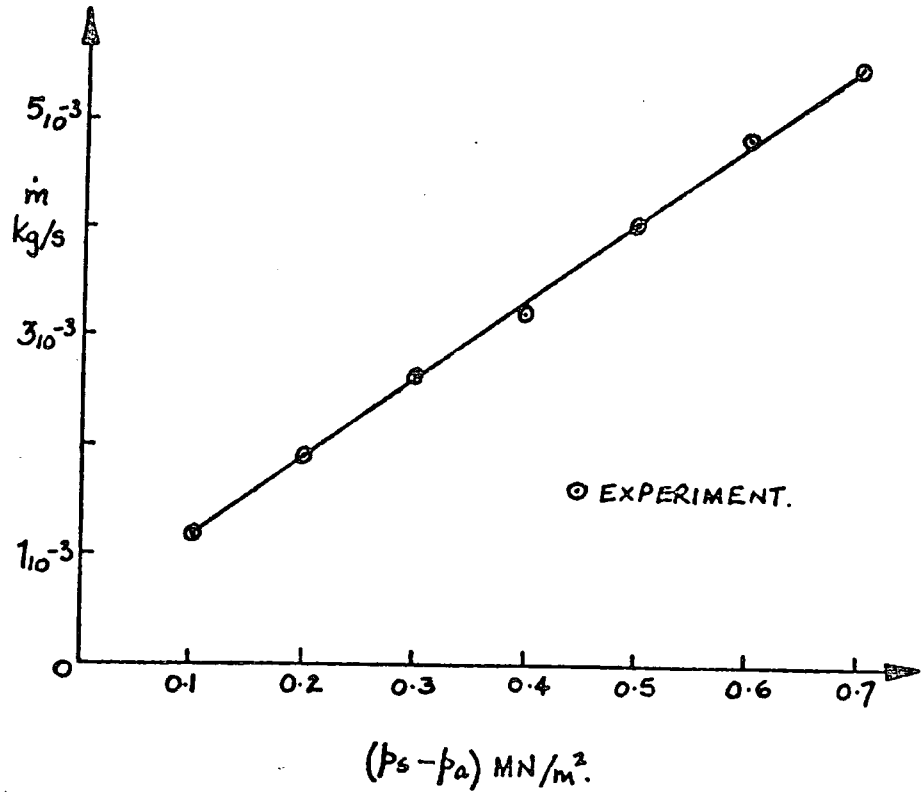

Fig. 1 Mass flow rate vs supply pressure.

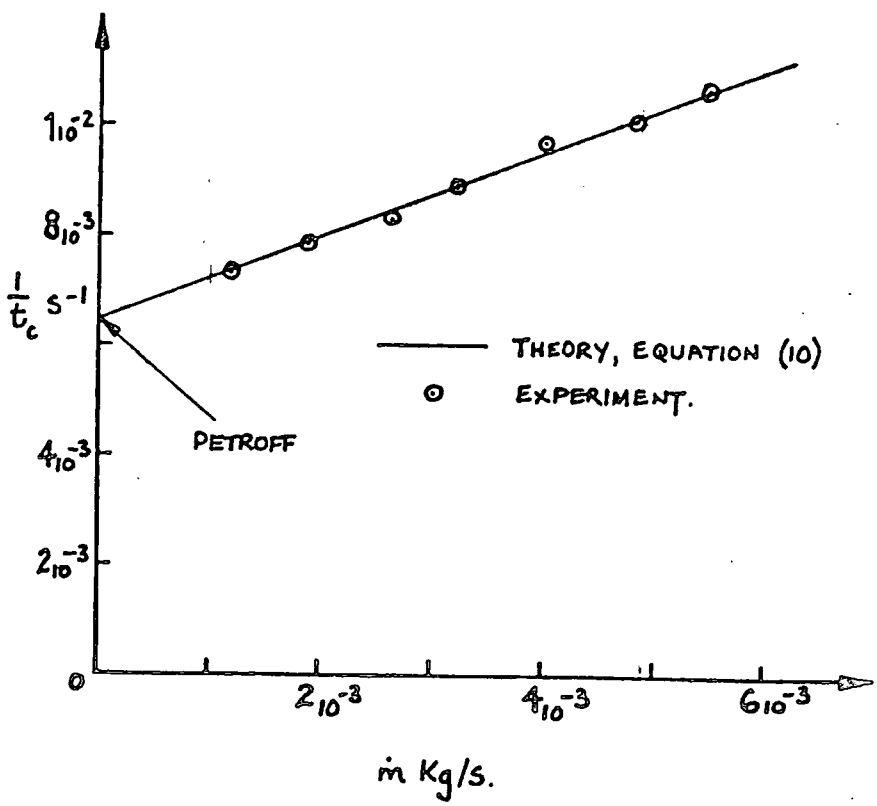

Fig. 2 Variation of $1/t_c$ with mass flow rate.

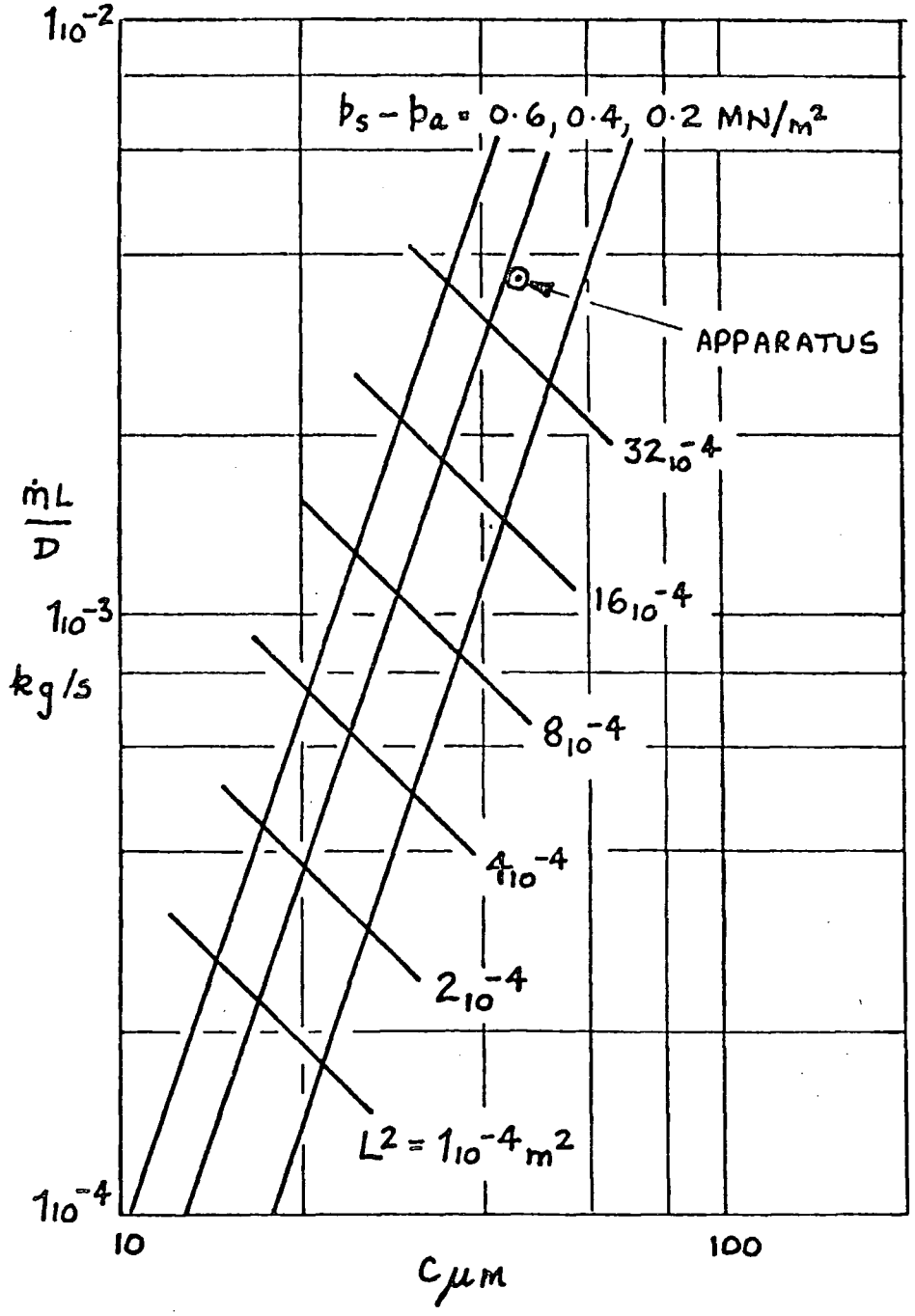

SHIRES' DATA FOR AIR AT 15°C, p_a = 0·1MN/m².
K_{go} = 0·4, ε = 0·0, l = 0·25L.

Fig. 3 Data for minimum friction design.

APPENDIX 2

6th International
GAS BEARING SYMPOSIUM
March 27-29, 1974
University of Southampton

PAPER C4

THE STEADY STATE AND DYNAMIC BEHAVIOUR OF THE TURBO-BEARING

J. Bennett, B.Sc.
and
H. Marsh, S.M., M.A., Ph.D.
University of Durham, U.K.

Summary

The turbo-bearing is an externally pressurised gas bearing with inclined supply holes, so that the gas enters the bearing clearance with a high angular momentum. There is a change of angular momentum for the gas and this produces a driving torque on the rotor. The paper describes a method for designing the turbo-bearing and the theory is confirmed by the experiments. It is shown that the inclined supply holes have no adverse effect on the load carrying capacity or stiffness of the bearing. The onset of half speed whirl has been investigated by driving the rotor to high speeds and it has been shown that the whirl onset speed is dependent on the direction of rotation.

Held at the University of Southampton, England.
Symposium organised and sponsored by BHRA Fluid Engineering, Cranfield, Bedford in conjunction with the Gas Bearing Advisory Service of the University of Southampton.

Nomenclature

c	radial clearance,
c_e	end clearance,
d	diameter of supply holes,
I_p	polar inertia of rotor,
I_T	transverse inertia of rotor,
L	length of bearing,
$\dot{m}$	mass flow rate of gas,
n	number of supply holes,
p_a	ambient pressure,
p_s	supply pressure,
R_i	inner radius of thrust plates,
R_o	radius of journal bearing,
S_A	angular stiffness,
S_T	translational stiffness,
t_c	time constant,
T_{th}	thrust bearing torque,
T_B	bearing torque,
T_R	rotor torque,
T_1	driving torque,
T_2	frictional torque in journal bearing,
V	velocity in the supply holes,
ϕ	inclination of the supply holes,
μ	viscosity,
ρ	density,
ω	angular velocity,
ω_∞	steady state angular velocity

Introduction

The turbo-bearing is a self driving externally pressurised journal bearing in which the supply jets are inclined so that the gas enters the bearing with a high tangential velocity. It has been known for many years that small errors in the manufacture of conventional externally pressurised bearings can lead to non-radial supply holes and this usually results in a system where the rotor rotates, even when there is no externally applied torque. The turbo-bearing uses this same effect, the supply holes being inclined at a large angle, typically 60°, to the radial direction. The gas enters the bearing clearance with a high angular momentum and leaves at the two ends of the bearing with low angular momentum. This change of angular momentum requires a torque applied to the lubricant, this being provided by the rotor and bearing. There is, therefore, a driving torque on the rotor and the rotor accelerates until the driving torque is equal to the frictional torque predicted from the Petroff analysis. This method of driving the rotor is extremely simple and it is completely silent. The gas supplied to the bearing both supports and drives the rotor. In an earlier paper, reference (1), this form of drive was compared with a bearing system where the rotor was driven by a small impulse turbine.

The predicted performance of the turbo-bearing

In the turbo-bearing, the gas enters the bearing clearance through small supply holes which are inclined at an angle θ to the radial direction, as shown in Figure 1. The experiments described in this paper have all been performed with a bearing having inclined plain jets and annular orifices, since the use of simple orifices may result in large recess volumes and pneumatic hammer. The gas flows along the supply holes with a velocity V and enters the bearing clearance with an angular momentum $V R_o \sin\theta$. At the two ends of the bearing, the gas leaves with a mass averaged tangential velocity of $\omega R_o/2$. If the mass flow rate of the gas is $\dot{m}$, then this change of angular momentum requires a torque T_1 which is given by,

$$T_1 = \dot{m}\left(V R_o \sin\theta - \frac{\omega R_o^2}{2} \right) \qquad (1)$$

This torque is provided by the rotor and the bearing,

$$T_1 = T_B + T_R \qquad (2)$$

The mean tangential velocity of the gas decreases to $\omega R_o/2$ soon after leaving the supply holes and the change of angular momentum is therefore caused by viscous forces in the neighbourhood of the supply holes.

The tangential velocity of the gas leaving the tilted supply holes is $V \sin\theta$ relative to the bearing and $(V \sin\theta - \omega R_o)$ relative to the rotor surface. It is assumed that the torques on the bearing and rotor are in proportion to the relative tangential velocities of the gas and the two surfaces,

$$\frac{T_B}{T_R} = \frac{V \sin\theta}{V \sin\theta - \omega R_o} \qquad (3)$$

From equations (1), (2), and (3), the driving torque on the rotor is given by

$$T_R = \frac{\dot{m} R_o}{2} (V \sin\theta - \omega R_o) \qquad (4)$$

This driving torque is opposed by the frictional torque T_2 which may be obtained

from the Petroff equation,

$$T_2 = \frac{2 \pi \mu R_o^3 L \omega}{c} \tag{5}$$

The net torque on the rotor is equal to the difference between the driving torque T_R and the frictional torque T_2.

The equation describing the acceleration of the rotor is

$$I_p \frac{d\omega}{dt} = \frac{\dot{m} R_o}{2} (V \sin \theta - \omega R_o) - \frac{2 \pi \mu R_o^3 L \omega}{c} \tag{6}$$

or

$$I_p \frac{d\omega}{dt} + \left[\frac{2 \pi \mu R_o^3 L}{c} + \frac{\dot{m} R_o^2}{2} \right] \omega = \frac{\dot{m} R_o V \sin \theta}{2} \tag{7}$$

When released from rest, the rotor accelerates and the angular velocity is given by

$$\omega = \omega_\infty \left(1 - e^{-t/t_c}\right) \tag{8}$$

where ω_∞ is the ultimate steady angular velocity. The reciprocal of the time constant is related to the mass flow rate of the gas by the equation

$$\frac{1}{t_c} = \frac{1}{I_p} \left[\frac{2 \pi \mu R_o^3 L}{c} + \frac{\dot{m} R_o^2}{2} \right] \tag{9}$$

It is interesting to note that this equation shows that the time constant is independent of the angle ϑ, the inclination of the supply holes. The time constant for the turbo-bearing is independent of the angle ϑ, so that all turbo-bearings have the same time constant and this is equal to the time constant for a conventional bearing with radial supply holes.

The rotor of the turbo-bearing accelerates and approaches a steady angular velocity which is given by

$$\omega_\infty = \frac{\dot{m} R_o V \sin \theta}{2} \left[\frac{1}{\frac{2 \pi \mu R_o^3 L}{c} + \frac{\dot{m} R_o^2}{2}} \right] \tag{10}$$

or

$$= \frac{V \sin \theta}{R_o} \left[\frac{1}{1 + \frac{4 \pi \mu R_o L}{\dot{m} c}} \right] \tag{11}$$

The form of equation (11) confirms that the surface velocity of the rotor cannot exceed the tangential velocity of the gas entering the bearing clearance.

The steady state angular velocity, ω_∞, is dependent on the velocity of the gas, V, and this is related to the mass flow rate by the continuity equation for the supply holes,

$$\dot{m} = n \frac{\pi d^2}{4} \rho V \tag{12}$$

where n is the number of supply holes of diameter d. In an annular orifice type of bearing, the total orifice area is $n \pi d c$, so that for a given clearance and total orifice area,

$$nd = \text{constant} \qquad (13)$$

From equations (12) and (13), it is clear that a high velocity in the supply holes is obtained by designing a bearing with many supply holes of small diameter, the condition for an annular orifice bearing being $d \gg 4c$. The Mach number of the flow in the supply holes is typically 0.3 to 0.5 and the effect of compressibility must be considered when determining the velocity V. The calculations reported in this paper are based on the assumption that the gas enters the supply holes reversibly and adiabatically, an isentropic flow.

Experiments with a turbo-bearing

Experiments have been carried out on a turbo-bearing having a central row of 18 plain jets inclined at 60^{o} to the radial direction. The test bearing has the following dimensions and rotor inertias,

$L = 66.0$ mm, $\quad R_o = 25.4$ mm

$c = 45\ \mu$m, $\quad p_s - p_a = 0.3$ MN/m^2

$I_p = 4.237_{10}{}^{-4}$ kgm^2, $\quad I_T = 3.542_{10}{}^{-3}$ kg m^2

The diameter of the supply holes was determined by following the design method of Shires, reference (2), which was modified to allow for the intersection of the supply holes and bearing being approximately elliptical. The inclined plain jets have an annular restriction with an area given by

$$\text{(ellipse perimeter) x (radial clearance)} \qquad (14)$$

The design is based on a gauge pressure factor of 0.4. The nominal diameter of the inclined supply holes is 0.38 mm.

The mass flow rate of the air supplied to the bearing was determined for several supply pressures by using the weighing technique described in reference (1). Figure 2 shows the mass flow rate as a function of supply pressure and in Figure 3, the corresponding air velocity V is also given as a function of supply pressure. From Figures 2 and 3, it is seen that since the mass flow rate varies almost linearly with the absolute supply pressure, the velocity V is almost constant for supply pressures $(p_s - p_a)$ greater than 0.2 MN/m^2. At the higher pressures, the Mach number of the flow in the supply holes is 0.42.

The analysis for the behaviour of the turbo-bearing is based on the assumption that the torques on the bearing and rotor are in proportion to the relative tangential velocities of the jet and the two surfaces, equation (3). If this assumption is valid, then the reciprocal of the time constant is given by

$$\frac{1}{t_c} = \frac{1}{I_p} \left[\frac{2 \pi \mu R_o^3 L}{c} + \frac{\dot{m} R_o^2}{2} \right]$$

The test bearing consists of a journal bearing with two thrust bearings which are fed by the air leaving the two ends of the journal bearing. The dimensions of the two plain thrust bearings are

$R_o = 25.4$ mm $\quad R_i = 17.2$ mm

$c_e = 90\ \mu m$ (clearance at each end)

and the frictional torque caused by each thrust bearing is

$$T_{th} = \frac{\mu \omega}{2c_e} (R_o^4 - R_i^4) \qquad (15)$$

In addition, there is a further torque on the thrust faces of the rotor which is caused by the change of angular momentum of the air as it flows through the thrust bearing. It is not possible to give an accurate estimate for this additional torque, since it is not known what proportion of the angular momentum of the air leaving the journal bearing is conserved as the high speed flow turns the sharp corner to enter the thrust bearing.

The small torque associated with the change of angular momentum of the air is therefore neglected.

The reciprocal of the time constant for the experimental turbo-bearing is related to the mass flow rate of the air,

$$\frac{1}{t_c} = \frac{1}{I_p} \left[\frac{2 \pi \mu R_o^3 L}{c} + \frac{\mu (R_o^4 - R_i^4)}{c_e} + \frac{\dot{m} R_o^2}{2} \right] \qquad (16)$$

The experimental values of the time constant, t_c, were measured during acceleration from rest for several supply pressures and Figure 4 shows the variation of the reciprocal of the time constant with the mass flow rate. The close agreement between the experiments and the theory provides strong support for the original hypothesis concerning the ratio of the torques on the rotor and bearing, equation (3).

Having measured the mass flow rate and calculated the velocity of the air in the supply holes, it is now possible to estimate the steady state angular velocity of the rotor. For the journal bearing with the two thrust plates, the angular velocity approaches the value

$$\omega_\infty = \frac{\dot{m} R_o V \sin \theta}{2} \left[\frac{1}{\frac{2 \pi \mu R_o^3 L}{c} + \frac{\mu (R_o^4 - R_i^4)}{c_e} + \frac{\dot{m} R_o^2}{2}} \right] \qquad (17)$$

The theoretical and experimental values for the steady state angular velocity are compared in Figure 5. It is seen that the experimental values are always less than the predicted values, the maximum error being 19%. This difference may be caused by the supply holes being slightly larger in diameter than the diameter of the drill, 0.38 mm and Figure 5 shows that the experimental results are consistent with a supply hole diameter of 0.41 mm.

The translational and angular stiffnesses of this turbo-bearing are shown in Figure 6 as functions of the supply pressure. The two stiffnesses are typical of the corresponding conventional bearing with radial supply holes, thus showing that the inclination of the supply holes has no adverse effect on either the load carrying capacity or stiffness.

In the experiments with the turbo-bearing in the self driving mode of operation, it remained stable at all speeds up to the steady state angular velocity. However, it is important to know whether the system is operating close to the onset of a self excited instability. The rotor was therefore designed with two small air turbines so that it could be driven to high speeds in either direction

of rotation. The rotor could therefore operate with a surface velocity which was in the same direction or in the opposite direction to the air leaving the supply holes. Figure 7 shows the variation in the whirl onset speeds as a function of supply pressure for the two directions of rotation. When the rotor is driven in the same direction as the air entering the clearance, then the whirl onset speed for this system is well beyond the steady state angular velocity. The steady state angular velocity is determined by the bearing parameters, whereas for a conical half speed whirl, as found in these experiments, the whirl onset speed is also a function of the rotor transverse and polar inertias. If the transverse inertia of the rotor were increased, then the conical whirl onset speed would decrease, but the steady state angular velocity would remain unchanged. As with any bearing system, the turbo-bearing must be designed so that the whirl onset speed is greater than the steady state angular velocity.

From Figure 7, it is seen that when the rotor is driven in the opposite direction to the air leaving the supply, the whirl onset speed is significantly increased. The mode of whirl remained conical and the frequency of the self excited motion was about one half of the rotor frequency. These experiments support the earlier work of Tondl, reference (3), who showed that the whirl onset speed was increased when the journal rotated in the opposite direction to the incoming air. The reason for this improvement in stability is not yet fully understood and research on this topic is continuing.

Conclusions

In the turbo-bearing, the gas enters the bearing clearance through inclined supply holes so that it acts as a lubricant and also provides a driving torque on the rotor. This method of drive is completely silent and in some applications, it can lead to a reduction in the total amount of gas required, since there is then no need for a drive turbine. This paper describes the method of design for the turbo-bearing and the experiments show good agreement with the predicted performance. The translational and angular stiffnesses are typical of a bearing with plain jets, thus showing that the tilting of the supply holes has no adverse effect on stiffness or load carrying capacity. The experiments with the driven rotor indicate that the whirl onset speed of the tilted jet bearing is dependent on the direction of rotation. When the rotor is driven in the same direction as the air entering the bearing, then for this apparatus, a conical half speed whirl occurs at a speed which is far beyond the steady state speed of the self driving turbo-bearing. When the direction of rotation is reversed, so that the rotor surface moves in the opposite direction to the air entering the bearing, then there is a significant increase in the whirl onset speed, as reported in the work of Tondl, reference (3).

It is hoped that the research described in this paper may encourage the designers of gas bearings to investigate the possibility of using the lubricant gas to provide a driving torque.

Acknowledgements

The authors would like to thank the Science Research Council for a grant to support research on gas lubricated bearings.

References

(1) Marsh, H., Drive systems for gas bearings, Proc. 5th Gas Bearing Symposium, Southampton, 1971

(2) Shires, G.L., The design of externally pressurised bearings, Chapter 4 in Gas Lubricated Bearings, ed. N.S. Grassam and J.W. Powell, Butterworths, 1964

(3) Tondl, A., Bearings with tangential gas supply, 3rd Gas Bearing Symposium, Southampton, 1967

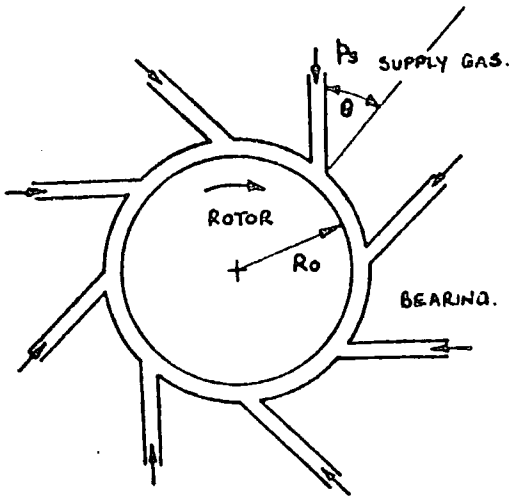

Fig. 1 The turbo - bearing.

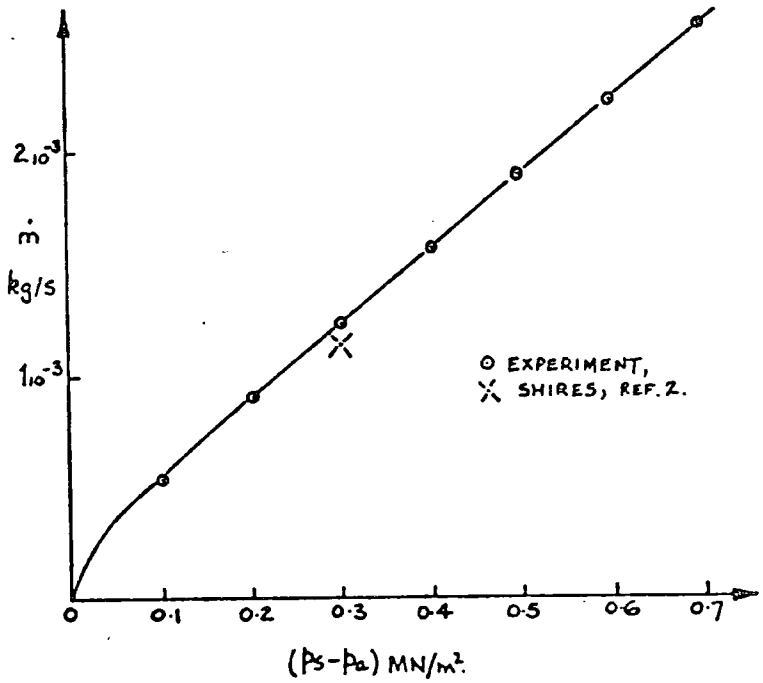

Fig. 2 Mass flow rate vs supply pressure.

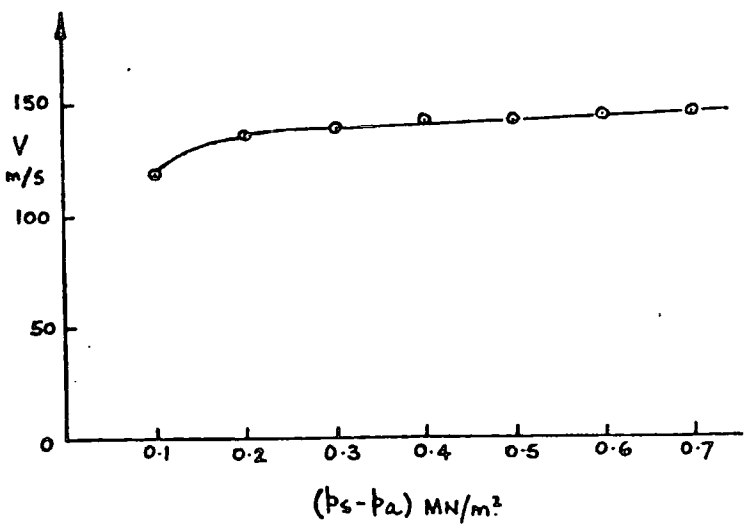

Fig. 3 Air velocity in supply holes.

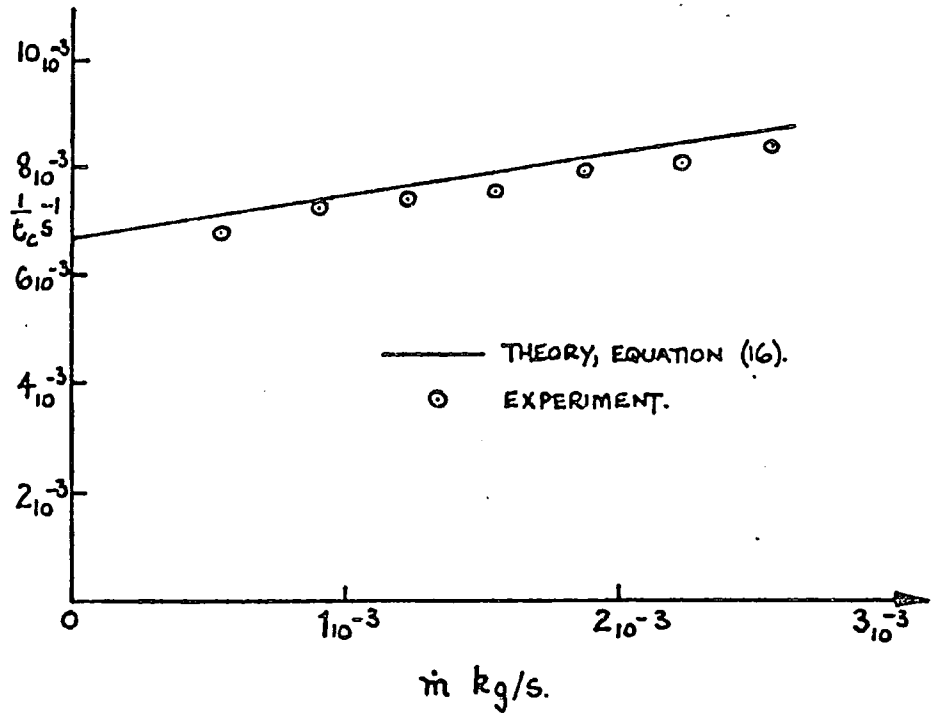

Fig. 4 Time constant vs. mass flow rate.

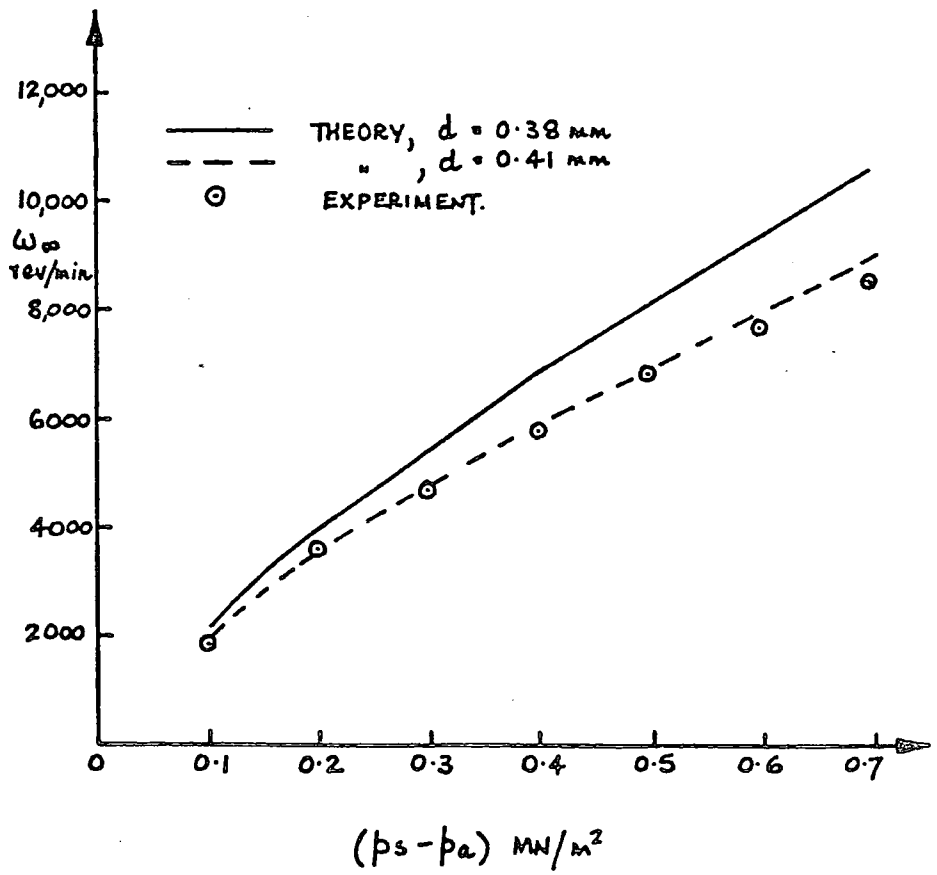

Fig. 5 The steady state angular velocity.

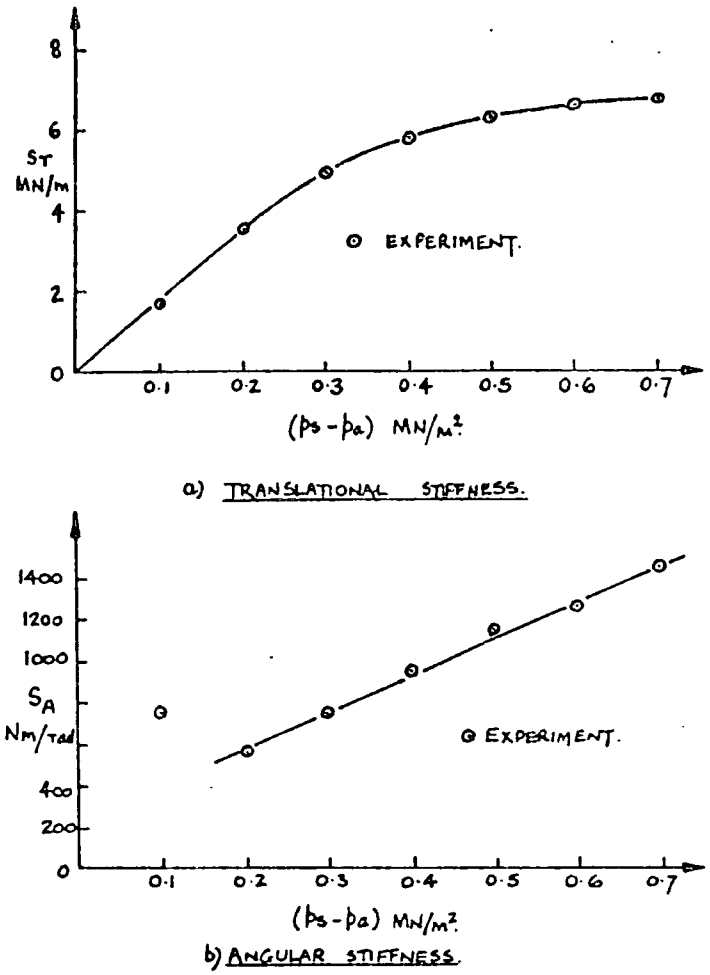

Fig. 6 Stiffness vs. supply pressure.

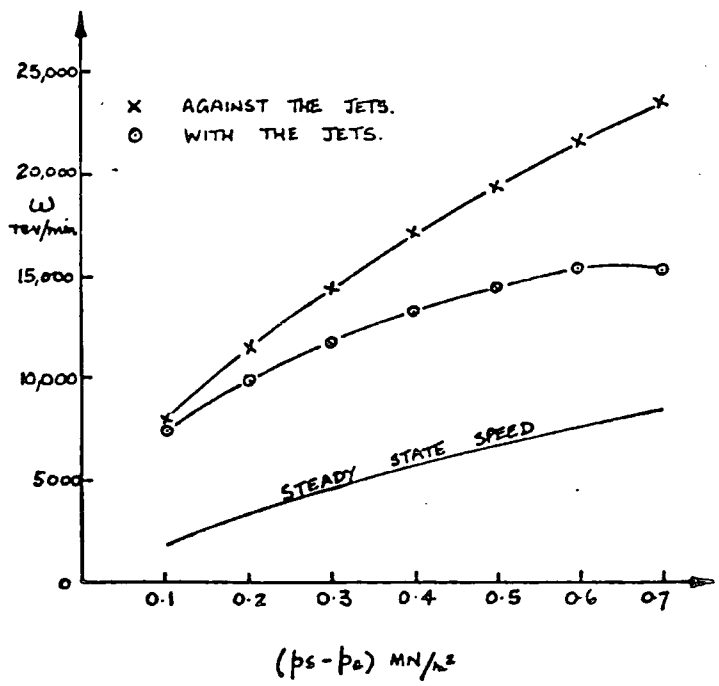

Fig. 7 Whirl onset speeds vs. supply pressure.

APPENDIX 3

VISCOSITY DETERMINATION

Distilled water was used as the lubricant. The viscosity of the water as a function of temperature was measured experimentally and the results obtained were used throughout the experimental work described in this thesis.

The apparatus used for determining the viscosity was a miniature U-tube viscometer. A U-tube viscometer consists of a glass capillary tube formed into a 'U' shape. Each side of the 'U' has a bulb let into it and these are separated by a fine capillary. A sample of water is put into one bulb between specified etched marks and the time it takes to flow through the capillary from one bulb to another can be related to the viscosity. The U-tube is suspended in a thermal water bath so that a plot of viscosity versus temperature can be obtained. The density of the water as a function of temperature is also measured using a specific gravity bottle. From the time period measurements the viscosity can be obtained from,

$$\nu = Bt + C/t$$

$$\text{and } \nu = \mu/\rho \qquad \text{(A3)}$$

(B and C are constants of the viscometer)

For large time periods the constant C in equation (A3) above can be neglected The results obtained from these experiments can be found in Figs. (A3a) and (A3b) and table (A3c).

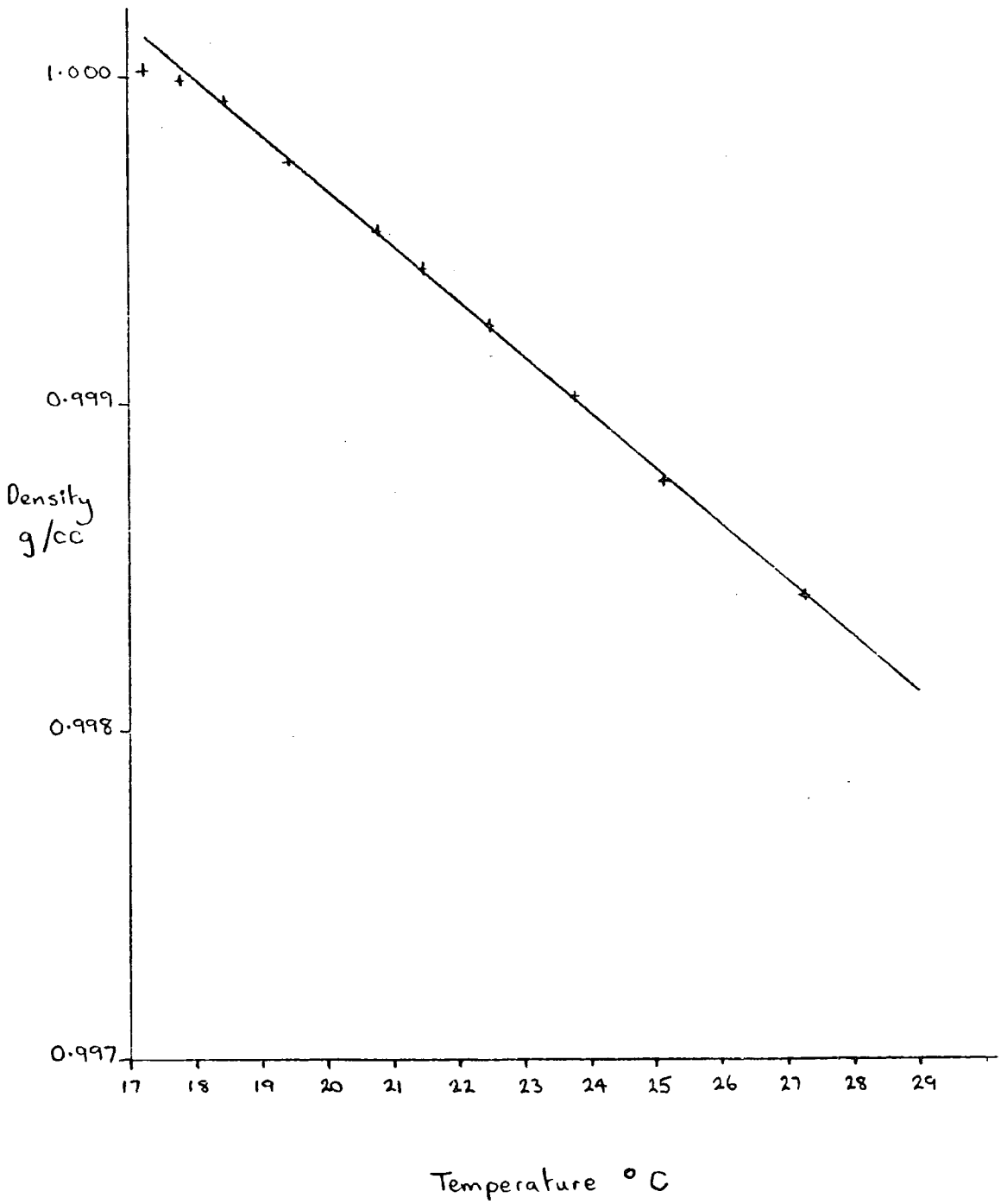

Fig. (A 3a) Plot of the variation of density with temperature of distilled water.

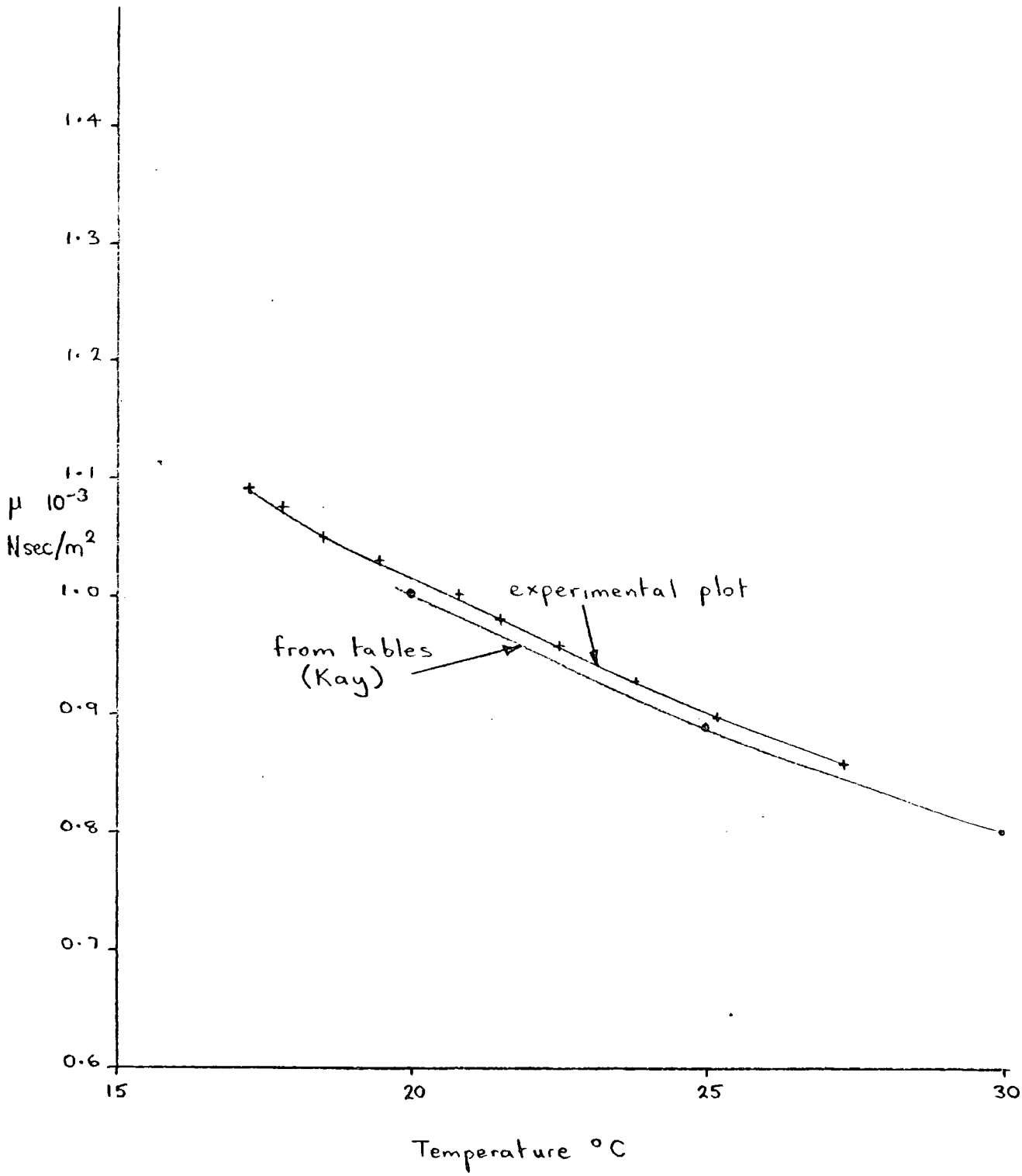

Fig.(A3b) Plot of the variation of viscosity with temperature of distilled water.

Table (A 3c) Viscosity Determination: (All runs carried out with an M1 Viscometer)

T°C (measured with Hg. in glass)	1. Time (secs)	2. Time (secs)	Average Time (secs)	ν cS	mass bottle + water (g)	mass bottle (g)	mass of water(g)	(50 cc bottle) density g/cc	viscosity (SI) 10^{-3} Nsec/m^2
17.25	1710.0	1708.3	1709.2	1.092	89.7892	39.7892	50.001	1.00002	1.092
17.80	1683.4	1681.2	1682.3	1.076	89.7877	"	49.9995	0.99999	1.076
18.50	1644.0	1641.5	1642.8	1.051	89.7843	"	49.9961	0.999921	1.051
19.45	1611.8	1612.1	1611.9	1.030	89.7753	"	49.9871	0.999741	1.030
20.80	1561.1	1560.8	1561.0	1.001	89.7643	"	49.9761	0.999522	1.001
21.50	1536.8	1535.2	1536.0	0.981	89.7594	"	49.9702	0.999405	0.980
22.50	1498.1	1499.9	1499.0	0.957	89.7500	"	49.9600	0.99924	0.956
23.80	1452.0	1450.4	1451.2	0.929	89.7351	"	49.951	0.99902	0.928
25.15	1404.3	1406.9	1405.6	0.899	89.7266	"	49.938	0.99876	0.898
27.30	1340.8	1341.0	1340.9	0.857	89.7087	"	49.9205	0.99841	0.856

B = calibration constant = 0.0006399 (mm^2/sec)/second $\quad \nu = Bt \quad$ t = time (secs)

APPENDIX 4

```
C      FRICTION BEARING (DESIGN)
1      REAL L1,L2,L3,L4,L5,LB
2      REAL MR, MR1,MD,MASS
3      DIMENSION ECC(2,100)
4      READ(5,3215)((ECC(I,M),I=1,2),M=1,100)
5   3215 FORMAT(9X,F4.2,8X,F9.2)
C      TO FIND DISC SIZE
6      DO 9876 M=1,5
7      READ(5,1000)C,R,R1,L1,L2,L3,L4,L5,LB
8   1000 FORMAT (F10.7,8(F8.4))
9      RO=7900
10     VIS=0.001
11     RIPM=(RO*3.142*L1*R**4)/2
12     RIPS=RO*3.142*L2*R1**4
13     RIPE=RO*3.142*L3*R1**4
14     RIPDH=RO*3.142*L4*R**4
15     RIP1= RIPM+RIPS+RIPE+RIPDH
16     A=((L1+L2)/2)**2
17     B=(((L3+L1)/2)+L2+L4+L5)**2
18     D=(((L1+L4)/2)+L2)**2
19     G=(((L1+L5)/2)+L2+L4)**2
20     RITC=RO*3.142*L1*R**2*((R**2)/4+(L1**2)/12)
21     RITS=2*RO*3.142*L2*R1**2*((R1**2)/4+(L2**2)/12+A)
22     RITE=2*RO*3.142*L3*R1**2*((R1**2)/4+(L3**2)/12+B)
23     RITDH=2*RO*3.142*L4*R**2*((R**2)/4+(L4**2)/12+D)
24     RIT1+RITC+RITS+RITE+RITDH
25     DO 2000 N=1,1000
26     RD=N*0.001
27     RIPD=RO*3.142*L5*RD**4
28     RITD=2*RO*3.142*L5*RD**2*((RD**2)/4=(L5**2)/12+G)
```

```
29        RIP=RIPD+RIP1
30        RIT=RITD+RIT1
31        AA=RIT-RIP*2
32        IF(AA.EQ.0.0.OR.AA.LT.0.0.) GO TO 3000
33   2000 CONTINUE
C         TIME CONSTANT
34        TC=(RIP*C)/(2*3.142*R**3*LB*VIS)
C         THE MASS
35        MR=RO*3.142*R**2*(L1+2*L4)
36        MR1=RC*3.142*R1**2*(2*L2+2*L3)
37        MD=2*RO*3.142*RD**2*L5
38        MASS=MR+MR1+MD
39        WRITE(6,7779)
40   7779 FORMAT (1H1//3X,'****')
41        WRITE(6,6000)
42   6000 FORMAT(6X,'RADIUS OF SHAFT(M)',3X,'LENGTH OF BUSH(M)',3X,'RADIAL CL
          *EARANCE(M)',3X,'RADIUS OF DISCS(M)')
43        WRITE (6,7000)R,LB,C,RD
44   7000 FORMAT(9X,F8.4,11X,F8.4,15X,F9.7,10X,F8.4)
45        WRITE(6,8000)
46   8000 FORMAT(6X,'R1(M)',6X,'L1(M)',6X','L2(M)',6X,'L3(M)',6X,'L4(M)', 6X
          *,'L5(M)')
47        WRITE(6,9000)R1,L1,L2,L3,L4,L5
48   9000 FORMAT (4X,F8.4,5(3X,F8.4))
49        WRITE(6,9100)MASS
50   9100 FORMAT (6X,'MASS OF ROTOR(KG)=',F8.4)
51        WRITE(6,9898)TC
52   9898 FORMAT(/6X,'TIME CONSTANT=',F7.2,1X,'SECS')
53        WRITE(6,1212)
```

```
1212 FORMAT(//6X,'SAFE WORKING STRESS FOR MILD STEEL=1.5*10**8 N/M**2')
     WRITE(6,9200)
9200 FORMAT(////6X,'ECCENTRICITY',4X,'RPM',4X,'REYNOLDS NO',4X,'MASS FL
    *OW RATE(KG/SEC)',4X,'%EFFECT',4X,'ONSET(RPM)', 2X,
    *'SOLID STRESS(N/M**2)',1X,'HOLE STRESS(N/M**2)')
     DO 4000 N=1,100
     E=ECC(1,N)
     A=ECC(2,N)
     IF(A.EQ.0.0) GO TO 4000
     REV=(MASS*9.81*30*C**2)/(R*3.142*VIS*LB**3*A)
     RON=(2*30/3.142)*SQRT(9.81/(C*E))
     REN=(2*REV*3.142*R*C)/((VIS/1000)*60)
     FLOW=(R*3.142*REV*10**3*C*LB*E)/30
C    ASSUMING THROWN
     RP=0.28
     WR=3.142*REV/30
     STH=((3+RP)/4)*RO*WR**2*(RD**2+R1**2*((1-RP)/(3+RP)))
     STS=((3+RP)/8)*RO*WR**2*RD**2
     STH=STH/10**8
     STS=STS/10**8
     RATIOP=(FLOW*C*10**2)/(2*3.142*R*LB*VIS)
     WRITE(6,9300)E,REV,REN,FLOW,RATIOP,RON,STS,STH
9300 FORMAT(10X,F4.2,6X,F7.1,5X,F7.1,9X,F9.6,13X,F7.3,4X,F8.1,
    *6X,F6.3,1X,'X10**8',12X,F6.3,1X,'X10**8')
4000 CONTINUE
9876 CONTINUE
     STOP
     END
```

Input to the program:

c = bearing radial clearance

R = radius of the shaft

R1 = radius of the shaft stubbs and recesses

LB = length of the bearing

L1 = length of the centre portion of the shaft

L2 = length of the shaft recesses

L3 = length of the shaft stubbs

L4 = length of the disc mounts

L5 = disc thickness

ECC = eccentricity array

The array ECC (2,100) consists of eccentricity values ranging from 0.01 to 0.99 and the corresponding values of the expression:

$$\frac{\pi \varepsilon}{4(1-\varepsilon^2)^2}\left(\left(\frac{16}{\pi^2}-1\right)\varepsilon^2+1\right)^{1/2}$$

This expression arises from the Ocvirk solution for Reynolds equation and is used in the program to predict the bearing load carrying capacity.

Output from the program:

The bearing and shaft dimensions

The calculated disc diameter

The mass of the rotor

The deceleration time constant

For each value of eccentricity in the range 0.01 to 0.99:

The rotational speed

The rotational Reynolds number

The lubricant mass flow rate

The ratio of the lubricant momentum torque to the shear torque

The predicted onset speed for translational whirl

The disc stresses

REFERENCES

1. Reynolds, O. On the theory of lubrication and its application to Mr. Beauchamp Towers' experiments, including an experimental determination of the viscosity of olive oil. Phil. Trans. R. Soc., 177, 1886, pp. 157-234.

2. Taylor, G.I., Stability of a viscous liquid contained between two rotating cylinders, Phil. Trans., A223, 1923, pp. 289-343.

3. Taylor, G.I., Fluid friction between rotating cylinders, Proc. R. Soc. of London, vol. 157A, 1936, pp. 546-564.

4. Wilcock, D.F., Turbulence in high speed journal bearings, Trans. A.S.M.E., vol. 72, 1950, pp. 825-834.

5. Castle, P., Mobbs, F.R., and Markho, P.H., Visual observations and torque measurements in the Taylor vortex regime between eccentric rotating cylinders, Journal of Lubrication Technology, Trans. A.S.M.E., vol. 93, No. 1, Jan. 1971, p. 121.

6. Smith, M.I. and Fuller, D.D., Journal bearing operation at super-laminar speeds, Trans. A.S.M.E. vol. 78, 1956, pp. 469-474.

7. Huggins, N.J., Tests on a 24 in. diameter journal bearing: transition from laminar to turbulent flow, Proc. Inst. Mech. Engrs., vol. 181, part 3B, 1966-1967, pp. 81-88.

8. Jackson, P.A., Robati, B., Mobbs, F.R., Secondary flows between eccentric rotating cylinders at sub-critical Taylor Numbers, Proc. 2nd Leeds -Lyon Symposium on Tribology, 1975, pp. 9-14.

9. Zarti, A.S., Jones, C.D. and Mobbs, F.R., The influence of cylinder radius ratio on the variation of the critical Taylor Number with eccentricity ratio, Proc. 2nd Leeds-Lyon Symposium on Tribology, 1975, pp. 23-27.

10. Cole, J.A. and Hughes, C.J., Oil flow and film extent in complete journal bearings, The Engineer, 201, 1956, pp. 255-263.

11. Cole, J.A., Experiments on the flow in rotating annular clearances, Proc. Conf. on Lub. and Wear, Inst. Mech. Engrs.,London, 1957, paper 15, pp. 16-19.

12. Short, M.G., Jackson, J.H., Wavy mode super-laminar flow between concentric and eccentric rotating cylinders: stroboscopic flow visualization and torque measurement, Proc. 2nd. Leeds-Lyon Symposium on Tribology, 1975, pp. 28-33.

13. Bennett, J. and Marsh, H., The frictional torque in externally pressurised bearings, Proc. 6th Gas Bearing Symposium, Southampton 1974.

14. Marsh, H., Drive systems for gas bearings, Proc. 5th Gas Bearing Symposium, Southampton 1971.

15. Bennett, J. and Marsh, H., The steady state and dynamic behaviour of the turbo-bearing, Proc. 6th Gas Bearing Symposium, Southampton, 1974.

16. Hampson, L.G., The effects of friction reducing polymers on the operation of Journal Bearings, Ph. D. Thesis, March, 1973, Durham University.

17. Constantinescu, V.N., On turbulent lubrication, Proc. Inst. Mech. Engrs., 1959, Vol. 173, No. 38, pp. 881-900.

18. Ng, C.W. and Pan, C.H.T., A linearized turbulent lubrication theory, Journal of Basic Engineering, Trans. A.S.M.E., 1965, vol. 87, No. 4, p. 675.

19. Hirs, G.G., A bulk-flow theory for turbulence in lubrication films, A.S.M.E. - A.S.L.E. Conference, New York, 1972, Paper 72 - Lub -12.